行政院國家科學委員會補助專題研究計畫■ 成 果 報 告 □期中進度報告

計畫名稱：高分子/無機材量子點雷射的製備及特性研究

計畫類別：■ 個別型計畫　　□ 整合型計畫
計畫編號：NSC－93－2216－E－009－002
執行期間：93 年 8 月 1 日至 94 年 7 月 31 日

計畫主持人：黃華宗
共同主持人：
計畫參與人員：

成果報告類型(依經費核定清單規定繳交)：□精簡報告　■完整報告

本成果報告包括以下應繳交之附件：
□赴國外出差或研習心得報告一份
□赴大陸地區出差或研習心得報告一份
□出席國際學術會議心得報告及發表之論文各一份
□國際合作研究計畫國外研究報告書一份

處理方式：除產學合作研究計畫、提升產業技術及人才培育研究計畫、列管計畫及下列情形者外，得立即公開查詢
□涉及專利或其他智慧財產權，□一年□二年後可公開查詢

執行單位：國立交通大學材料科學與工程研究所

中　華　民　國　九　十　四　年　八　月　三　日

高分子/無機材量子點雷射的製備及特性研究

摘要

近幾年來由於奈米材料具有包羅萬象的新穎物理及化學性質不斷的被發現，這些現象驅使著科學家對於合成具低維度結構的奈米材料，例如零維度的奈米粒子及一維度的奈米線感到相當濃厚的興趣。本研究主要致力於具低維度的氧化鋅奈米材料包含奈米柱、奈米錐陣列以及奈米複合材料合成和性質探討

本研究第一部分是探討在基板上直接成長出一維單晶氧化鋅奈米柱。利用一種新穎的兩步驟合成方法，我們已經可以在極為低溫 90 ^{o}C的水溶液中長出高密度且平均直徑約 45 奈米的氧化鋅奈米柱。值得注意的是之所以在低溫下可以製備出氧化鋅奈米柱是因為藉由氧化鋅奈米結構基板的幫助，這裡所扮演作用如同是自身種子作用以利於控制氧化鋅奈米柱的成核種子及直徑大小。

本研究第二部分是利用一種溫和化學製程方法成長具高順向性排列及獨立式的氧化鋅奈米錐陣列。除此之外我們利用此種方法合成出一些極為新穎的氧化鋅奈米結構材料，例如”奈米錐/柱”陣列，奈米刷子，奈米筆及”奈米柱/板”陣列。利用x光繞射分析發現氧化鋅奈米錐是屬於六方柱wurtzite結構並且其成長軸方向完美順著基材方向成長。從高解析度穿透式電子顯微鏡中可知奈米錐是單晶構造。在室溫下量測奈米錐可發現在波長 378 nm左右有著高強度的紫外光發光。我們也針對氧化鋅奈米錐陣列作場發射性質的探討，從研究結果發現在電流密度約為 0.1 μA/cm^{-1}時，起始電場強度約為 10.8 V/μm，並且當施加電場強度為 19.5 V/μm 時電流密度可達 1 mA/cm^{2}。

本研究第三部分是我們利用一種奈米粒子表面改質方法以獲得高透明度及安定發光的氧化鋅/聚乙基醇丙烯酸甲酯奈米複合材料。利用一種簡單且溫和的溶膠-凝膠反應中加入3-(Trimethoxysilyl)propyl methacrylate (TPM)安定劑以製備TPM-modified的氧化鋅奈米粒子。當奈米粒子表面覆蓋安定劑時可明顯提升奈米粒子的安定性並且改善奈米粒子和有機基材之間的互溶性。從實驗結果可知利用安定劑改質的奈米粒所製備出的複合材料具較佳的分散性及較佳可操縱性光的學性質。我們亦利用紫外–可見光吸收

光譜，粉末式 x 光繞射，穿透式電子顯微鏡及氫核磁共振光譜來對改質及非改質的氧化鋅奈米粒子作性質分析。最後並利用奈米粒子受光激發所產生的激發光來使高分子聚合，並可經由理論計算，利用兩道特定波長之雷射光束使其在光聚合性高分子表面產生干涉效應，進而造成干涉條紋，而此以干涉條紋的振幅和波峰大小可經由理論計算使其具有 DBR（distribute bragg's reflector mirror）的效用，使得此一有機量子點固態雷射的結構更為簡單。

Synthesis and Characterization of Polymer/Inorganic Material Quantum Dots Laser

Abstract

Growing low-dimensional nanostructured materials, such as zero-dimensional nanoparticles, and one-dimensional nanorowires (nanorods), have attracted great interested due to their novel physical and chemical properties. This dissertation work concerns the synthesis and characteristics of low-dimensional ZnO nanostructures containing nanorods, well-aligned nanotips arrays, nanoparticles/Poly(hydroxyethyl methacrylate) nanohybrid Film.

In the first part of the project, we discuss the synthesis of one-dimensional single crystal ZnO nanorods directly grown on the substrates. Employing a novel two steps procedure, the high density of ZnO nanorods with a diameter about 45 nm can be successfully grown on the substrate in aqueous solution at attractive low temperature in 90 ^{o}C. Notably, low-temperature growth of ZnO nanorods can be achieved via the help of ZnO nanostructured (ZnO nanoparticles/ITO) substrate, as self-seeding purpose, which can be used to be effectively control of the diameter and nuclei sites of ZnO nanorods.

In the second part of the project, we have proposed highly aligned and free-standing ZnO nanotip arrays grown on the ZnO films by soft chemical method. In addition, the soft growing method also has been extended to synthesize a novel of fascinating ZnO nanostructures, such as nanotips/rod arrays, nanopaintbrushs, nanopencils, nanorods/nanoplate arrays. X-ray diffraction analysis shows that the ZnO nanotips are hexagonal wurtzite structure, and the *c*-axes of nanotips are perfectly along the substrate surface normal. HRTEM demonstrates the ZnO nanotip to be a single crystal. Room temperature photoluminescence of the ZnO nanotips has a strong UV emission band at 378 nm. The field emission of ZnO nanotip arrays shows a turn-on field of about 10.8 V/μm at a current density of 0.1 $\mu A/cm^{-1}$ and emission current density up to about 1 mA/cm^2 at a bias field of 19.5 V/μm.

In the last part of the project, high transparent and stable luminescent ZnO/Poly(hydroxyethyl methacrylate) nanocomposites have been synthesized via a nanoparticle surface modified method. 3-(Trimethoxysilyl)propyl methacrylate (TPM) was used as the stabilizing agent in the simple, mild sol-gel route to prepare the TPM-modified ZnO nanoparticles. The existence of TPM agent on the nanoparticle surface effectively promotes the stability of colloidal ZnO nanoparticles and the compatibility between inorganic nanoparticles and organic matrix in solid nanohybrid. The resulting ZnO/PHEMA nanocomposites with TPM-modified nanoparticles have a better dispersibility and controllable luminescent properties. The characteristics of TPM-modified and unmodified ZnO nanoparticles have been studied by ultraviolet-visible (UV-vis) absorption spectroscopy, powder X-ray diffraction (XRD), transmission electron microscopy (TEM), Fourier transform infrared (FTIR) and ^{1}H NMR spectroscopy.

TABLE OF CONTENTS

LIST OF TABLES

LIST OF FIGURES

Chapter 1 Introduction

Chapter 2 Literature Review

Chapter 3 A Novel Low Temperature Growth and Characterization of Single Crystal ZnO Nanorods

Chapter 4 Low-temperature Solution Approach Toward Highly Aligned ZnO Nanotip Arrays

Chapter 5 Effect of Surface Stabilization of Nanoparticles on Luminescent Characteristics in ZnO/Poly(hydroxyethyl methacrylate) Nanohybrid Film

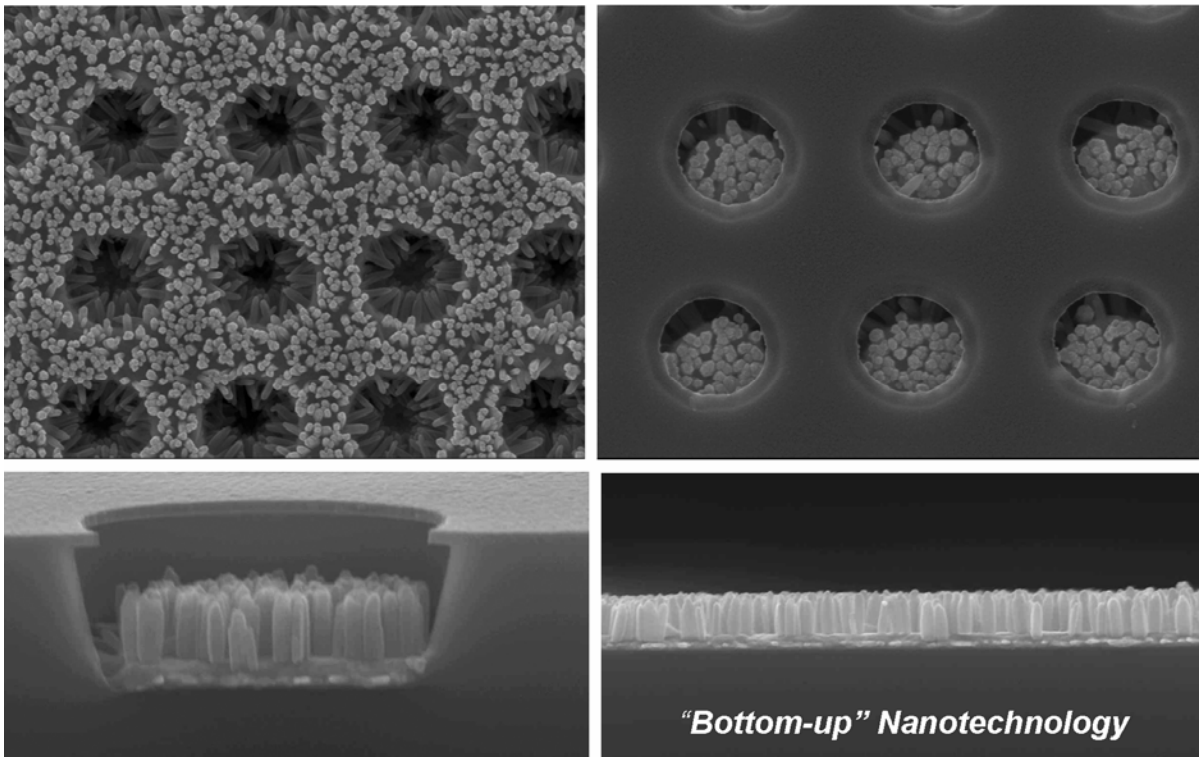

Chapter 1

Introduction

1.1 Background

"There's plenty of room at the bottom, that...almost any chemically stable structure, that can be specified, can in fact be built…."

Richard P. Feynamn [1]

Since the famous statement by Richard P. Feynman in a talk to the American Physical Society nearly 50 years ago, there has been driving force toward the fabrication of materials using the synthesis routes that build molecules from the level of "bottom-up" synthesis. The "bottom-up" synthesis is considered to give more control over the structure and design of nanomaterials than the "top-down" synthesis, in that one starts with bulk materials and sculpts downward to get to the nanoscale.

"Top-down" Approach

"Top-down" approach has been enormously successful, as the evidence by the progress in the microelectronic industry [2]. The technology is partly dominated by the ever shrinking of devices in the semiconductor progress and supported by the availability of characterization. The trend of decrease device dimensions has followed the well-known Moore's law [3] predicted in 1965 and illustrated in Figure 1-1. The figure shows that the dimension of a device halves approximately 18-24 months and today's transistor were fallen in the nanometer range. The astonishing rate of progress will be difficult to continue much past 2010, however, due to a combination of technological and economic reasons. For instance, the widening of the band gap of semiconductors occurs when the size of materials reaches de Broglies's wavelength.

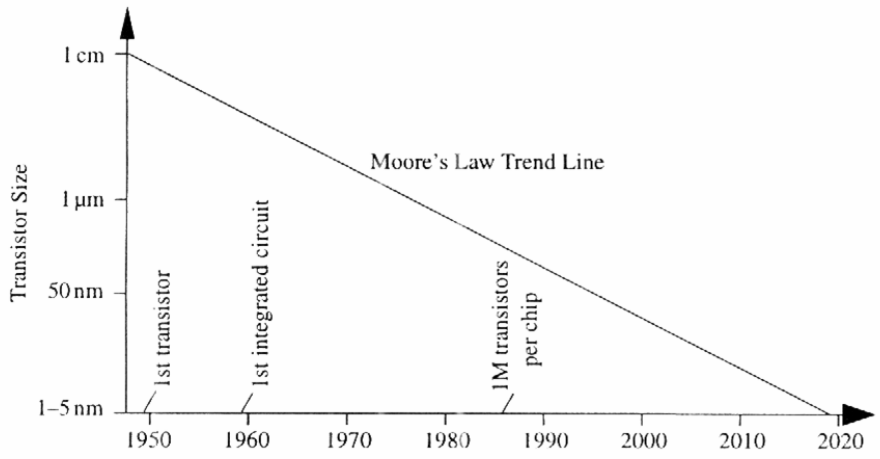

Figure 1-1 "Moore's Law" plot of transistor size *versus* year. [From ref. 4]

"Bottom-up" Approach

Another approach to nanofabrication is the so-called "bottom-up" approach. The approach refers to build-up materials from the bottom: atom-by-atom, molecular-by-molecules, or cluster-by-cluster. The approach has the potential to go far beyond of the limits of top-down technology by defining nanosystems through building structures molecules-by-molecules and even replication themselves.

Nanometer Scale Structures—Nanostructures

The development of structures with dimension in nanoscale range presents an exciting and rapidly expanding area of research in materials science. Figure 1-1 gives a partial list of zero-dimensional nanostructures, listing some of important objects from the microscopic to macroscopic world [4]. A "nano" represents one billionth, or 10^{-9}. Generally, in a wider meaning of the nanostructures, any material that has at least one dimensions below 100 nm. Reducing 1, 2, 3, dimensions (D) of bulk materials to the nanometer scale produces nanometer thick 2D layer, 1D nanowires, 0 D nanoparticles, respectively.

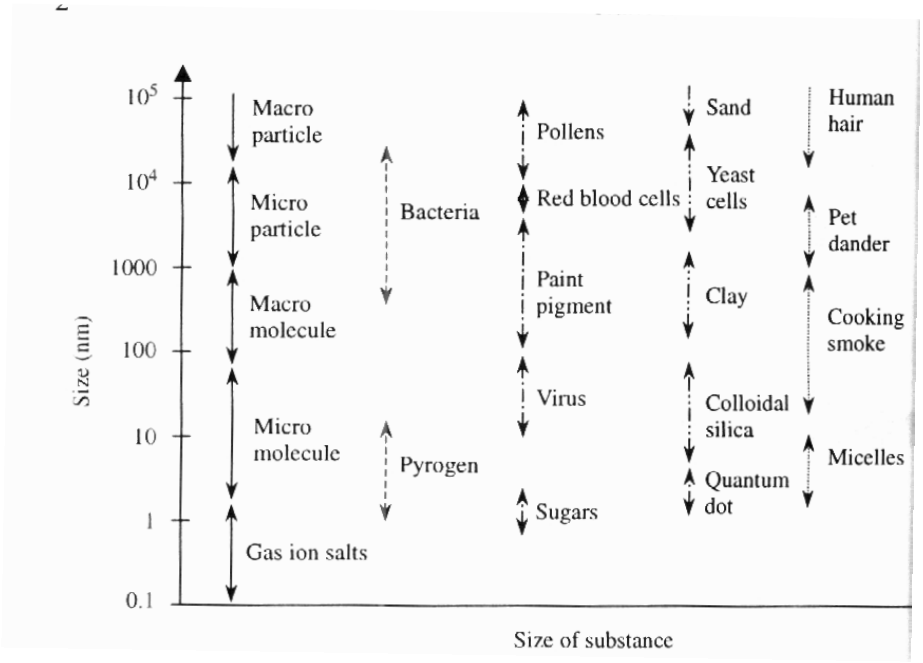

Figure 1-2 Examples of zero-dimensional nanostructures with typical ranges of dimension. [From ref. 4]

Two-dimensional Nanostructures—Thin Film

Among nanostructures, thin film structures are the best developed, and many methods have been developed and improved. Different vapor-phase growth methods (such as evaporation , molecular beam, chemical vapor deposition, atomic layer deposition) and liquid-phase growth methods (such as electrochemical deposition , Langmuir-Boldgett, self-assembled monolayers, chemical solution deposition) have been developed to grow various thin films. These synthesis methods allow the intensive study of properties and application of many different materials.

One-dimensional Nanostructures—Nanowires, Nanorods

One-dimensional nanostructures, such as nanowires [5], nanorods … etc, have been the extensively studies due to their novel physical properties and potential to revolutionize broad area of nanotechnology. One-dimensional nanostructures are the smallest dimensional structures that can act both as interconnect for the transport of charge carrier, thus are ideally studied to the critical and ubiquitous task of moving charges in nanodevices [6,7]. As semiconductor nanowires, on the other hand, provide all the properties of traditional semiconductor, such as excellent optical and electric properties, as well as new benefits form the reduced dimensions of the materials, such as possible carrier mobility enhancement. However, compared with that in two-dimensional thin film systems and zero-dimensional nanoparticles, the research progress on nanowires has been rare, due to the difficulties associated with synthesizing nanowires with well-controlled composition. In general, the techniques employed to produce nanowires include thermal evaporation, chemical vapor deposition, anodic aluminum template, and hydrolysis reaction etc. The detailed description will be presented in Chapter 2.

Zero-dimensional Nanostructures—Nanoparticles (NPs)

Individual molecules, quantum dots, nanocrystals, and nanoparticles, which can be classified as zero-dimensional structures, are attractive building blocks for bottom-up approach of nanoscale devices. Although numerous techniques have been developed for synthesizing NPs, most practical application of nanomaterials will require high-quality suitable product (monodispersion, uniform shape, high stability of NPs).

Nanoparticles possess a large fraction of surface atoms per unit volume. Due to the vast surface area, all nanoparticle materials have a huge surface energy and, thus often form agglomeration as a result of attractive van der Waals force to minimize the total surface energy. In many applications and processing where well-dispersed particles or stabilized dispersion are required, and undesirable agglomeration and coagulation in the synthesis and processing steps must be prevented. Producing unagglomerated particles can be achieved by two conceptually different ways: electrostatic stabilization, and by steric stabilization [4].

Electrostatic Stabilization [8]

When the nanoparticles are ultra-small, and are dispersed in a polar solvent, van der Waals force and Brownian motion play important role, whereas the influence of gravity becomes negligible. The method is to disperse the particles by electrostatic repulsion resulting from the interaction between the electric double layers surrounding the particles. A typical example, the synergistic and concurrent particles preparation and electrostatic stabilization is illustrated by classical synthesis of 3 nm diameter ZnO particles [9]. This process involved the hydrolysis and condensation of ethanol zinc acetate dihydrate solution in lithium hydroxide monohydrate. The ZnO nanoparticles formed at coated by an electric double layer (composed of carboxylic acid ions and the cations of zinc) responsible for Coulombic responsible which decays exponential with increasing interparticles instance. There is a weak minimum repulsion in the van der Waals energy at an interparticle separation which approximately corresponds to the diameter of stabilized ZnO nanoparticles. The stable stable distance of particle separation depends not only on the charges of the particles, but also the concentration of ion in the diffuse region of the double layer. It also should be noted that electrostatic stabilization is limited by the following factors:

- It is only applicable to dilute systems.
- It is not applicable to electrolyte sensitive systems.
- It is almost not possible to redisperse the aggregated particles.
- It is difficult to apply to multiple phase systems.

Steric Stabilization

One alternative way to produce unagglomerated particles is accomplished by absorbing polymer and/or surfactant onto the surface of nanoparticle colloids. This idea is borrowed from the physical basis of steric stabilization: a volume restriction effect arising from the decrease in possible configuration (entropy; ΔS) in the region between the two surface when the two particles contact one another and an osmotic effect due to the relatively high concentration of absorbed polymeric molecules in the region when the two particles.

Steric stabilization possesses several advantages over electrostatic stabilization [4]:

- It is thermodynamic stabilization method, so that the particles are always redispersible.
- A very high concentration can be accommodated, and the dispersion medium can be completely depleted.
- It is not electrolyte sensitive.
- It is suitable to multiple phase systems

Size of Quantization Effects

Dimensionality plays a critical role in determining the electronic and optical properties of materials. When the size of materials in a micrometer scale, the physical properties exhibit the same as that of bulk value; however, when the size of materials in a nanometer scale, the physical properties may exhibit a distinctively different from that of the bulk value. As a result, materials scientist interested in nanotechnology have mostly devote to the study of "the quantum-sized effects" owing to the spatial confinement of delocalized electrons in confined grain sizes. For example, bulk gold is chemically inert and thus considered to be not useful as a catalyst. However, nanostructured gold can have very excellent catalyst properties as first demonstrated by Haruta et al. [10]. Optical, mechanical, magnetic and thermal properties of nanostructured materials may also have similar shift. As an example is that the gold can appear blue, purple, red, or orange, as it size varies from 500 nm to 1 nm [11]. Similarly semiconductor (III-V) nanostructures exhibit a systematic blue-shift of photoluminescence emission when their size is smaller than 10–20 nm exciton diameter of corresponding bulk materials [12]. In the nano-size regime, these novel optical properties arise as a result of a change in the electric band structure. The energy states of a semiconductor material as it become in smaller size can be described initially as bulk material orbits which become discretely quantized band states in nanoparticles, and finally, quasi-uncontinuous energy bands in the molecule (Figure 1-3).

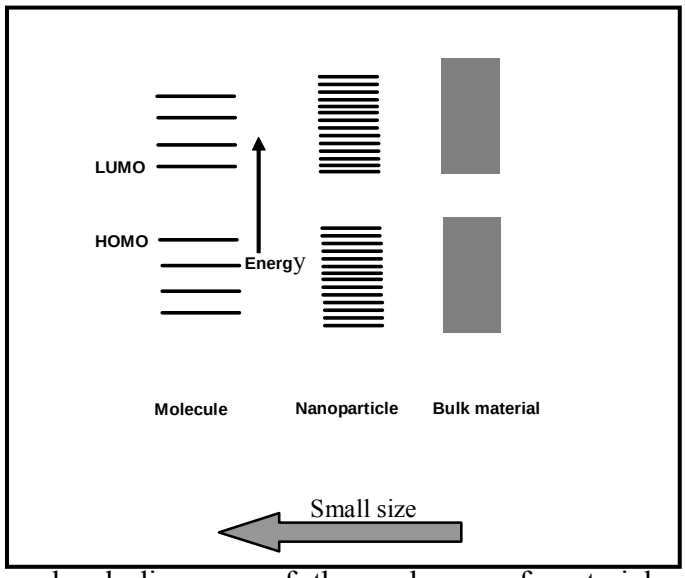

Figure 1-3 Energy level diagrams of three classes of materials showing discrete energies into molecules energy bands.

InorganicNanoparticles/Organic Polymer Nanohybrid

Recent extensive investigation into integration of organic and inorganic materials at nanoscale hybrid structures enables active devices that inherit the superior optoelectronic characteristic of nanoparticles (NPs) and possess advantages of polymers such as flexibility, film integrity, and conformity. The control of the particle size, size distribution and dispersion homogeneity over entire matrix is the critical prerequisite to assure the optical and electrical properties of the nanocomposites for nanodevice applications. Some of these applications for these nanohybrids materials are summarized in Table 1-1. It is apparent that the applications of nanohybrids range from electroluminescence to catalysis, solar cells, and storage.

Table 1-1 Examples of some application of nanohybrids

Field	Applications examples	Reference
Electroluminescence	Device1: Ag/Mg:Ag/40 nmAlq_3/CdSe (ZnS) NPs/TPD/ITO EL: wavelength ~560 nm; external efficiency:~ 0.52 %	[13]
	Device 2:Ca:Al/MEH-PPV: doped InAs-ZnSe NPs/ITO EL: wavelength 1000 nm–1300 nm; external efficiency:~ 0.5 %	[14]
Catalysits	Pt nanoparticles for hydrogenation of cyclohexane with 100 % conversion	[15]
Solar cells	Device 1:Al/PPV: doped ZnO NPs/ITO	[16]
	Devices2: Au/PA-PPV/TiO_2 NPs/ITO	[17]
Magnetic Storage	Fe_2O_3 nanoparticles in magnetic media storage	[18]

1.2 Overview of the Project

Thesis Outline

The dissertation is divided into three parts: first part (chapter 1 to chapter 2), comprise introduction and literature review. The second part (chapter 3 to chapter 5), describes the experiments, results, and discussions. The last part (chapter 6), presents a brief summary.

This thesis is organized in the following manner:

- **In chapter 2**, I describe a series of methodology used to produce one-dimensional ZnO nanostructures.

- **In chapter 3**, I present a soft chemical method for growth of single crystal ZnO nanords directly grown on ZnO nanostructured substrates. The structures, appearances and optical properties of ZnO nanorods also have been characterized in this chapter.

- **In chapter 4**, I further use the soft chemical approach to grow vertical and isolated single crystal ZnO nanotip arrays on different ZnO substrates. Results of optical and field emission measurement on ZnO nanotip arrays will also be presented.

- **In chapter 5**, I present the synthesis of high transparent and stable luminescent ZnO/PHEMA nanocomposites via a nanoparticle surface modified method. The characteristics of TPM-modified and unmodified ZnO nanoparticles have been characterized by UV-vis, XRD, TEM, FTIR and ^{1}H NMR analysis.

- **In chapter 6**, I conclude a brief summary.

1.3Reference

[1] R. Feynman. There' plenty of room at the bottom: an invitation to center a new field of physics. Engineer & Science Magazine, California Institute of Technology, USA; 1960.

[2] J. R. Health, P. J. Kuekes. G. S. Sinder, R. S. Williams, Science 280 (1998) 1716.

[3] B. E. Deal, Interface 6 (1976) 18.

[4] G. Z. Gao, Nanostructures & Nanomaterials, Synthesis, Properties & Nanomaterials, Imperical College Press, 2004.

[5] M. H. Haung, Y. Wu, H. Feick, N. Tran, E. Webber, P. Yang, Adv. Mater. 13 (2001) 113.

[6] Y. Wu, R. Fan, P. Yang, Int. J. Nano. 1 (2002) 1.

[7] Y. Wu, H. Yan, M. Huang, B. Messer, J. H. Song, P. Yang, Chem. Eur. J. 8 (2002) 1260.

[8] P. C. Pierre, Introduction to Sol-Gel Processing, Kluwer, New Work, 1981.

[9] L. Spanhel and M. A. Anderson, J. Am. Chem. Soc., 113 (1991) 2826.

[10] M. H. Hartua, Catal Today 36 (1997) 153.

[11] J. P. Wilcoxon, J. E. Martin, F. Parsapour, B. Wiedenman, D. F. Kelley, J. Chem. Phys. 108 (1998) 9137.

[12] C. B. Murry, D. J. Norris, M. G. Bawendi, J. Am. Chem. Soc. 115 (1993) 8706.

[13] N. Tessler, V. Medvedev, M. Kazes, S. H. Kan, U. Banin, Science 295 (2002) 1506.

[14] S. Coe, W. K. Woo, M. Bawendi, W. Bulovic, Nature 429 (2002) 800.

[15] A. B. R. Mayer, J. E. Mark, Colloid Poly. Si., 275 (1997) 333.

[16] W. J. E. Beek, M. M. Wienk, R. A. J. Janssen, Adv. Mater. 16 (2004) 1099.

[17] A. C. Arango, L. R. Johnson, V. N. Bliznyuk, Z. Schlesinger, S. A. Carter, H. H. Horhold, Adv. Mater. 12 (2000) 1689.

[18] D. Y. Godovsky, Biopolymers/PVA Hydrogels/Anionic Polymerization Nanocomposites, 153 (2000) 163

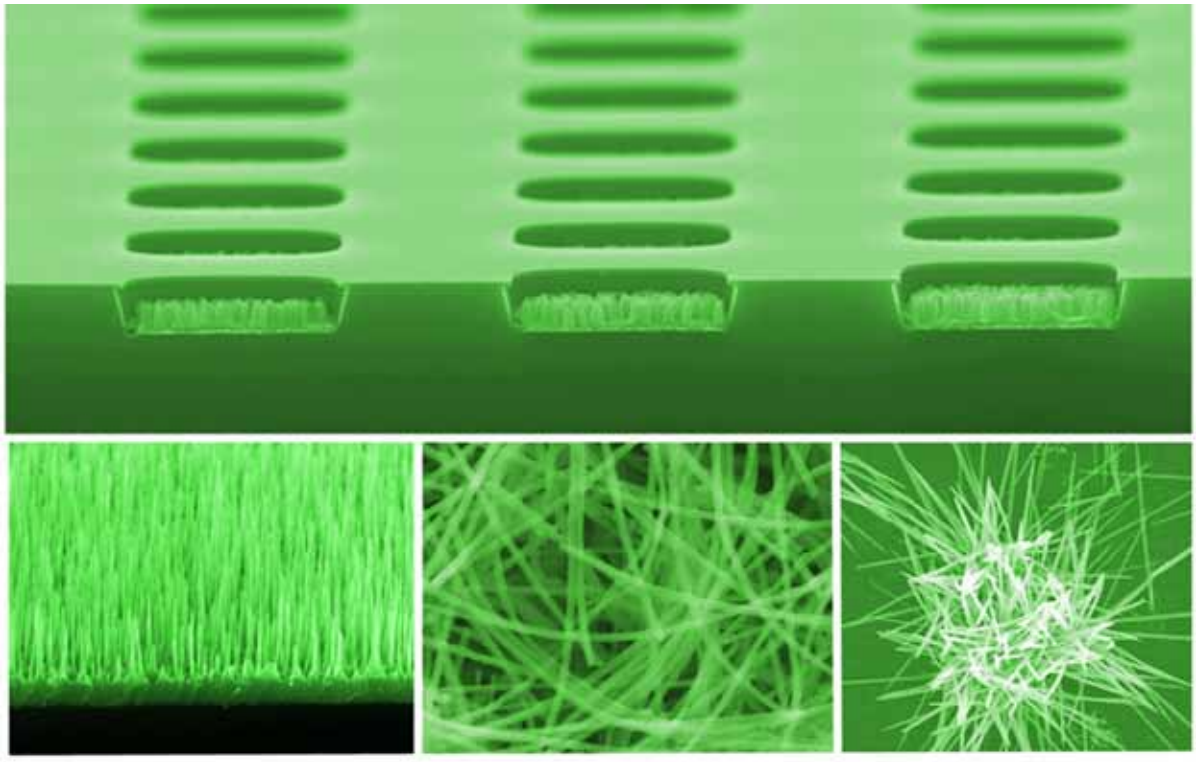

Chapter 2

Literature Review

This chapter first reviews the progress achievements in the synthesis of one-dimensional nanostructures materials. Based on the different media in the reaction system, the synthesis methods can be generally grouped into two major categories: vapor-based growth and liquid-based growth. Over the past two decades tremendous efforts have been carried out in the field of synthesis carbon nanotubes and 1D semiconductor materials, thus, our review in this chapter will be only focused on 1D ZnO nanostructures. Finally, a brief introduction of physical properties and potential application of 1D ZnO nanostructures are also described.

2.1 Strategies for Synthesis 1D ZnO Nanostructures

Since the successful synthesis of micron-size whiskers using chemical reaction under vacuum in the early 1960's [1], the investigation and formation of one-dimensional nanostructures have attracted considerable attentions. Up to date, many techniques have been developed in the synthesis of 1D nanostructures employing variety of novel

nanotechnology.

Table 2-1 summarizes the different processing techniques available for synthesis one-dimensional ZnO nanostructures.

Methodology	**Processing Route**	**Nanostructured Materials**	**Reference**
Vapor-Based Growth	Thermal Evaporation	Wires	[2-10]
		Belts	[11-13]
		Rods	[14-17]
		Tubes	[17-20]
	Chemical Vapor Deposition	Wires	[21-24]
		Rods	[25-29]
		Tubes	[30-31]
		Belts	[32]
		Needles	[33-35]
Liquid-Based Growth	Anodic Alumina Oxide Template	Wires	[36-37]
	Dissolution-Condensation Growth	Rods	[38]
	Hydrolysis Reaction	Wires	[39]
		Rods	[40-43]
		Tubes	[44]

Vapor-based Growth

In this section, two vapor-based methods for preparing 1D ZnO nanostructures are introduced: the thermal evaporation, and chemical vapor deposition.

2.1.1 Thermal Evaporation

Since Sears was the first to explore the preparation of micro-size mercury whisker by axial screw dislocation in 1955, thermal evaporation has become one of the most commonly employed in the synthesis of 1D nanostructure materials. Nowadays, the thermal evaporation growth (vapor-solid process) has been widely used to synthesize a variety of ZnO nanostructures [2-10]. In principle, the thermal vaporization is a simple process in which the vapor is generated by vaporization; subsequently the resultant vapor transports and direct condenses the growth of species on the desirable substrate.

A typical example of 1D ZnO growth *via* the vapor-solid mechanism was reported by Wang and co-workers (see Figure 1a) [4]. A horizontal tube furnace of 50–100 cm length is used. Vaporization process is conducted in argon from several ten torr to ~600 torr. The powder sources are placed in an aluminum boat and holding at a high temperature of approximately 800–1400 ^{o}C to flow the source into the tube, some of which condense in the form of novel ZnO nanostructures (see Figure 2-1b) [4,45]. The morphology of products depends on the processing parameter, i.e, growth temperature, pressure, substrate, and atmosphere. The growth of 1D ZnO via thermal evaporation process may be involved with impurity metal.

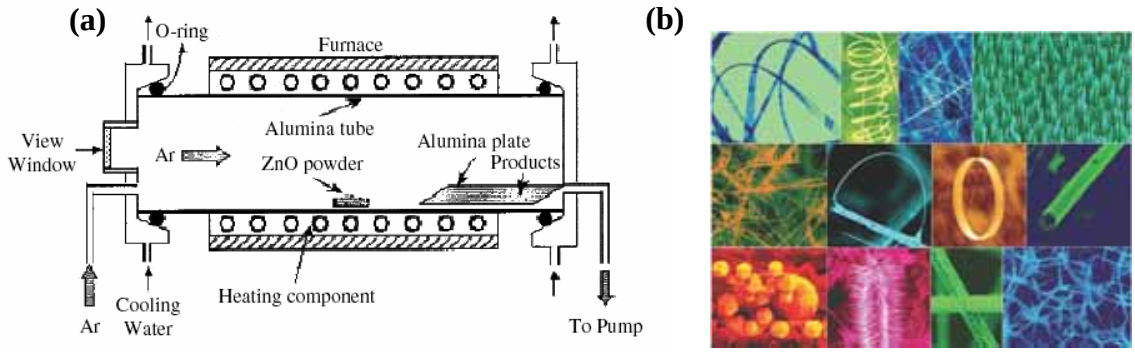

Figure 2-1 (a) Schematic diagram of experimental apparatus for growth nanostructures by thermal evaporation growth. (b) SEM images of ZnO nanostructures. [From ref. 4, 45]

2.1.2 Vapor-Liquid-Solid Growth Mechanism

Among the vapor-based methods, the vapor-liquid-solid (VLS) process seems to be the most effective method for creating 1D nanowires with single crystalline structure. Wanger *et al*. [46] first proposed the VLS mechanism to explain the growth of micron-sized silicon whisker in 1960s. In the VLS mechanism, metal catalysts are used to form liquid alloys with dissolution of gaseous reactants. The anisotropic growth of nanowire is mainly induced and promoted by the solid-liquid interface energy of liquid droplets.

The impurity metal, such Au [2], Sn [47], Co, [48] and NiO [21] are known to be catalyst for guiding ZnO nanowires growth on to a specific substrate. The method of growing ZnO nanowires *via* VLS mechanism has been well adopted by Yang *et al*., [2] mainly relying on Au catalyst-induced anisotropic growth of nanowires. They explained the catalyst-induced growth process involving three stages (see Figure 2-2): deposition a layer of metal catalyst (I); nucleation formation of the nano-sized liquid alloy droplet (Zn:Au) (II) and growth of ZnO nanowires from the supersaturation droplets of reactants by the VLS mechanism (III). The temperature of formation the liquid alloy droplets should be as high as 880–1000 ^{o}C when using Au as catalyst.

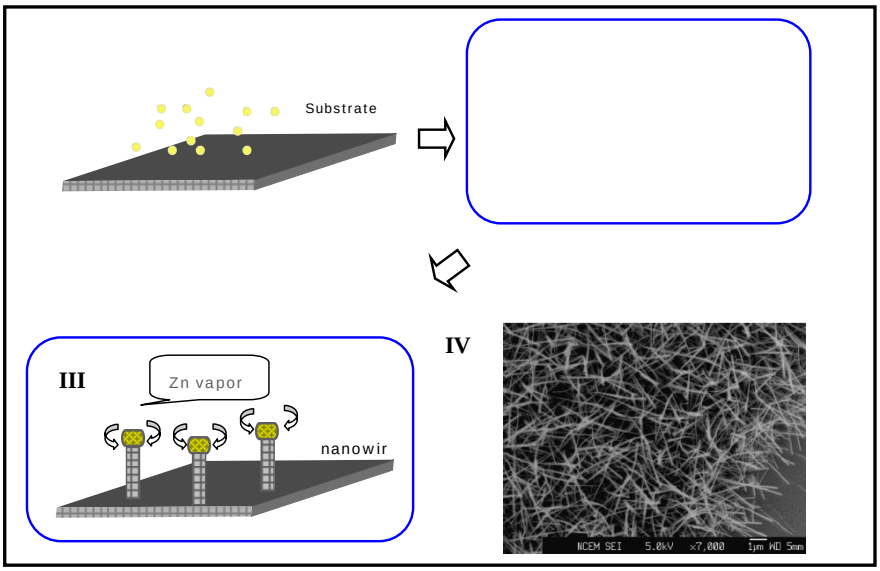

Figure 2-2 Scheme diagram of ZnO nanowires growth with Au particles as seeds for vapor-liquid-solid (VLS) mechanism. (I) Deposition of nano-sized Au particles on a Si substrate. (II) Formation a liquid alloy after heating to about 880 ^{o}C in a Zn and CO/CO_2 vapor. (III) After the alloy reaching a supersaturated with vapor sources, the nuclei of ZnO crystals precipitate and further grow into the nanowires. (IV) SEM image of ZnO nanowires grown on Si (100). [From ref. 2]

The size of catalyst is recognized to be closely related the diameter of the nanowires, so that small size of metal cluster produces a small size nanowire [2]. By optimizing the growth condition and superior properties of metal catalysts, the possibility of thermal evaporation growth of quantum-sized ZnO nanostructures was suggested. For example, the extraordinarily small size of single crystalline ZnO nanobelts with an average width of 5.5 nm has recently been reported via a solid-vapor deposition process, in which nanobelts deposits on the silicon substrate coated with a thin layer of tin catalyst under a 250~300 ^{o}C and 250~300 bar environment [49].

Sapphire is an ideal substrate to generate aligned ZnO nanorods on the substrate surface. The sapphire substrate has lattice constant a = 4.57 Å, c = 12.94 Å and small lattice mismatch (~0.1 % at room temperature) with ZnO. It has been proved that single crystalline nanorod can grow parallel to each other and perpendicular to the substrate surface (see Figure 2-3), owing to good epitaxial growth interface between the (0001) plane of ZnO crystal and the (110) plane of sapphire. Nowadays, the VLS mechanism is extensively applied to control the growth direction of nanowires on the substrate and allows for formation patterns of ZnO nanowires [2,3]. By combining the selected area deposition of catalyst, ZnO nanowires have been grown as forests of vertically aligned ZnO nanowires (see Figure 2-3B). This process has two main disadvantages: the aligned nanowires are required at relative high temperature (> 880 ^{o}C) growth and expensive sapphire substrates restrict the large-scale production and wide applications of 1D ZnO arrays.

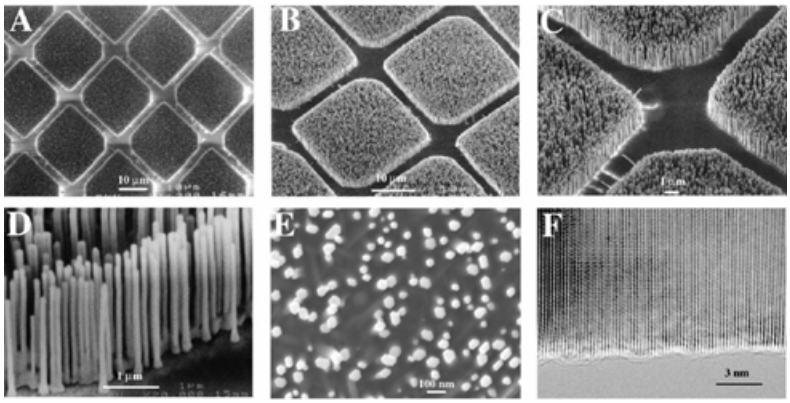

Figure 2-3 ZnO nanowires arrays grown on sapphire (0001) substrate. [From ref. 3]

2.1.1.3 Chemical Vapor Deposition (CVD)

The temperature for preparing aligned ZnO nanowire arrays via the VLS process is too high and not suitable for the fabrication of aluminum-based metallization of electronic devices (melting point of aluminum ~700 ^{o}C). As a result, it is desirable to grow aligned 1D ZnO arrays in a controlled low-temperature growth fashion.

CVD is of particular interest since it has a powerful approach for crystal film growth at a relative low temperature. In this approach, the active gaseous molecules are generated and transported into reaction chamber. The gaseous molecules will be either thermal dissociation or chemical reaction on a heat substrate surface to form stable solid film. Generally, CVD can be classified according to the type of heating method, such as thermally activated CVD, photo-assisted CVD, plasma-enhanced CVD (PECVD), metal-organic chemical vapor deposition (MOCVD) and mtalorganic vapor-phase epitaxial growth (MOVPE). Wangrt and Eillis was the first used the CVD method to grow whisker in 1964 and then Givargizov extended this method to synthesize a variety of whiskers (such as Ge, GaAs, InP and Si).

Recently, Wu's group [25] was among the first of several groups that developed and optimized a related metal-organic chemical vapor deposition (MOCVD) method to obtain aligned ZnO nanorods on silicon and sapphire substrate at ~500 ^{o}C. By employing zinc acetylacetonate hydrate compound as the metal-organic precursor, the vaporizing temperature of precursor can be maintained at temperature as low as 130–140 ^{o}C. Park *et al.* [33] also employed this interesting method to form vertically well-aligned ZnO nanoneedles on (111) Si substrates, where the needles with sharp tips and uniform distribution in their diameter. Furthermore, a number of hosts have been extensively used the MOCVD method to develop a controllable *in suit* doping of manganese in ZnO nanorods, while it still maintaining wurtzite structure [35,50].

Similar to route of MOCVD, the preferentially aligned ZnO nanorod arrays can also be achieved by MOVPE, according to Park et al. [51]. In this method, the nanorods possess a higher crystallography quality and a greater tendency to form regular arrays on the sapphire (0001) substrate than those reported using other vapor-based method. Due to more

uniform vaporized gas and better control of growth conditions obtained in the reaction chamber, the diameter of nanorods can be effectively controlled by varying the reaction time. A drawback of this method is that it needs to operate in the low-vapor-pressure. Therefore, expensive vacuum equipment is required.

Recently, this method has been used to fabricate nanocsale multiple-quantum-well heterostructures of ZnO/ZnOMgO nanords arrays (see Figure 2-4) [52]. These quantum structures in a single nanorod would enable novel physical properties from quantum confinement effect.

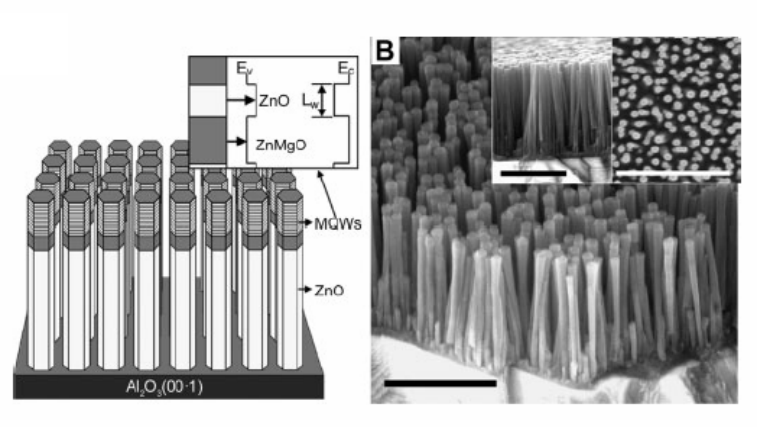

Liquid-based Growth

In this section, three liquid-based growth methods have been used to prepare a number of 1D ZnO nanostructure materials: including anodic alumina oxide template, orient-attachment growth, and hydrolysis reaction. In contrast to the techniques discussed above, the liquid-based method has several advantages, such as environment friendliness, easily large scaling, low producing cost, and low-temperature growth condition.

2.1.4 Anodic Alumina Oxide (AAO) Template

Among the numerous liquid-based methods, anodic alumina oxide (AAO) template has attracted interesting due to its versatility and facility. Anodic alumina oxide is a thermally and chemically stable template; that has uniform, cylindrical pores with diameter ranging from 10 nm to 200 nm (I). The pores are arranged in regular hexagonal arrays and the pore density can be as high as 10^{11} pores per square centimeter. In this technique, the high density nanochannels can be filled with metals or semiconductor materials by pressurized liquid injection, polymerization, sol-gel colloids and electrochemical deposition to form 1D nanowires in the membrane (II). If the template of membrane is dissolved in a chemical solution, the free-standing nanowire arrays are obtained (III). Although the AAO template-assisted method has been demonstrated to be efficient approach of large-area (up to several cm^2) nanowire arrays, it still has a drawback. Most of the AAO-template synthesis of nanowires is polycrystal or amorphous structures. The polycrystalline/amorphous nanowires could be severely limited their application in optoelectronic nanodevices.

Martin and co-workers [37] recently reported that high density of ZnO nanofibrils with an average diameter of 200 nm were fabricated by filling ZnO colloidal solutions into AAO template. So-gel reaction was applied to synthesize ZnO colloids. After the membrane was immersed into the ZnO colloids, the template was then dried in room temperature, and fired it in dry air at 120 ^{o}C to obtain free-standing polycrystalline nanofibers.

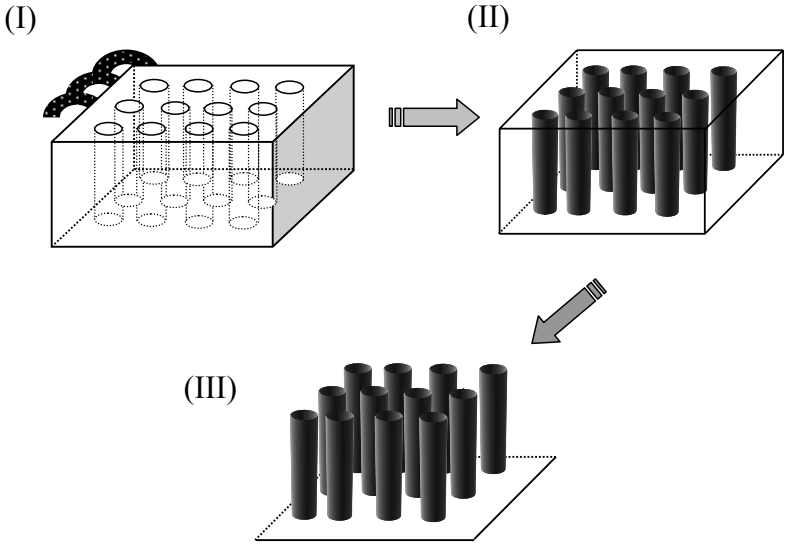

Figure 2-5 Schematic outlines of fabrication free-standing nanowire arrays by AAO template method.

2.1.5 Orient-attachment Growth

Nanocrystals growth in solution generally comprises the fast nucleation of primary particles and the subsequently crystal growth *via* two primary mechanism of coarsening and aggregation processes. Penn and Banfield [53] proposed a new crystal growth mechanism called "orient-attachment" growth in which the anatase and iron oxide can coalesce together under hydrothermal condition. In the nanocrystals aggregates process, the lattice plane at the interface of adjacent oriented particles may not perfectly align and result in a dislocation at the contact particles. These defects would influence subsequent ocarsening and final structures of crystal.

Single crystal ZnO nanorods can also be formed *via* a self-assembly mechanism of aggregated nanoparticles in methanol, as Weller *et al* [38] has demonstrated in recent year. This approach uses an extremely simple, low-temperature (60 ^{o}C), liquid-based growth. The first step of this approach involved the formation of the quasi-spherical particles with size of ~3 nm through a sol-gel reaction (Figure 2-6a). The concentration of colloids was then increased by evaporation of the solvent and aged at 60 ^{o}C in different length of time. Specifically, the length of rod-like nanoparticles increased with reaction time, but the width of nanorods grew only slightly (see Figure 2-6b). This process thus enables the single crystalline ZnO nanorods to grow in the absence of a template. Weller used an "oriented attachment" mechanism to explain anisotropic growth of nanorod, in which aggregated nanoparticles serve as seeds for further crystal growth. The "orient-attachment" growth has the advantages of producing nanorods very quickly and massively. However, the control of nucleation site and orientation of the nanorods on the substrate would be very difficult.

Hydrothermal synthetic route is similar to orient-attachment method. It also has been explored as another possible way to produce single crystal ZnO nanorods by liquid-based reaction. In this process, a mixture of alkali aqueous solution and complex agent such as ethylenediamine is put into the Telfon-lined autoclave, where the complex agent are usually used to control the growth rate of different faces. The whole reaction are kept at evaluated temperature (180–230 ^{o}C) and pressure (0.1–15 MPa) environment to lead ZnO crystal growth. For example, Zeng et al. [54] have prepared the nearly monodispersed ZnO nanorods with high crystalline in the diameter regime of 50 nm under a high-pressure and

high-temperature (180 ^{o}C) solutions of Zn alkali.

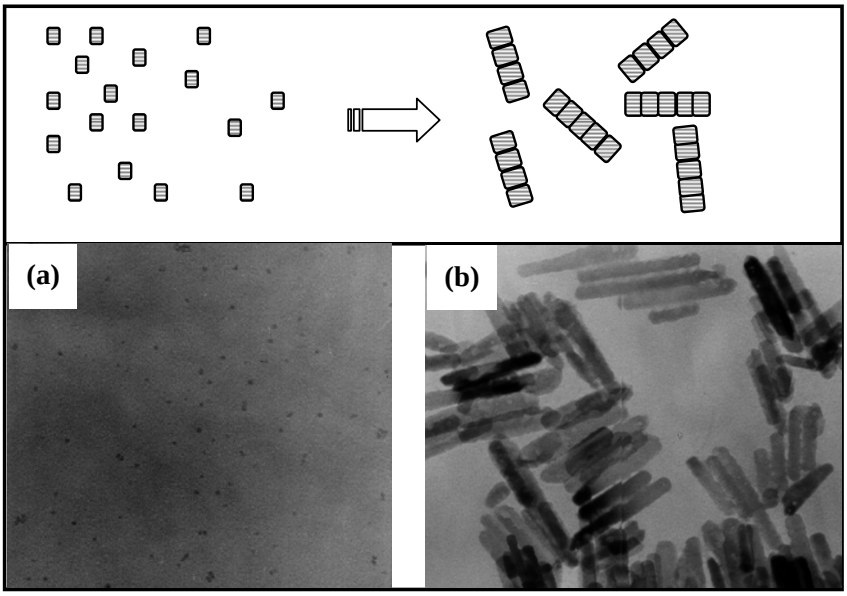

2.1.6 Hydrolysis Reaction

Despite the described progress of the liquid-based methodology for synthesis single crystal 1D ZnO, there is still remained some problems in their synthesis, such as mass production and well aligned growth of ZnO on the substrates. But, the Vayssieres's group [55] proposed a metal-oxide crystals growth method called "purposed-built materials" or we called "soft chemical route", as a new candidate for growing single crystals ZnO. This method is capable of controlling growth directly on the substrate and acquiring a large-scaled production of 1D ZnO arrays. In additional, these ordered ZnO arrays can prepare by hydrolysis reaction of zinc salt precursor in an aqueous at attractive low temperature of 95 ^{o}C. Since the electrical and optical properties of 1D ZnO nanostructures are size-dependent, the growth of high crystal quality ZnO with well-defined and nanometer-sized diameter is highly desirable. The soft chemical route can obtain large quantities of ZnO submicrods, however, the product size and morphology can not controlled very well, which will be the focus in our research.

Nucleation and Growth Model

The easiest method to prepare uniformly sized colloids metal oxide is based on (forced) hydrolysis of metal salt solution. The monodispersive particles can be obtained by carefully controlling the kinetics of the precipitation in ionic solution. It is well known that most polyvalent cations readily hydrolyze, and that deprotonation of coordinated water molecules is greatly accelerated with increasing temperature. Therefore, increasing temperature will result in an increasing amount of deprotonated molecules because hydrolysis products are intermediates to the precipitation of metal oxides.

In the formation of new crystal from solution, the nucleation plays an important role in controlling the final particles size and distribution. Essentially, there are three kind of nucleation process: homogenous nucleation, heterogeneous nucleation and secondary nucleation. Homogenous nucleation occurs in the absence of any solid interface, as nucleating acid. On the other hand, heterogeneous nucleation allows the formation of nuclei on the foreign solid interface.

In the classical theory of homogenous nucleation, the overall free energy change (ΔG) for spherical particles, is the sum of the free energy of formation of a new volume and free energy of new surface creation.

$$\Delta G = -4/\nu \cdot \pi \cdot r^3 \cdot k_B \cdot T \cdot \ln (S) + 4 \pi \cdot r^2 \gamma$$

Where ν is the molecular volume of the precipitated particle, r is the radius of the embryo, k_B is the Boltzmann's constant, S is the saturation ratio and γ is the surface free energy per unit surface area.

Once the solution reaches a saturation ratio ($S > 1$), ΔG has a positive maximum at a critical size. This maximum free energy is the activation energy for nucleation. In the most case of metal oxide, however, homogenous nucleation in the absence of a solid interface solution needs a higher activation energy barrier. Therefore, the heterogeneous

nucleation mechanism will be more favorable to crystal growth in the solution. Based on the model of hetero-nucleation, the crystal nucleation and growth in the solutions are controlled by interface free energy. Generally, the interfacial energy between the crystal and the substrate is smaller than the interfacial energy between the crystal and the solution. When the reactant species is a supersaturated, thereby a new crystal only forms on the substrate.

2.2 Properties and Potential Applications of 1D ZnO Nanostructures

In this chapter, we have been focused on studying the issue of synthesis 1D ZnO nanostructures as mentioned above. One signification for literature review in this chapter is the physical properties and potential applications for 1D ZnO nanostructures.

Zinc oxide has been know and extensively studied over the past two decades. ZnO is a very promising material for optical, electrical, catalytic and piezoelectric applications. Therefore, it has emerged as one of most used semiconductor oxides employed in catalysts, solar cell, UV LEDs, optical waveguides, varistors, gas senosor, surface acoustic wave devices, transparent conducting glass and field emission devices.

2.2.1 The Structures and General Properties of ZnO

Zinc Oxide (ZnO) has a wurtzite (hexagonal; space group *C6mc*) structures with lattice constant $a = b = 3.25$ Å and $c = 5.12$ Å, where layers occupied by zinc atoms alternate with layers occupied by oxygen atoms. The zinc atoms are tetrahedrally coordinate to four oxygen atoms, and the *d*-electrons of zinc hybridize with the *p*-electron of oxygen (see Figure 2-7).

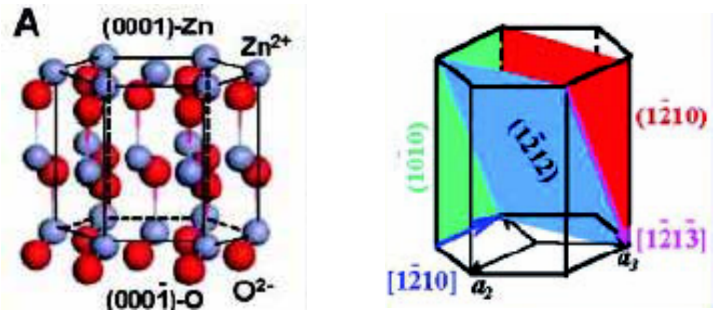

To realize any type of devices technology, it is difficult to understand their character without a basic knowledge of basic material parameters. Table 2-2 summarizes the material parameters of wurtzite ZnO [57]. ZnO is an II–VI compound semiconductor with direct band gap of 3.4 eV at room temperature, and shows optical properties similar to observed in GaN. The optical band gap of ZnO can be tuned *via* divalent substitution on the cation site, as called dopants. Cd substitution (doping) can lead to a reduction in the energy gap to ~ 3.0 eV, whereas Mg substitution can increase the energy gap to as high as ~4.0 eV [58]. The electron Hall mobility in single crystal ZnO is between 100 and 200 cm^2/V s and the hole Hall mobility is on the order of 5 cm^2/V s at room temperature. The carrier effective mass in ZnO is basically equal to 0.24 m_0 and 0.59 m_0 for electrons and holes, respectively.

Lately, both ZnO film and 1D ZnO single crystalline nanostructures show excellent optical characteristics. In some respects, the physical properties of ZnO compare favorably to those of the GaN. The high exciton binding energy (60 meV) in ZnO wurtzite crystals, significantly larger than that of GaN (25 meV), that ensures an efficient exciton relate photon emission process under low threshold excitation energy at room temperature. The binding energy of ZnO has greater than thermal energy at room temperature (26 meV). As such, it offers a candidate host for developing a room temperature UV laser [3]. Furthermore, ZnO has higher optical gain (300 cm^{-1}) than GaN (100 cm^{-1}) at room temperature.

2.2.2 Application of 1D ZnO Nanowires

In contrast to bulk materials, the low-dimensional nanoscale materials comprise large surface area and possible quantum confinement effect that may exhibit new distinct electrical, chemical, optical, and thermal properties. At present, many researches have been extensively devoted to explore these novel physical properties and take advantage of these properties in advanced nanodevice applications.

Recent progress in processing and novel applications for related 1D ZnO nanomaterials are listed below:

- Synthesis single-crystal ZnO nanowires via a VLS growth mechanism [2,3]
- Room temperature ultraviolet lasing in ZnO nanowire arrays [3]
- Growth aligned submicron ZnO rods in low-temperature aqueous solution [55]
- Field electron emission from vertically aligned ZnO nanowire arrays [59]
- Synthesis of single-crystal complete nanorings of ZnO via a spontaneous self-coiling process [56]
- Quantum confinement observed in ZnO/ZnMgO nanorods heterostructures [52]
- Fabrication of *p*-GaN/*n*-ZnO nanorods heterojunction EL devices [60]

Hydrogen Storage

Hydrogen storage in 1D nanostructure, such CNTs, has attracted a great deal attention. Hydrogen storage capacity would be potentially useful for fuel cell in electric vehicles or laptop computer application. Recently, Wan et al. [61] have reported that the hydrogen storage capacity of about 0.83 % is achieved in ZnO nanowires under the pressure of 3.03 Mpa at room temperature and about 71 % of the storage hydrogen is released under ambient pressure.

Gas Sensors

Among major application of 1D ZnO nanostructures is likely related the sensing of gas molecules. Because of the high surface-to-volume ratio of 1D ZnO nanostructures, their electronic properties are extremely sensitive to species absorbed on the surface. For example, Wang and *co*-workers [62,63] have demonstrated the perspective of gas sensor using the microelectromechanical system based on ZnO nanowires. They reported that ZnO nanowires have a high sensitivity and fast response to ethanol gas molecules at a work temperature of 300 ^{o}C. In another demonstration, the same group also observed that the

positive temperature coefficient resistance of Cd-doped ZnO nanowires strongly depends on porous surface states produced by water molecules absorption. Hence, the Cd-doped ZnO nanowires might show a promising application for humidity sensors.

Field-emission Devices

Because of the unique geometries of 1D nanowires and nanotubes, combined with their high flexibility and hardness resulting from defect-free lattices, these materials are attractive as cold cathode for device that use field emission electron sources and flat panel display. Le and co-workers [59] were first group to explore the field emission characteristics of well-aligned ZnO nanowires. The single crystalline nanowire arrays exhibited a turn-on electric field of about 6.0 V/μm and the emission current density reached about 1 mA/cm^2 at an applied field of 11.0 V/μm.

Wan et al. [64] have reported the turn-on field in the tetrapod-like ZnO nanostructures almost as low as 1.6 V/μm at the current density of 1 μA/ cm^2. Ren et al. [65] subsequently developed an extremely low operating electric field of ZnO nanowires grown on carbon cloth. In particular, a turn-on electric field of as low as 0.7 V/μm is needed to obtain an emission current density of 1 mA/cm^2, which is comparable with those for other field emitters as carbon nanotubes emitters. The field emission properties in various ZnO nanostructure emitters are summarized in Table 2-3.

Electroluminescence Devices

One of the more exciting applications for 1D ZnO nanowires is the light-emitting diodes (LEDs). Because of the superior characteristic of direct and wide band gap with a large exciton binding energy (60 meV), the ZnO materials are attractive much attentions especially for short-wavelength emitting devices application. Like ordinary electroluminescence devices, the ZnO-based EL device typically comprises ZnO p-n homojunction structure and n-ZnO/p-GaN heterojunction structure. The latter generates luminescence; however, has lower luminescence efficiency due to the large lattice mismatch at junction interface. This problem may be resolved by employing the growth 1D

nanorods, as nanosize junctions, since the growth mechanism of nanorods is completely different. Yi *et al*. [60] have demonstrated the electroluminescence from the p-GaN/n-ZnO nanorod arrays heterostructure EL devices (see Figure 2-8). The p-n heterojunctions nanorod arrays device shows a high current density and strong luminescence at a reverse-bias of 3V.

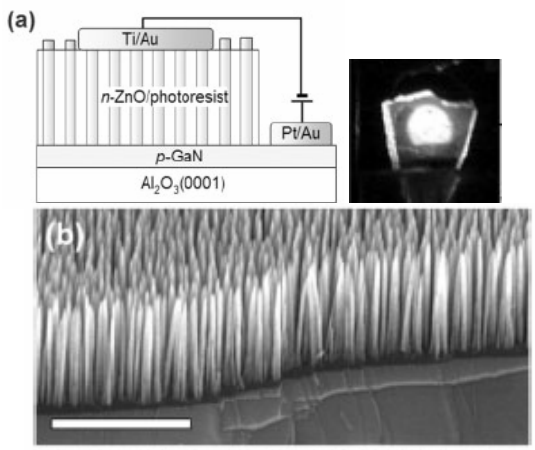

F

Table 2-2 Properties of wurtzite ZnO. [57]

Property	Value
Lattice parameter at 300 K	
a_0	0.32495 nm
c_0	0.52069 nm
a_0/c_0	1.602
u	0.345
Density	5.606 g/cm^3
Stable phase at 300 K	Wurtzite
Melting point	1975 ^{o}C
Thermal conductivity	0.6, 1–1.2
Linear expansion coefficient (/C)	a_0: 6.5×10^{-6} c_0: 3.0×10^{-6}
Static dielectric constant	8.656
Refractive index	2.008, 2.029
Energy gap	3.4 eV , direct
Intrinsic carrier concentration	< 10^6 meV
Exciton binding energy	60 meV
Electron effective mass	0.24m$_0$
Electron Hall mobility at 300K for low *n*-type conductivity	100–200 cm^2/V s
Hole effective mass	0.59 m$_0$
Hole Hall mobility at 300 K for low *p*-type conductivity	5–50 cm^2/V s

Table 2-3 Summary of emission turn-on fields and threshold fields (field required to generate a current density of 10 μA/cm^2 and 1 mA/cm^2, respectively) for various ZnO nanostructures emitters.

Nanostructures materials	Fabrication method & substrate temperature (^{o}C)	Turn-on field (V/μm)	Threshold field (V/μm)	Reference
ZnO nanowire arrays	thermal evaporation & 550 ^{o}C	6.0	11.0	[59]
ZnO nanoneedle arrays	thermal evaporation & 370 ^{o}C	2.4	6.5	[66]
Tetrapod-like ZnO	thermal evaporation & 900 ^{o}C	1.6	4.5	[64]
Gallium-doped ZnO nanofiber arrays	thermal evaporation & 830 ^{o}C	2.5	6	[67]
ZnO nanopins	thermal evaporation & 600–700 ^{o}C	1.92	5.9	[68]
ZnO nanowires grown on carbon cloth	thermal evaporation & 720–750 ^{o}C	0.2	0.7	[65]
ZnO nanoneedles arrays	PE-CVD & 550 ^{o}C	24.0	> 40.0	[69]
ZnO nanotip arrays	Hydrolysis & 95^{o}C	10.8	19.5	[70]
ZnO nanoneedles	thermal evaporation & 500–550 ^{o}C	2.5	4.0	[71]
ZnO nanowires	thermal evaporation & 650 ^{o}C	2.4	>10	[72]

2.3 Motivation

Even though several groups have been extensively working to develop 1D ZnO on the substrate by using vapor-based growth, to date successful preparing ZnO nanorods *via* the liquid-based methods have rarely been achieved.

The first purpose of this research is to use the soft chemical route to produce small diameter of ZnO nanorods on the nanostructured (ZnO nanoparticles/ITO) substrates, by controlling the nuclei of them on the nanometer scale at which they grow. In this way, the ZnO nanorod is created using the recognized "bottom up" approach that is characteristic of nanotechnology. In the second purpose, we devote to grow highly aligned and free-standing ZnO nanotip arrays grown on the ZnO films. The soft growing method also has been extended to synthesize a series of novel geometric structures, including nanotips/rod arrays, nanopaintbrushs and nanopencils. In the third objective, highly transparent and stable luminescent ZnO/Poly(hydroxyethyl methacrylate) nanocomposites have been synthesized via a nanoparticle surface modified method. The resulting ZnO/PHEMA nanocomposites with TPM-modified nanoparticles have a better dispersibility and controllable luminescent properties.

2.4 Reference

[1] G. W. Sear, Acta Metal, 3 (1955) 361.

[2] M. H. Haung, Y. Wu, H. Feick, N. Tran, E. Webber, P. Yang, Adv. Mater. 13 (2001) 113.

[3] M. H. Huang, S. Mao, H. Feick, H. Yan, Y. Wu, H. Kind, E. Weber, R. Russo, P. Yang, Science 292 (2001) 1897.

[4] Z. R. Dai, Z. W. Pan, Z. L. Wang, Adv. Funct. Mater. 13 (2003) 9.

[5] B. D. Yao, Y. F. Chen, N. Wang, Appl. Phys. Lett. 81 (2002) 757.

[6] D. Banerjee, J. Y. Lao, D. Z. Wang, J. Y. Huang, Z. F. Ren, D. Steeves, B. Kimball, M. Sennett, Appl. Phys. Lett. 83 (2003) 2061.

[7] H. J. Yuan, S. S. Xie, D. F. Liu, X. Q. Yan, Z. P. Zhou, L. J. Ci, J. X. Wang, Y. Gao, L. Song, L. F. Liu, W. Y. Zhou, G. Wang, Chem. Phys. Lett. 371 (2003) 337.

[8] Y. C. Kong, D. P. Yu, B. Zhang, W. Fang, S. Q. Feng, Appl. Phys. Lett. 78 (2001) 407.

[9] Y. W. Wang, L. D. Zhang, G. Z. Wang, X. S. Peng, Z. Q. Chu, C. H. Liang, J. Cryst. Growth 234 (2002) 171.

[10] S. C. Lyu, Y. Zhang, C. J. Lee, Chem. Mater. 15 (2003) 3294.

[11] X. Y. Kong, Y. Ding, Z. L. Wang, J. Phys. Chem. B 108 (2004) 570.

[12] X. Y. Kong, Z. L. Wang, Nano Lett. 12 (2003) 1625.

[13] R. S. Yang, Y. Ding, Z. L. Wang, Nano Lett. 4 (2004) 1309.

[14] Y. Dai, Y. Zhang, Q. K. Li, C. W. Nan, Chem. Phys. Lett. 358 (2002) 83.

[15] J. Y. Lao, J. Y. Huang, D. Z. Wang, Z. F. Ren, Nano Lett. 3 (2003) 235.

[16] V. A. L. Roy, A. B. Djursic, W. K. Chan, J. Gao, H. F. Lui, C. Surya, Appl. Phys. Lett. 83 (2003) 141.

[17] H. Chik, J. Liang, S. G. Cloutier, N. Kouklin, J. M. Xu, Appl. Phys. Lett. 84 (2004) 3376.

[18] J. Q. Hu, Q. Li, X. M. Meng, C. S. Lee, S. T. Lee, Chem. Mater. 15 (2003) 305.

[19] Y. J. Xing, Z. H. Xi, Z. Q. Xue, X. D. Zhang, J. H. Song, R. M. Wang, J. Xu, Y. Song, S. L. Zhang, D. P. Yu, Appl. Phys. Lett. 83 (2003) 1689.

[20] B. P. Zhang, N. T. Binh, K. Wakatsuki, Y. Segawa, Y. Yamada, N. Usami, M. Kawasaki, H. Koinuma, Appl. Phys. Lett. 84 (2004) 4098.

[21] S. C. Lyu, Y. Zhang, H. Ruh, H. J. Lee, H. W. Shim, E. K. Suh, C. J. Lee, Chem. Phys. Lett. 363 (2002) 134.

[22] C. Y. Geng, Y. Jiang, Y. Yao, X. M. Meng, J. A. Zapien, C. S. Lee, Y. Lifshitz, and S. T. Lee, Adv. Funct. Mater. 14 (2004) 589.

[23] S. Y. Bae, H. W. Seo, J. H. Park, J. Phys. Chem. B 108 (2004) 5206.

[24] M.C. Jeong, B. Y. Oh, W. Lee, J. M. Myoung, J. Cryst. Growth 268 (2004) 149.

[25] J. J. Wu, S. C. Liu, Adv. Mater. 14(2002) 215

[26] B. P. Zhang, N. T. Binh, Y. Segawa, K. Wakatsuki, N. Usami, Appl. Phys. Lett. 83 (2003) 1365.

[27] H. T. Yuan, Y. Zhang, J. Cryst. Growth 263 (2004) 119.

[28] S X. Liu, X. H. Wu, H. Cao, R. P. H. Chang, J. Appl. Phys. 95 (2004) 3141.

[29] G. Z. Wang, N. G. Ma, C. J. Deng, P. Yu, C. Y. To, N. C. Hung,M. Aravind, D. H. L. Ng, Mater. Lett. 58 (2004) 2195.

[30] B. P. Zhang, N. T. Binh, K. Wakatsuki, Y. Segawa, Y. Yamada, N. Usami, M. Kawasaki, H. Koinuma, Appl. Phys. Lett. 84 (2004) 4098.

[31] J. J. Wu, S. C. Liu, C. T. Wu, K. H. Chen, L. C. Chen, Appl. Phys. Lett. 81 (2002) 1312.

[32] J. Zhang. W. Y. Yu, L. D. Zhang, Phys. Lett. A 229 (2002) 276.

[33] W. I. Park, G. C. Yi, M. Y. Kim, S. J. Pennycook, Adv. Mater. 14 (2002) 1841.

[34] S. Muthukumar, H. Sheng, J. Zhong, Z. Zhang, N. W. Emanaetoglu, Y. Lu, IEEE Trans. Nanotechnol. 2 (2003) 50.

[35] J. Zhang, S. Muthkumar, Y. Chen, Y. Lu, H. M. Ng, W. Jiang, E. L. Garfunkel, Appl.

Phys. Lett. 83 (2003) 3401.

[36] Y. Li, G. W. Meng, L. D. Zhang, F. Phillipp, Appl. Phys. Lett. 76 (2000) 2011.

[37] B. B. Lakshmi, P.K. Dorhout, C. R. Martin, Chem. Mater. 9 (1997) 857

[38] C. Pacholski, A. Kornowski, H. Weller, Angew. Chem. Int. Ed. 7 (2002) 41.

[39] L. Vayssieres, Adv. Mater. 15 (2003) 464.

[40] B. Liu, H. C. Zheng, Langmuir 20 (2004) 4196.

[41] J. Zhang, L. –D. Sun, X. –C. Jiang, C. –S. Liao, C. –H. Yan, Crystal. Growth & Design 4 (2004) 309.

[42] X. P. Gao, Z. F. Zheng, H. Y. Zhu, G. L. Pan, J. L Bao, F. Wu, D. Y. Song, Chem. Commun. (2004) 1428.

[43] B. Cheng, E. T. Samulski, Chem. Commun. (2004) 986.

[44] L. Vayssieres, K. Keis, A. Hagfeldt, S. E. Lindquist, Chem. Mater. 13 (2001) 4395.

[45] Z. L. Wang, Materials Today 7 (2004) 26.

[46] R. S. Wanger, W. C. Ellis, Appl. Phys. Lett. 4 (1964) 89.

[47] P. X. Gao, Y. Ding, Z. L. Wang, Nano. Lett. 3 (2003) 1315.

[48] C. J. Lee, T. J. Lee, S. C. Lyu, Y. Zhang, H. Ruh, H. J. Lee, Appl. Phys. Lett. 19 (2002) 3648.

[49] X. Wang, Y. Ding, C. J. Summers, Z. L. Wang, J. Phys. Chem. B 103 (2004) 9701.

[50] J. J. Wu, S. C. Liu, M. H. Wang, Appl. Phys. Lett. 85 (2004) 1027.

[51] W. I. Park, D. H. Kim, S. –W. Jung, G. –C. Yi, Appl. Phys. Lett. 80 (2002) 4232.

[52] W. I. Park, G. –C. Yi, M. Y. Kim, S. J. Pennycook, Adv. Mater. 15 (2003) 526

[53] J. F. Banfield, S. A. Welch, H. Zhang, T. T. Ebert, R. L. Penn, Science 289 (2000) 751.

[54] B. Liu, H. C. Zhang, J. Am. Chem. Soc. 125 (2003) 4430.

[55] L. Vayssieres, K. Kesis, S. E. Lindquist, A. Hagfeldt, J. Phys. Chem. B 105 (2001) 3350.

[56] X. Y, Kong, Y. Ding, R. Yang, Z. L. Wang, Science 303 (2003) 1348.

[57] S. J. Pearton, D. P. Norton, K. Ip, Y. W. Heo, T. Steiner, J. Vac. Sci. Technol. B 22 (2003) 932.

[58] L. K. Singh, H. Mohan, Indian, J. Pure Appl. Phys. 13 (1975) 222.

[59] C. J. Lee, T. J. Lee, S. C. Lyu, Y. Zhang, Appl. Phys. Lett. 81 (2002) 3648.

[60] W. I. Park, G. –C. Yi, Adv. Mater. 16 (2004) 87.

[61] Q. Wan, C. L. Lin, X. B. Yu, T. H. Wang, Appl. Phys. Lett. 84 (2004) 124.

[62] Q. Wan, Q. H. Li, Y. J. Chen, T. H. Wang, X. L. He, J. P. Li, C. L. Lin, Appl. Phys. Lett. 84 (2004) 3654.

[63] Q. Wan, Q. H. Li, Y. J. Chen, T. H. Wang, X. L. He, X. G. Gao, J. P. Li, Appl. Phys. Lett. 84 (2004) 3085.

[64] Q. Wan, K. Yu, T. H. Wang, C. L. Lin, Appl. Phys. Lett. 83 (2003) 2253.

[65] S. H. Jo, D. Banerjee, Z. F. Ren, Appl. Phys. Lett. 85 (2004) 1407.

[66] Y. W. Zhu, H. Z. Zhang, X. C. Sun, S. Q. Feng, J. Xu, Q. Zhao, B. Xiang, R. M. Wang, D. P. Yu, ppl. Pys. Lett. 83 (2003) 144.

[67] C. X. Xu, X. W. Sun, B. J. Chen, Appl. Phys. Lett. 84 (2004) 1540.

[68] C. X. Xu, X. W. Sun, Appl. Phys. Lett. 83 (2003) 3806.

[69] Y. K. Tseng, C. –J. Huang, H. –M. Cheng, I. –N. Lin, K. –S. Liu, I. –C. Chen, Adv. Funct. Mater 13 (2003) 811.

[70] C. H. Hung, W. T. Wang, J. Cryst. Growth 268 (2004) 242.

[71] Y. B. Li, Y. Bando, D. Golberg, Appl. Phys. Lett. 84 (2004) 3603

[72] S. Y. Li, P. Lin, C. Y. Lee, T. Y. Tseng, J. Appl. Phys. 95 (2004) 3711

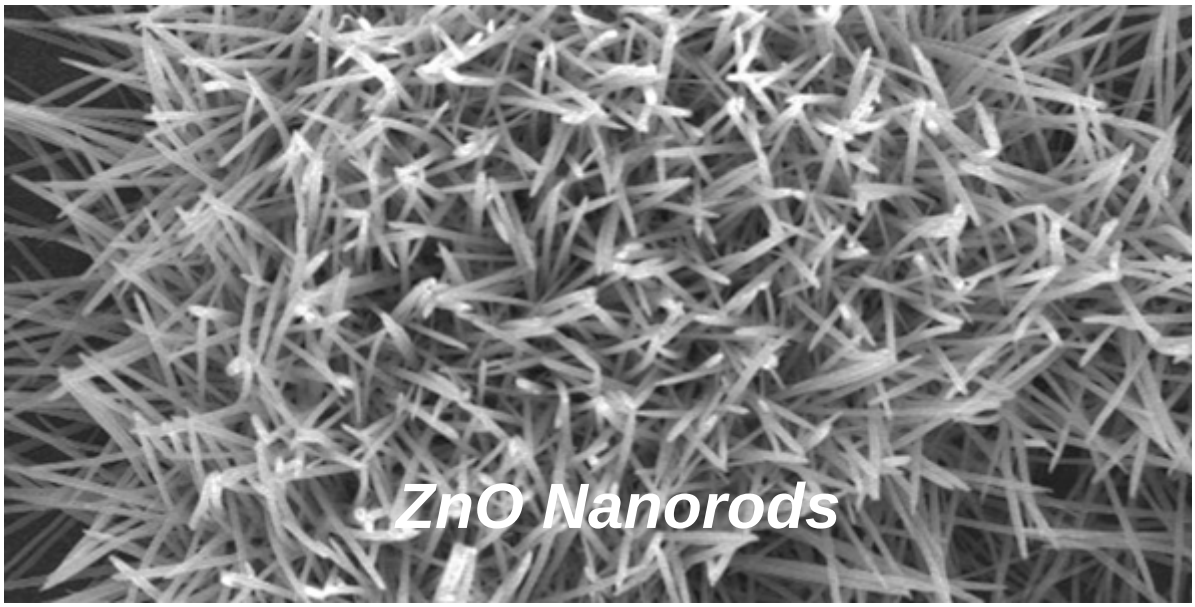

Chapter 3

A Novel Low Temperature Growth and Characterization of Single Crystal ZnO Nanorods

3.1 Introduction

One-dimensional (1 D) nanoscale materials have received considerable attention due to their remarkable properties applied in optoelectronic and electronic nanodevices [1-2]. Particularly, semiconductor nanomaterials such as GaN [3], CdS [4], Si [5] and MnO_2 [6] have been highly interested for the fundamental concepts of quantum size effect on optical, electrical and mechanical properties. Among them, ZnO notably possesses the unique properties such as wide direct-band gap (3.4 eV) and large exciton binding energy (60 meV) at room temperature, leading to a wide variety of potential applications in catalysts, gas sensors, piezoelectric devices, and solar cells[7,8]. Moreover, ZnO nanowire array is shown to have a UV laser emission in the room temperature, as has been observed by Yang et al.[9]. Generally, 1 D ZnO nanowhisker can be prepared by various methods, including using anodic alumina template [10], vapor-liquid-solid (VLS) mechanism [11], mtalorganic vapor-phase epitaxial growth (MOVPE) [12,13] and common thermal evaporation method

[14-17]. However, all of above methods always require quite extreme conditions and expensive equipments. Contrariwise, the soft chemical process provides a mild condition with a low-cost and well-controlled method to synthesize 1 D nanoscale materials. Until now, the most effective ways to fabricate 1 D ZnO nanostructures by employing soft solution process are microemulsions–growth [18], thermal decomposition reaction in solvent [19] and spray pyrolysis [20]. Although the soft chemical method can be used to grow one-dimensional ZnO nanomaterials, however, most ZnO nanorods are randomly grown in the solutions, which limit their applications in nanodevices. Recently, ZnO microrod arrays have been be produced by using soft chemical method [21], however, the preparation of small diameter nanorods (diameter < 100 nm) with controlled nano-size nucleation are still highly required. Although the well-aligned ZnO microrods can be produced in soft solution [16], the controlled nano-size nucleation and growth mechanism to obtain aligned anisotropic array are still needed. As shown in Figure 1, though the ZnO columns can be fabricated based on the method reported before [16], the product usually has a quite large size to submicron (~650 nm in diameter) scale and non-uniform size distribution (typically from 300 nm to 1 μm). Herein, we demonstrate an effective technique to directly grow single crystal ZnO nanorods on substrates with high density. Notably, we employ ZnO nanostructured (ZnO nanoparticles/ITO) substrates, as self-seeding to control ZnO nanorod growth, which not only has an attractive low temperature (ca. 90 ^{o}C) feature but also prevents from using exotic metal as catalysts. The exclusion of exotic metal catalysta is very important for fabricating reliable nanodevices based on high quality 1 D nanorods, because even very low impurity concentration of catalyst could dopant species into semiconductor nanorods and significantly affect the properties of nanodevices. In this study, the ZnO nanostructured substrate is shown to be helpful to the ZnO nanorods formation by soft solution method, and a novel two-step procedure is proposed. In the first step, uniform ZnO nanoparticle colloids were synthesized by sol-gel reaction. Second, ITO glass substrates covered with ZnO nanoparticle seeds were used to grow the nanorods from the hydrolysis-condensation of Zn^{2+} salt aqueous solution.

3.2 Experimental Section

The schematic diagram illustrating the ZnO nanorods formation processes is shown in

Figure 3-2.

3.2.1 Preparation of ~4.3 nm ZnO nanoparticle seeds

The ZnO nanoparticles used in this study were prepared by sol-gel reaction in the presence of cetyltrimethylammonium hydroxide (CTAOH) as both catalysts and surfactants. First, 0.01 M of zinc acetate [$Zn(CH_3COOH)_2 \cdot 2H_2O$] was dissolved in ethanol under vigorous stirring at 60 ^oC for 1 hour and cooled to 0 ^oC. The cetyltrimethylammonium hydroxide was then added into the solution with a molar ratio of Zn^{2+}/CTAOH=1:1.6 under constant stirring for 30 min. The mixture was then subsequently refluxed at 60 ^oC for 2 h and allowed cooling to room temperature.

3.2.2 Growth of ZnO nanorods

The ZnO nanoparticle colloids in ethanol solution were directly dipped onto ITO substrate and dried at room temperature. Prior to nanorod growth, the substrate was under the heat treatment in dry air at 300℃ for 12h (Figure 1b). Then the ZnO nanostuctured substrates were immersed in equimolar of zinc nitrate ($Zn(NO)_3 \cdot 6H_2O$) and methenamine ($C_6H_{12}N_4$) aqueous solutions at 90 ^oC for 24h (Figure 1c). The thin film was formed above the nanostructured substrate. Subsequently, the product was thoroughly washed with deionized water and allowed drying in air at room temperature.

The as-grown products were further characterized and analyzed by scanning electron microscopy (SEM) (Hitachi S-4700 FEG at 15 kV), Transmission electron microscopy (TEM) (JOEL 2000FX at 200 kV) and Philip Tecnai 20 high-resolution TEM (HRTEM) at 200 kV equipped with a GATAN digital photograph system and energy dispersion x-ray spectroscopy (EDS). The absorption spectrum was recorded on a HP8453 UV-VIS spectrometer. The Raman spectra were measured on Renishaw system 2000 micro-Raman spectrometer with a 514 Ar^+ laser as excitation source. Photoluminescence (PL) spectra were also performed at room temperature using He-Cd laser line of 325 nm. An x-ray diffraction study of the samples was carried out with MAC Sience MXP18 X-ray diffractometer（30 kV, 20 mA）with copper target at a scanning rate of 4^o/min.

3.3 Characterization

3.3.1 ZnO nanoparticles seeds

UV-vis, TEM and XRD

The UV-vis absorbance spectrum of the ZnO nanoparticle colloids is shown in Figure 3-3. The absorption spectrum shows a well-defined exciton band at 327 nm and significant blue shift relative to the bulk exciton absorption (373 nm) [22]. This shift phenomenon mainly corresponds to the confinement effect of the small size ZnO nanoparticle colloids (particle size ≤ 7 nm) [23]. According to the experimental relationship between the absorption shoulder ($\lambda_{1/2}$) and the particle size reported by Meulenkamp [24], the diameter difference of the nanopartices during aging at 60 ^{o}C can be monitored. After aging for 2h, the particles average diameter is estimated to ~3.6 nm, which consists with our TEM measurement. In the TEM image as shown in Figure 3-3, the nanoparticles are essentially monodispersed. Moreover, the nanoparticles are almost fully well separated, indicating that CTAOH surfactants efficiently cap on the particle surfaces and successfully prevent the aggregation from sol-gel reaction.

3.2.2 Characterization of the as-grown ZnO nanorods

SEM

Figure 3-4 shows the typical field emission SEM images of ZnO nanorods grown on nanostructured substrate at 90 ^{o}C aqueous solution. As observed in Figure 3.2, these images show clearly that highly density and straight nanorods can grow over through the whole surface of these substrates. Although the nanorods are not perfectly aligned on the substrate, they have a tendency to grow toward perpendicular to the substrate. The nanorods grown with 10×10^{-3}, 8.4×10^{-3} and 6.8×10^{-3} M Zn^{2+} aqueous solutions at 90 ^{o}C for 24h exhibit mean diameters about 50, 45 and 40 nm, respectively (Fig. 3–4(a-b-c). We also investigated the nanorods growth at higher concentration (17×10^{-3}, 20×10^{-3} M), the diameters of nanorods were increased to about 100 nm, implying that the diameters of nanorods are dependent on aqueous solution concentration. Meanwhile, as shown in the inset of Figure 3.4a, the ZnO nanorod has a hexagonal prismatic cross-section and hemisphere appearance at ends. In order to identify the growing site of the nanorods on the nanostructured substrate, the pure ITO substrates were used without ZnO nanoparticles at the

same experiment conditions. As approach, there is barely nanorod grown on the whole substrates, indicating that ZnO nanoparticle really play a crucial role in ZnO nanorods growth mechanism.

XRD and Raman

The crystal structure of as-grown ZnO nanorods was investigated using XRD (Figure 3-5a); the [002] reflection apparently has sharpened up comparative to the [101] maximum reflection of ZnO zincite (JCPDS 36-1451). It showed that the ZnO nanorods were grown with c-axis orientation and trend towards to substrate surface. Figure 3-5b shows Raman spectra for ITO substrate and ZnO nanorods growth on the substrate. Clearly, the ZnO nanorods have only one peak at 432 cm^{-1} corresponding to ZnO optical phonons E_2 mode [25].

TEM and EDS

In order to characterize the ZnO nanorods in advanced, TEM was employed to observe the nanorod microstructure. To prepare TEM sample, the nanorods were scraped from substrate, briefly ultrasonicated in methanol and then dispersed onto a carbon film covered copper grid. In Figure 3-6a, the bright–field TEM image shows that the nanorods are straight and have a uniform diameter. The typical diameter and length-to-diameter ratios of the nanorods are about 50 nm and 25, respectively. It is notable that the individual nanorod has a hemisphere appearance at the end in Figure 3-6a as well as in Figure 3-4a, whereas the other nanorod end is shaped like a flatness appearance. This observation suggests that the nanorods would be grown from the well-defined faceted end to the hemisphere end, which is similar to the previous reports on the single crystal ZnO whiskers [26,18]. In addition, the EDS analysis of nanorods showed the nanorods contain only Zn and O, indicating that there is no other metal impurity as catalyst (Figure 3-6c). The HRTEM lattice fringes image and selected area electron diffraction pattern (SAED) shown in Figure 3.4b reveal that in this selected area, the nanorods possess a single crystal hexagonal structure without dislocation and stacking fault. The image also confirms that the nanorods grow along the [0001] direction (indicated with an arrow).

Photoluminescence

Photoluminescence (PL) of the ZnO nanorods were measured in room temperature and the spectra were shown in Figure 3-7. In Figure 3-7a, a sharp near band-edge emission at 378 nm and a broad green emission at ~580 nm were observed. The near band-edge emission is attributed to a well-known recombination of free excitons [27], and the green emission is resulted from the recombination of photogenerated hole with a singly ionized charge state of the specific defect [28]. In addition, the heat-treatment step could cause a further decrease intensity of the green emission and increase the intensity of band-edge emission (Figure 3-7b). This result can be attributed to the decrease of the amount of the singly ionized oxygen vacancies in the ZnO and acquired high crystal quality of ZnO nanorods with increasing the heat-treatment temperature.

3.2.3 Influence parameter of growth one-dimensional ZnO

Concentration of ZnO nanoseeds

In order to realize the influence of self-seeds on the nucleation and growth mechanism of ZnO nanorods, more detailed experiments were carried out. First, the effects of various concentrations in the nanoparticles seeds precursor were investigated. It was found that the average diameter of the nanorod increase to about 70± 25 nm, and the length increase to about ~3 μm when the precursor concentration increase to about ~0.05M (Figure 3-8a). This increase could be attributed to the seeds aggregation because high concentration precursor could form bigger nanoclusters and large size seeds, subsequently favored the growth of coarser nanorods. Figure 3-8b shows the TEM image of such nanorods, indicating the nanorods were straight along the longitudinal axis.

Heat-treatment temperature of nanoseeds

Nevertheless, we also found that low heat treatment temperature for preparing the nanostructured substrate can decrease the diameter of nanorods. As shown in Figure 3-9, when the substrate temperature was heated at ~250 ^{o}C, the bundle-like aggregation of ZnO nanorods about 30 nm in diameter and length in excess of 1 μm were produced.

Notably, when the heat treatment temperature of ZnO nano-seeded substrate was stetted

about 200 ^{o}C, the morphology of ZnO nanostructures became significant high ratio of wire-like appearances. Figure 3-10 shows the low-magnification SEM pictures of the final products after the hydrolysis-condensation of Zn^{2+} salt aqueous solution on seeded substrates. As shown in Figure 3.10a and Figure 3.10b, the morphology of final products is definitely different from the original ZnO nanoparticles and looks like 1D nanowire. The average diameter of the high-density nanowire-like materials is around 30 nm and the length is up to several micrometers. Thus it is suggested that the ZnO NPs could serve as seeds at the hydrolysis-condensation process and enhance the anisotropic growth of 1D nanomaterials.

TEM

Figure 3-11 displays TEM pictures of the final products, for which the sample is prepared by scratching and dispersing the final products on copper grid. As shown in Fig. 3-11(a) and Figure 3-11(b), there are several nanowire-like materials in this micrograph. Moreover, it is found some of them have different contrast in the central part and outside part (as indicated by the arrows in this picture). This result implies that some 1D ZnO nanomaterials have hollow and tubular nanostructures. Figure 3-11(b) the HRTEM image and corresponding selected area electron diffraction (SAED) pattern (inset) of tubular ZnO nanomaterials. The thickness of the nanotubes wall is approximately 6.5 nm. The selected area electron diffraction pattern (inset) implies the ZnO nanotube is a single crystal with growth direction along [001].

Based on the above observations, ZnO nanoparticle seeds have been demonstrated to have the essential effect on ZnO nanorod formation. In the present method, the nanorod growth mechanism can not be explained by using the well-known vapor-liquid-solid growth mechanism [11], in which a liquid metal droplet is located at the growth front. As a result, a possible mechanism for the hexagonal ZnO (*h*-ZnO) crystal growth in this case was believed to be related to common crystal growth as solution chemistry. For the metal oxide (*h*-ZnO) growth, nucleation always needs to overcome higher activation energy barrier, and the interface energy between *h*-ZnO/ITO substrate is usually smaller than that of *h*-ZnO/solution. Thus the nuclei will be favored to create on the ITO substrate than in the solution. Moreover, the nanoparticles on the substrate seem to be able to further lower the

h-ZnO/substrate interface energy so the nucleation of ZnO nanorods would take place in lower saturation ratio than those without. Because the ZnO nanoparticle have the hydroxyl group on the surface as ZnO/$Zn(OH)_2$ core-shell nanostructure [29], electrostatic absorption (binding) could promote to the metal organic molecule anchored on the nanoparticles surface. Upon the hydrolysis-condensation reaction, the as-prepared ZnO nanoparticles can serve as nuclei for the directly epitaxial growth of ZnO nanorods because they have the same crystal structure and lattice parameter. Compared with other reports [11-17], it should be emphasized that the much lower growth temperature in this research is of particular significance and can be very helpful to complex advanced nanodevice integration where the conducting layer such as metal can not survive at a high temperature.

3.4 Conclusions

In summary, we have demonstrated a novel two-step procedure for preparing large-scale growth of single crystal ZnO nanorods by a soft solution method without metal catalyst. XRD, Raman, SEM, TEM and HRTEM analysis indicated that the pure single crystal ZnO nanorods have the uniform size distribution and hexagonal wurtzite structure. The low-temperature growth can be achieved due to the help of ZnO self-seeds and it offers a desirable route for large-scale ZnO nanorods growth. The room temperature PL spectra of the ZnO nanorods exhibit a strong UV emission of 378 nm and a weak green emission of 580 nm. It should be noted that the low-temperature growth process requires no expensive and precise vacuum equipment so as to permit large-scale fabrication at low cost. Furthermore, the highly optical transparency and electrical conductivity of the ITO glass substrate can provide a great application potential in future optoelectronic nanodevice.

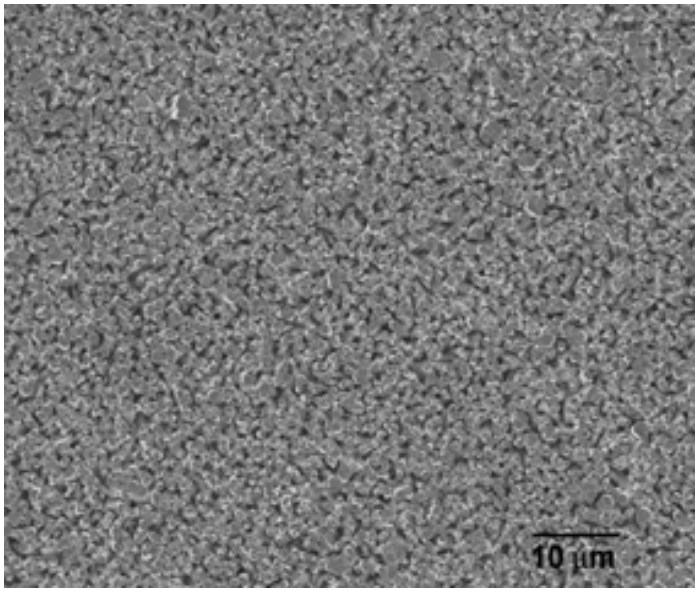

Figure 3-1 SEM image of ZnO columns synthesized based on the previously reported method. [From ref. 21]

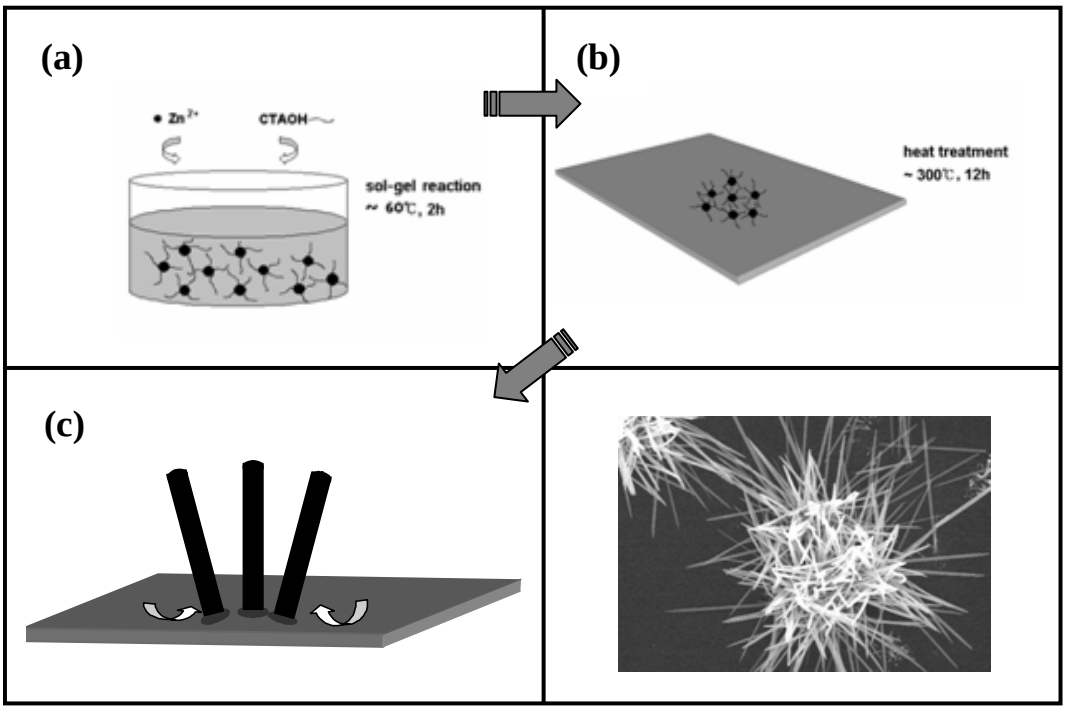

Figure 3-2 A schematic illustration for ZnO nanorod growth on nanostructured substrate by soft chemical method. (a)-(b) formation of ZnO nanoparticle colloids through sol-gel reaction and dispersion on ITO substrate; (c) the ZnO nanorods directly grow from the nanoparticles via hydrolysis-condensation process.

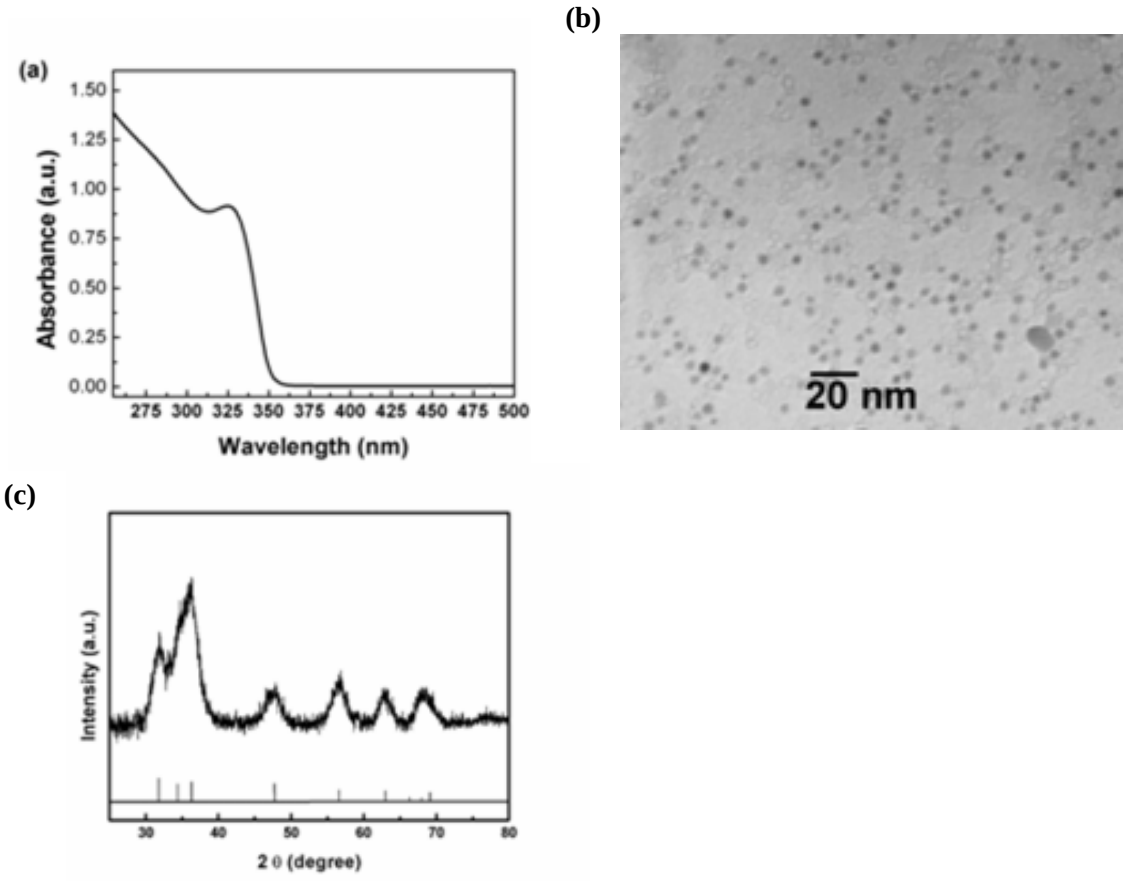

Figure 3-3 (a) Absorption spectra, (b) TEM image and (c) XRD pattern of CATOH-capped ZnO nanoparticles.

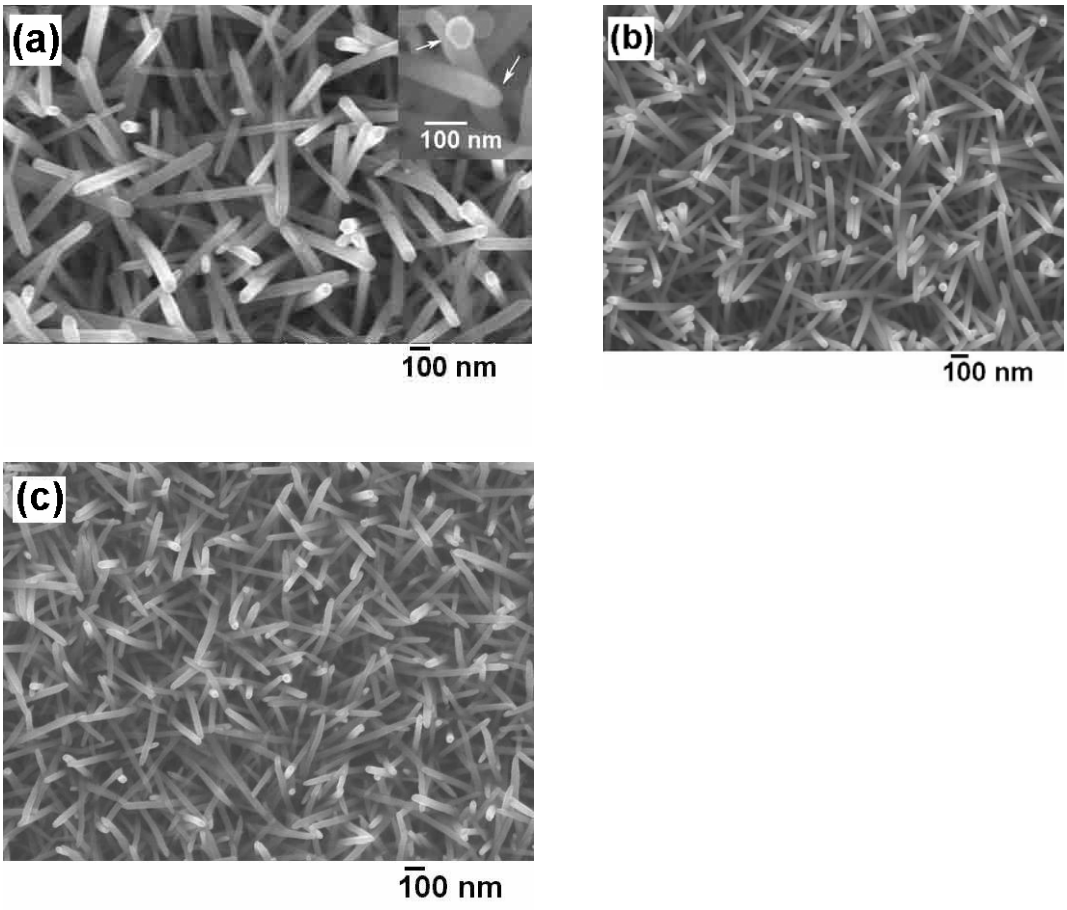

Figure 3-4 SEM image of ZnO nanorods grown in aqueous solution on the nanostructured substrates. The corresponding concentration of Zn^{2+} aqueous solutions is (a) 10×10^{-3}, (b) 8.4×10^{-3} and (c) 6.8×10^{-3} M. The inset in Fig. 3-4(a) exhibits hexagonal prismatic cross-section and a hemispherical end.

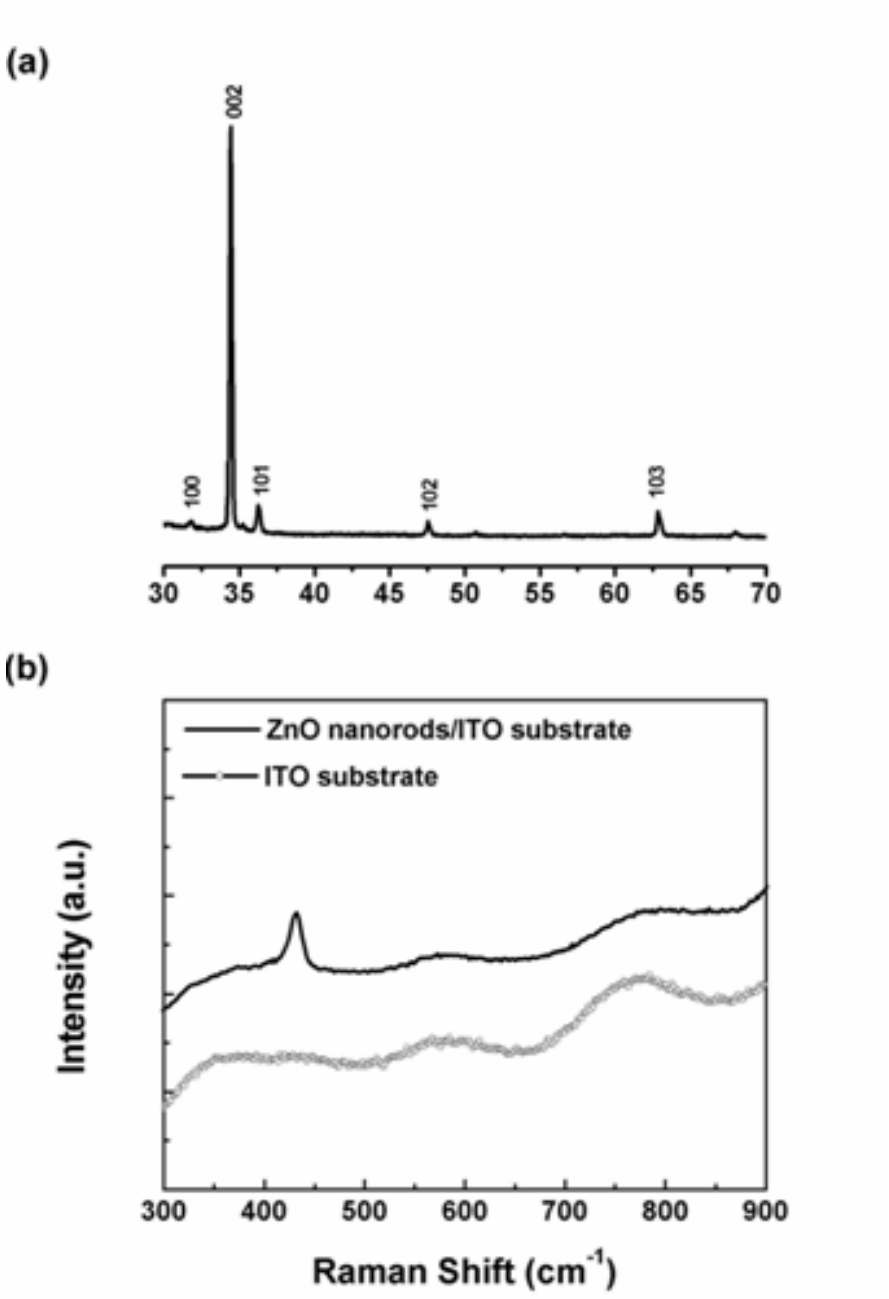

Figure 3-5 (a) XRD pattern and (b) Raman spectrum of the ZnO nanorods on ITO substrate.

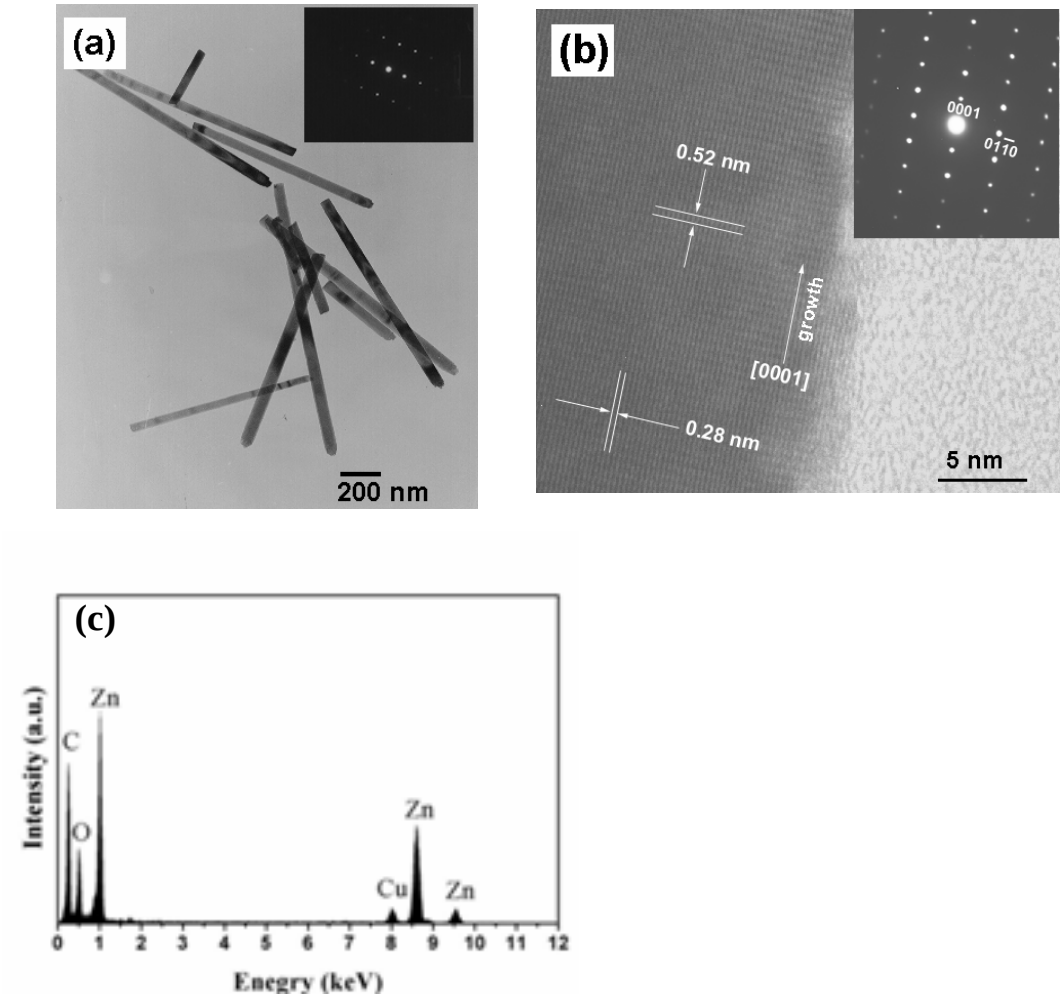

Figure 3-6 (a) TEM and select area diffraction image of single crystal ZnO nanorods grown in 10×10^{-3} M Zn^{2+} aqueous solution. The diffraction pattern shows that the nanorod grows along [0001] direction. (b) High resolution TEM image obtained from the edge of an individual nanorod and its corresponding SAED diffraction pattern (inset) (c) EDS analysis of ZnO nanorod.

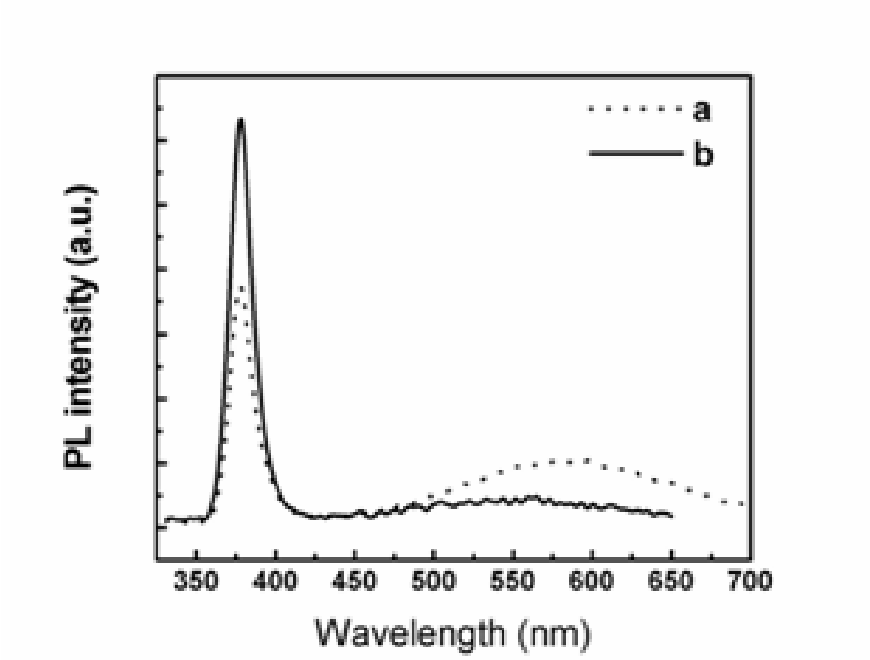

Figure 3-7 PL spectra of (a) the as-grown ZnO nanorods and (b) heat treated at 350 ^{o}C for 12 h.

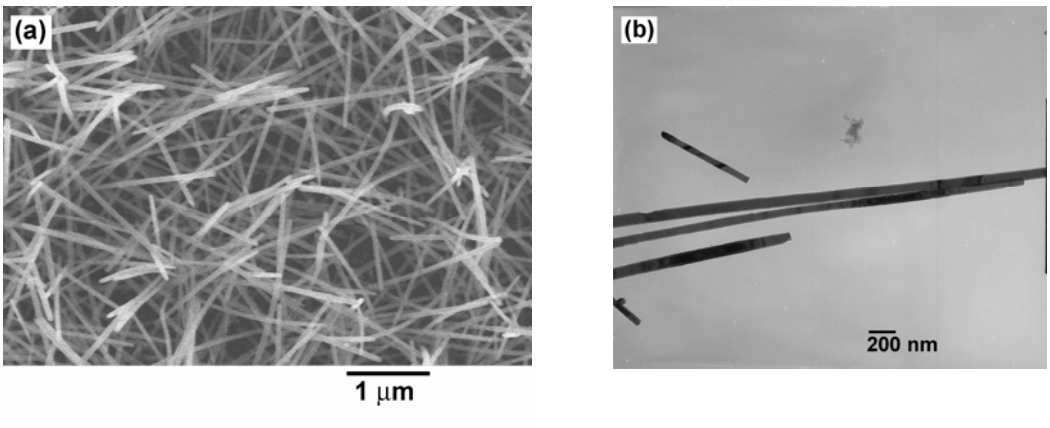

Fig. 3-8 (a) SEM and (b) TEM images of the ZnO nanorods grown under same condition but using precursor concentration of nanoparticles seeds about 0.05M.

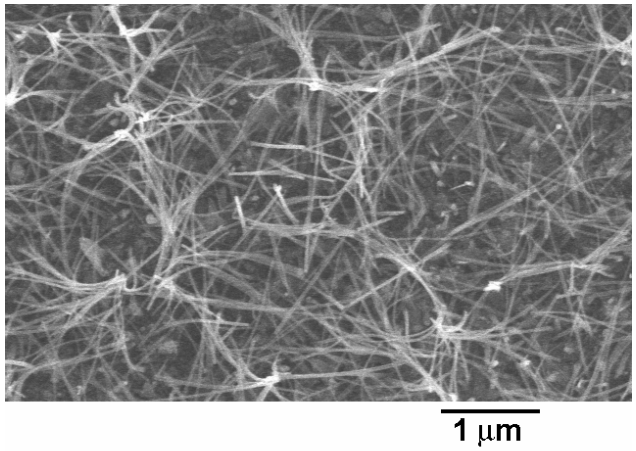

Figure 3-9 SEM image of the ZnO nanorods grown at the same condition but using the nanostructured substrate with low heat treatment temperature of ~250 ^{o}C.

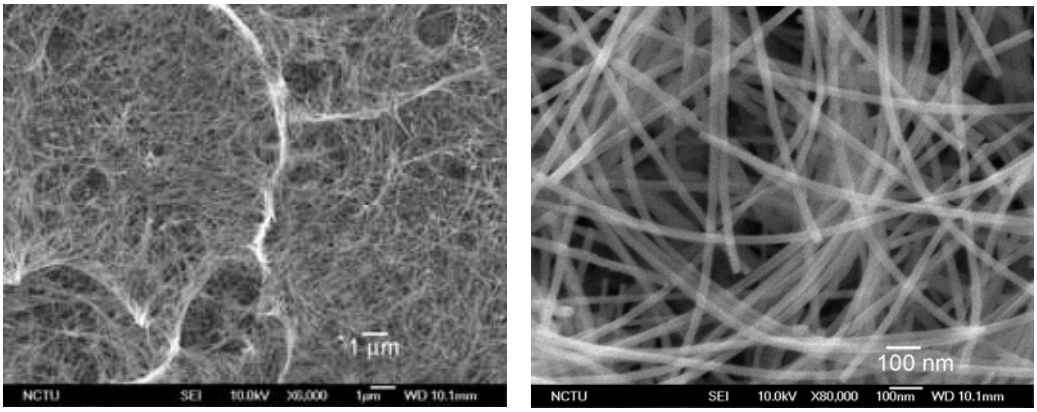

Figure 3-10 SEM image of the ZnO nanostructure grown at the same condition but using the nanostructured substrate with low heat treatment temperature of ~200 ^{o}C.

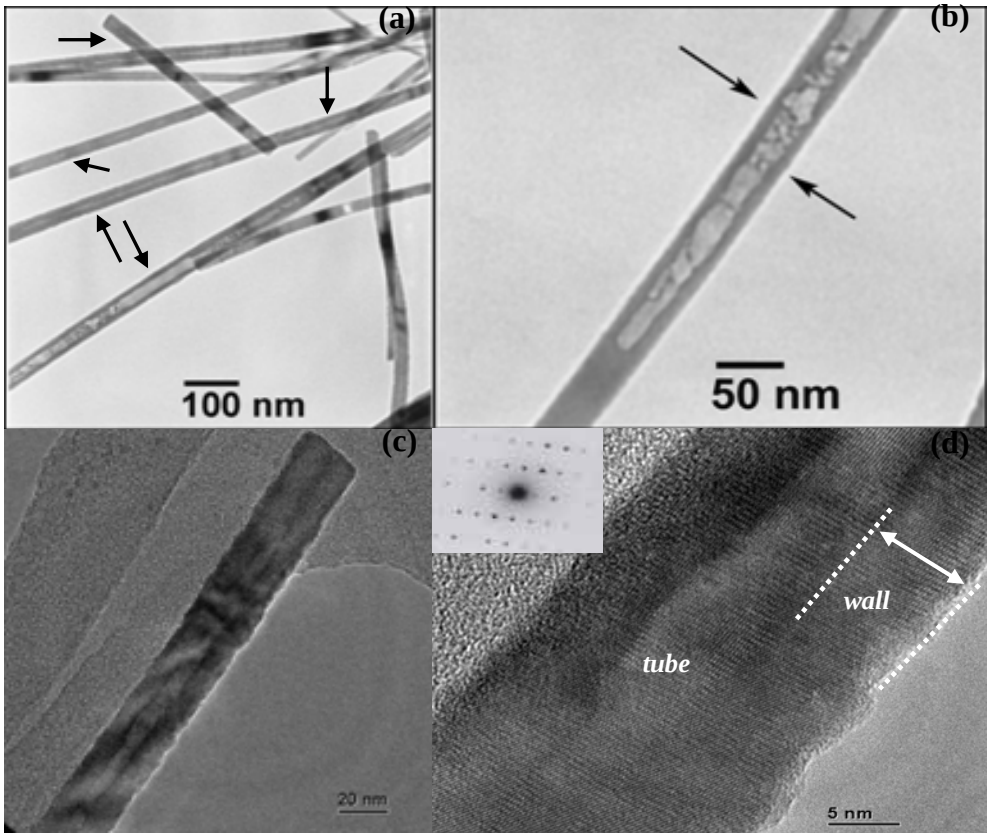

Figure 3-11 (a) A low magnification TEM image of as-synthesis ZnO nanotubes, (b,c) high magnification TEM images of a single nanotube, and (d) a HRTEM image of ZnO nanotube.

3.5 Reference

[1] Morales, A. M.; Libber, C. M. Science 279 (1998) 208.

[2] H. Dai, E. W. Wong, Y. Z. Lu, F. Shoushan, C. M. Libber, Nature 375 (1995) 769.

[3] W. Q. Ham, S. S. Fan, Q. Q. Li, Y. D. Hu, Science 277 (1997) 1287.

[4] J. H. Zhang, X. G. Yang, D. W. Wang, S. D. Li, Y. Xie, Y. N. Xia. Y. T. Qian, Adv. Mater. 12 (2000) 1348.

[5] J. H. Hu, T. W. Odom, C. M. Libber, Acc. Chem. Res. 32 (1999) 435.

[6] X. Wang, Y. Li, J. Am. Chem. Soc. 124 (2002) 2880.

[7] L. Vayssieres, K. Keis, A. Hagfeldt, S. –E. Lindquist, Chem. Mater. 13 (2001) 4386.

[8] K. Hara, T. Horiguchi, T. Kinoshita, K. Sayama, H. Sugihara, H. Arakawa, Sol. Energy Mater. Sol. Cells 64 (2000) 115.

[9] M. H. Huang, S. Mao, H. Feick, H. Yan, Y. Wu, H. Kind, E. Weber, R. Russo, P. Yang, Science 292 (2001) 1897.

[10] M. J. Zheng, L. D. Zhang, G. H. Li, W. Z. Shen, Chem. Phys. Lett. 363 (2002) 123.

[11] M. H. Haung, Y. Wu, H. Feick, N. Tran, E. Webber, P. Yang, Adv. Mater. 13 (2001) 113.

[12] J. – J. Wu, S. –C. Liu, Adv. Mater. 14 (2002) 215.

[13] W. I. Park, D. H. Kim, S. –W. Jung, G. –G. Yi, Appl. Phys. Lett. 80 (2002) 4232.

[14] B. D. Yao, Y. F. Chan, N. Wang, Appl. Phys. Lett. 81 (2002) 757.

[15] Z. W. Pan, Z. R. Dai, Z. L. Wang, Science 291 (2001) 1947.

[16] Y. C. Kong, D. P. Yu, B. Zhang, W. Fang, S. Q. Feng, Appl. Phys. Lett. 78 (2001) 407.

[17] Y. Dai, Y. Zhang, Q. K. Li, C. W. Nan, Chem. Phys. Lett. 358 (2002) 83.

[18] L. Guo, Y. L. Ji, H. Xu, P. Simon, Z. Wu, J. Am. Chem. Soc. 124 (2002) 14864.

[19] J. Zhang, L. D. Sun, C. S. Liao, C. H. Yan, Chem. Commun. (2002) 262.

[20] O. Milosevic, D. Uskokovic, Mater. Sci. Eng. A A168 (1993) 249.

[21] L. Vassieres, K. Keis, S. –E. Lindquist, A. Hagfeldt, J. Phys. Chem. B 105 (2001) 3350.

[22] M. Haase, H. Weller, A. Henglein, J. Phys. Chem. 92 (1988) 482.

[23] U. Koch, A. Fojtik, H. Weller, A. Henglein, Chem. Phys. Lett. 122 (1985) 507.

[24] E. A. Meulenkamp, J. Phys. Chem. B 102 (1998) 5566.

[25] X. L. Xu, S. P. Lau, J. S. Chen, G. Y. Chen, B. K. Tay, J. Cryst. Growth 223 (2001) 201.

[26] J. Q. Hu, Q. Li, N. B. Wong, C. S. Lee, S. T. Lee, Chem. Mater. 14 (2002) 1216.

[27] D. M. Bagnall, Y. F. Chen, Z. Zhu, T. Yao, M. Y. Shen, T. Goto, Appl. Phys. Lett. 73 (1998) 1038.

[28] K. Vanheusden, W. L. Warren, C. H. Seager, D. R. Tallant, J. A. Voigt, B. E. Gnade, J. Appl. Phys. 79 (1996) 7983.

[29] H. Zhou, H. Alves, D. M. Hofmann, W. Kriegseis, B. K. Meyer, G. Kaczmarzyk, A. Hoffmann, Appl. Phys. Lett. 80 (2002) 210.

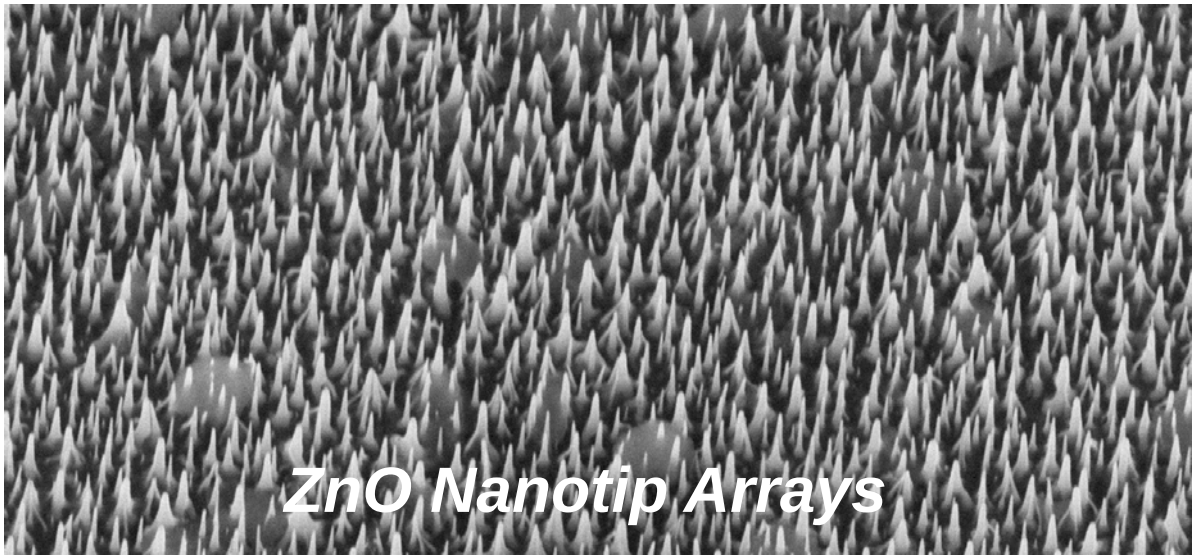

Chapter 4

Low-temperature Solution Approach Toward Highly Aligned ZnO Nanotip Arrays

4.1 Introduction

Owing to the unique geometries of small radii of curvature, the nanotips have attracted significant interests for the potential applications such as the probing tip for the high resolution imaging atomic force microscopy [1], the photonic crystal for waveguide and the field emitter for flat-plane displays [2]. For the field emitter arrays technologies, the manipulation of high density, vertical aligned and well-ordered fine tips are particularly desirable. Currently, developing high-performance field emitter mainly relies on materials with low work function and thermal stability under the high vacuum environment, such as carbon-based (carbon nanotubes, diamond-like carbon) [3], silicon-based (Si, SiN, SiCN) [4], oxide-based (MoO_2, MoO_3, ZnO) [5,6], and others semiconductor materials [7]. Among these materials, zinc oxide (ZnO) is a wide band-gap (3.4 eV) and large exciton binding energy (60 meV) semiconductor compound, which is useful for light emitting diodes, room temperature nanolasers, gas sensors, piezoelectric devices, and solar cells [8], etc.

Recently, one dimensional (1D) ZnO nanostrustures, such as nanowires, nanotubes and nanorods, have attracted great attentions due to the excellent physical and chemical properties that are highly different from the bulk materials. These properties are changed by quantum effects.

Generally, 1D ZnO nanostructures are synthesized by the following methods: anodic alumina template(AAO) [9], metal catalyst-assisted vapor phase transport (MCVPT) [10], metal-organic chemical vapor deposition (MOCVD) [11], metal-organic vapor epitaxy (MOVPE) [12] and common thermal evaporation method [13]. Much efforts have been devoted to obtain highly aligned and well-separated (i.e. isolated standing) 1D ZnO arrays, which are crucial for developing the next generation of nanoscale electronic and optoelectronic devices. Such perfectly aligned ZnO nanowire arrays are achieved via MCVPT or MOVPE techniques [8,10,14]. Huang et al. demonstrated the aligned ZnO nanowire arrays epitaxially grown on (0001) sapphire substrate by using MCVPT technique with the gold catalyst at 900–925 ^{o}C [8]. However, the necessary of relative high temperature and expensive sapphire substrates restrict the production and wide applications of 1D ZnO arrays. In addition, the MCVPT technique is not suitable for growing sharp tips since the metal catalyst droplets would form at the terminating growth front. Notably, the soft chemical route greatly facilitates the approach to scaled-up fabricated 1D ZnO nanostructures with relative low-cost, which also has been demonstrated to be very efficient in synthesizing single crystal structure at a remarkably low temperature [15]. Vayssieres et al. reported the aligned ZnO microsize rod arrays growing on conducting tin oxide glass by hydrothermal procedure at 95 ^{o}C aqueous solution [16]. Liu et al. utilized the well-defined (001) facet microrods as the substrates to grow helical structures of ZnO nanorod and column arrays [17]. Recently, we proposed the using of a layer of nanoparticles with self-seeding assistance to attain ZnO nanorods on ITO substrate [18]. However, the polycrystalline nano-seeds on the substrate generated the random orientations of our nanorods, so the nanorod alignment was unsatisfied. To date, fabricating perfectly aligned and well-isolated 1D ZnO nanoarrays on the Si substrates with soft chemical method is a valuable challenge, which would benefit in the electronic device integrations due to the mild growth conditions. To our knowledge, growing well-aligned ZnO nanotip (nanoneedle) arrays on Si substrate rarely succeeded except using the MOCVD-based method at temperature 400–500 ^{o}C [19,20].

In the chapter 4, we grew vertical and isolated single-crystal ZnO nanotip arrays on a ZnO thin film by soft chemical technique at a low temperature 95 ^{o}C without any metal catalyst or template. The field emission (FE) of our ZnO nanotip arrays shows a turn-on field of 10.8 V/μm at a current density of 0.1 μA/cm^{-1}. Moreover, we also successfully fabricated the self-oriented nanotip arrays on ZnO microrod by soft chemical route. This fascinating morphology suggested that our new strategy might provide an insight for building a controllable well-ordered multiple nanostructures at a significant low temperature.

4.2 Experimental Section

All the chemicals from Tokyo Chemical Industry were used as received without further purification. ZnO nanotip arrays growth was prepared by the wet chemical technique, as reported by Vayssieres et al [16]. In this study, 0.1 g of zinc nitrate ($Zn(NO)_3 \cdot 6H_2O$, 3×10^{-3} M) and 0.1 g of methenamine ($C_6H_{12}N_4$, 6×10^{-3} M) were dissolved in 100 ml aqueous solution as the precursor solution. Prior to growing ZnO nanotips, a thin ZnO layer (ca. 200 nm) was deposited on the Si substrate by radio frequency sputtering. The substrate was then put into a bottle filled with precursor aqueous solution in the oven at 95 ^{o}C for several hours. After the crystal growth, the final products were rinsed with distilled water several times, and then dried in oven at 100 ^{o}C for 4h. The morphology of as-synthesis products was further characterized and analyzed by scanning electron microscopy (SEM) (JOEL JSM-6500F at 10 kV) and high-resolution transmission electron microscopy (HR-TEM) (JOEL 2010F at 200 kV). Photoluminescence spectrum was also measured at room temperature using He-Cd laser with a wavelength 325 nm as excitation source.

4.3 Result and Discussion

SEM and TEM

The surface morphology of as-grown ZnO nanotip arrays on the ZnO film substrate was studied by the field-emission scanning electron microscope (FE-SEM). Figure 4-1a and Figure 4-1b show the top and tilted views of low-magnification SEM images. The numerous nanotips appear as bright dots and are well-separated across the entire substrate, implying that a large density of ZnO nanotips preferentially grew normally to the substrate

surface, and almost isolated from each other with a density of approximately 1.22×10^{10} tips/cm^2. The higher-magnification image (Fig. 4-1c) further shows the formation of a regular nanotip arrays with a perfectly vertical alignment. The nanotips are found to grow from the tops of nano-grained film and the spacing between well-oriented nanotips estimates about 100 nm. The detail morphology can be observed by high magnification side-view image, as shown in Figure 4-1d. The nanotips are parallel to each other and perpendicular to ZnO thin film. The base diameter of a nanotip is around 70 nm and the length is around 410 nm. The length could be further controlled by changing the growth parameters, such as reaction times. Typically, the length of a nanotip decreases to ~160 nm in 95 ^{o}C aqueous solution for 2 hours growth. In contrast to the hemispherical end and hexagonal-shaped structure of ZnO nanorod grown by hydrothermal techniques reported previously [16,18,21,22], the feature of ZnO nanotips in this study obviously has a sharp apex and conical morphology. The structural characterization of the ZnO nanotips was investigated by transmission electron microscopy (TEM) and the typical TEM image of an individual nanotip is depicted in Figure 4-1e. The nanotip end clearly has an extremely sharp morphology with an apex angle about 13^{o}. The high-resolution TEM image (HRTEM) in Figure 4-1f shows a single crystal structure of the ZnO nanotip. The lattice spacing of about 0.26 nm between adjacent lattice planes corresponds to the distance between (002) crystal planes, meaning that the [001] direction is a common growth direction of the ZnO nanotip. Energy dispersive X-ray spectroscopy (EDX) analysis shows the nanotips only contain Zn and O, confirming that no other metal impurity exists.

To study the effect of concentration and reaction time on growth of nanotips, the low concentration precursor (3×10^{-4} M) and longer reaction time (24 hours) were investigated. It reveals that the nanotips arrays have a lower density (Figure 4-2) on the ZnO film substrate in lower concentration solution. Figurer 4-3 shows the ZnO nanotip arrays grown on the ZnO film using higher reaction time (24 hours) at 95 ^{o}C aqueous solution. Obviously, the ZnO nanotip arrays have a bundling together structure grown on the ZnO thin film.

XRD

The crystal structure of ZnO nanotips was investigated by X-ray diffraction. As shown in Figure 4-4, only two diffraction peaks of (002) and (004) of wurtzite ZnO were observed, implying that the (002) planes of ZnO nanotips were perfectly oriented perpendicularly to the surface.

Photoluminescence

Photoluminescence spectrum (PL) of ZnO nanotip arrays was measured at room temperature using a He-Cd laser with an excitation wavelength of 325 nm. The PL spectrum in Figure 4-5 exhibits a strong UV emission at 378 nm (3.29 eV), agreeing well with the band gap of bulk ZnO (~380 nm) which comes from recombination of free excitons via exciton-exciton collision process [23]. Generally, a green-yellow emission could be observed in the PL spectrum, which comes from the recombination of photo-generated hole with a singly ionized charge state of specific defect [24]. However, the green-yellow emission was not appeared in our sample. Therefore, the results of PL spectrum show that our low temperature growth method can produce a low concentration of oxygen defects and high optical quality of singe crystal ZnO nanotips.

Growth mechanism

The growth mechanism of ZnO nanotip arrays on a substrate described here could be based on conventional crystal growth model of solution chemistry [16]. Accordingly, the crystal nucleation and growth in the solutions are controlled by interface free energy. In present work, the column-like (002) ZnO thin film was deposited on the Si substrate as a self-seeding and buffer layer prior to the crystal growth. Note that no any ZnO nanotip was formed on the bare Si substrate under the same growth conditions. Certainly, the ZnO film in our work can effectively provide nuclei sites and reduce interface energy barrier for ZnO crystal growth. Upon the hydrolysis-condensation reaction, the reactant [$Zn(OH)^{+}$] diffused onto the ZnO film surface and gradually formed a saturating situation between ZnO film/solution interface. As soon as reaching a critical saturation point, the nuclei of ZnO crystals simultaneously occurred on the column-like (002) ZnO film, then the ZnO crystals began to precipitate and resulted in a preferential orientation along ZnO [001] by directly homoepitaxial growth. The nano-grained {002} ZnO film provided perfectly well-separated and oriented nuclei for ZnO crystals growth, as demonstrated from HRTEM images

(Figure 4-6), producing a well-ordered and vertically aligned nanotip arrays on the substrate. Moreover, the concentration gradient of reactant created a driving force for further crystal growth. According to "the lowest energy" argument on polar crystal growth by Laudise's et al. [25], the growth velocity along <001> direction could be much higher than that along <101> and <100> directions. In fact, it is well-known that the crystal facets with a faster growth velocity are easier to disappear and eventually result in the appearance of the crystal only built up by slower growth rate facets. Recently, Park and co-works [19] also proposed that sharp-tipped ZnO nanoneedle formation could originate from a higher growth rate along c-axis direction than that along the in plane direction. We therefore conclude that the tips-like ZnO geometry mainly resulted from higher growth rate along <001> direction.

Nanostructures of ZnO

We found that the nanotip arrays can also be grown on ZnO microrods by similar low temperature technique which formed a "nanotips-rod" geometry. Prior to achieving desired nanostructures, the micro-size ZnO rods were deposited onto ITO substrate by equimolar (0.1 M) of zinc nitrate and methenamine aqueous solution at 90 ^{o}C for 24h. When the (001) facets of microrods served as nuclei sites, the ZnO nanotip arrays dispersively self-oriented along the well-defined hexagonal facet (001) plane with a density of about 200 tips/rod, as shown in Figure 4-7a. Comparing with the previous report of growing 1D ZnO on microrod-based substrates [17] which formed a much lower density (< 20 nanorods/rod) of helical-like ZnO nanorods, our method should base on different growth mechanism. Figure 4-7b is a higher-magnification SEM image taken from the top of a microrod. Obviously, the ZnO nanotips are precisely grown perpendicular to the (001) surface of the microrod, where these nanotips show a conical shaped cross-section and around 250 nm in length, with the base diameter of 60 nm and tip diameter less than 15 nm. The typical bright-field, dark-field images and the corresponding electron diffraction pattern of the ZnO nanostructures captured in side-view are also depicted in Figure 4-7(c-e), respectively. The results indicate that the homoepitaxial orientation growth of the nanotip arrays only occurred on the hexagonal basal plane of the microrod. Moreover, we also have successfully obtained some interesting architectures of ZnO nanostructures, including nanopaintbrushs (Figs. 4-8a) and nanopencils (Figure 4-8b). Figure 4-8a is the ZnO nanotip arrays grown on (001) microds under longer growth time while the precursor concentration does not vary,

there are many cluster-like nanowires grown from the ends of the rods resembles to the paintbrush structures, as we named nanopaintbrush, which typical consist of several microds base and connected with bundle-like of ZnO nanowires. In addition, the nanorods was also used to service as nucleation site, as shown in Figure 4-8b, apparently a nanotip with sharply ends epitaxially grow out of entire rods of (001) plane, showing the "pencil-like" nanostructures.

Field emission

The field emission measurement of ZnO nanotip arrays was carried out in a vacuum under a pressure of ~10^{-6} torr at room temperature (see Figure 4-9). A cylinder electrode of 2.2 mm diameter was placed above the nanotips top surface with a distance of 50 μm. Keithley 237 was employed as a power supply and a current meter. Figure 4-10a shows the typical result of the field emission current density versus the applied electric field. The turn-on electric field for the ZnO nanotips was about 10.8 V/μm at a current density of 0.1 μA/cm^{-1}, and the emission current density reached about 1 mA/cm^2 at a bias field of 19.5 V/μm. The field emission current-voltage characteristics can be expressed by Fowler-Nordheim (F-N) theory:

$$J = (AE^2\beta^2/\Phi)\exp(-B\,\Phi^{3/2}/\beta E)$$

Where

J is the emission current density (A/cm^2), E is the applied field (V/cm), β is the field enhancement factor related to the emitter geometry, Φ is the work function of the emitter, A and B are the constants with values of 1.56×10^{-10} (A V^{-2} eV) and 6.83×10^{9} (V $eV^{-3/2}$ μm^{-1}), respectively. By plotting $\ln(J/E^2)$ versus $1/E$ in Figure 4-10b, two-stages slope behaviors were observed in a measured range. Such characteristics are also perceived in many other types of field emitters [26], which may result from the variation of the tips local field. The β values are derived from fitting the experiment curve to F-N theory by assuming the ZnO nanotips work function of 5.4 eV. Therefore, the field enhancement factor of ZnO nanotip arrays was estimated to be about 590 for β_1 and 270 for β_2. These values are comparable to the reports of needle-like ZnO nanowires [27,28], indicating that the mild method for manufacturing ZnO nanotips arrays would have a great potential in field emitter technologies.

4.4 Conclusions

We have successfully produced uniformly well-separated ZnO nanotip arrays which are excellent oriented and vertically aligned on the ZnO film using a soft chemical route under simple and mild conditions. The soft growing method also has been extended to synthesize well-aligned nanotip arrays on ZnO microrods. The field-emission characteristics of ZnO nanotip arrays showed a turn-on field of about 10.8 V/μm at a current density of 0.1 $\mu A/cm^{-1}$. This advanced technique for ZnO nanotip array fabrication is believed to open novel possibilities for nanoscale optoelectronic device applications.

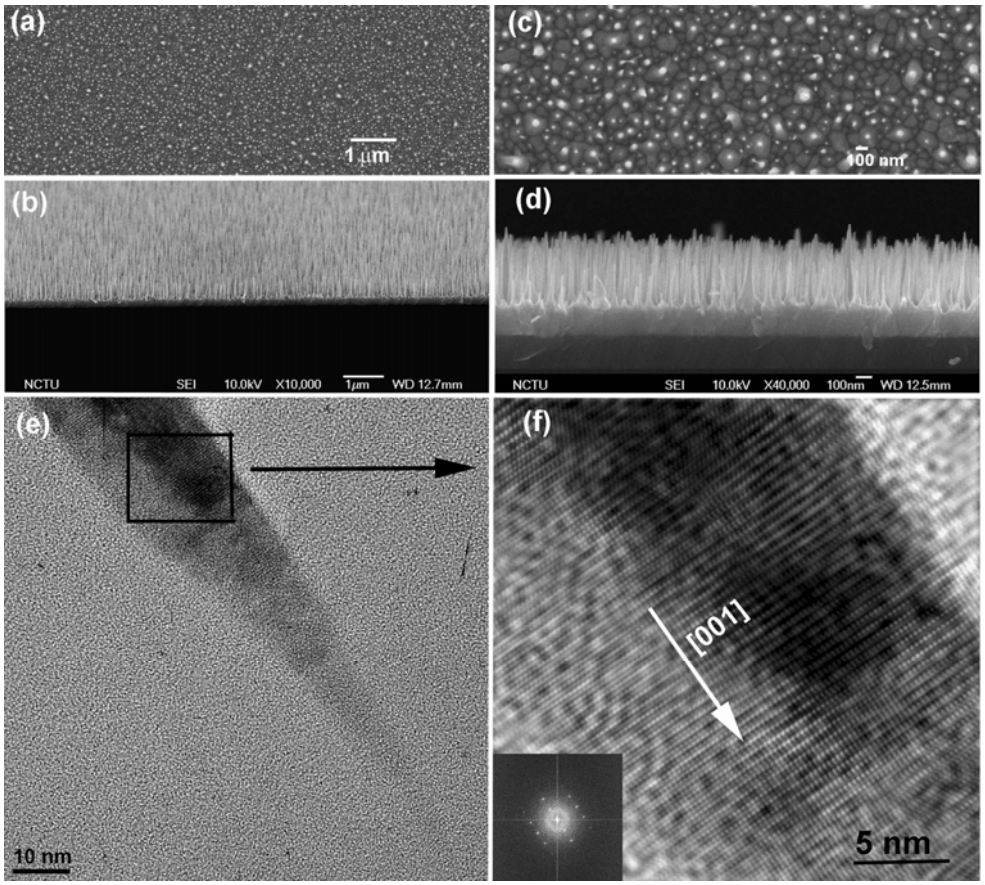

Figure 4-1 SEM images show highly aligned ZnO nanotip arrays grown on the ZnO thin film at 95 ^{o}C aqueous solution for 6 hours. Low-magnification images from (a) top view and (b) tilt view reveal that high density of well-oriented ZnO nanotips were dispersively distributed on the substrate. (c) Top and (d) side view of high-magnification SEM images. (e) TEM image of a typical ZnO nanotip. (f) High-resolution TEM image taken from the edge of ZnO nanotips and the corresponding fast Fourier-transform pattern (inset).

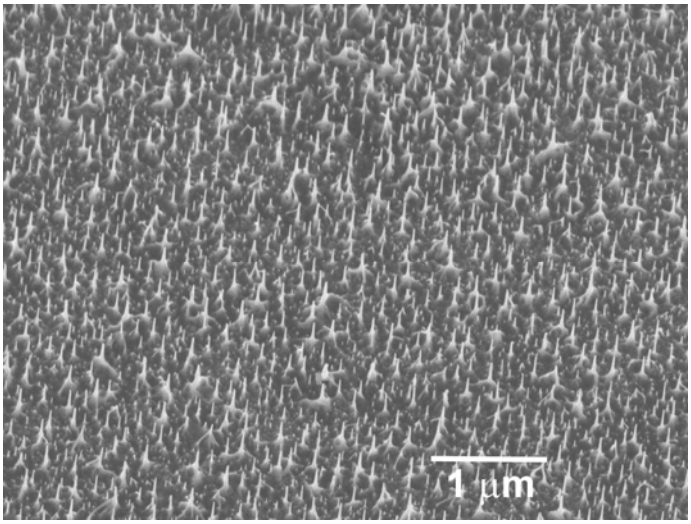

Figure 4-2 Low density ZnO nanotip arrays grown on thin film with low concentration of 3×10^{-4} M Zn^{2+}aqueous solution.

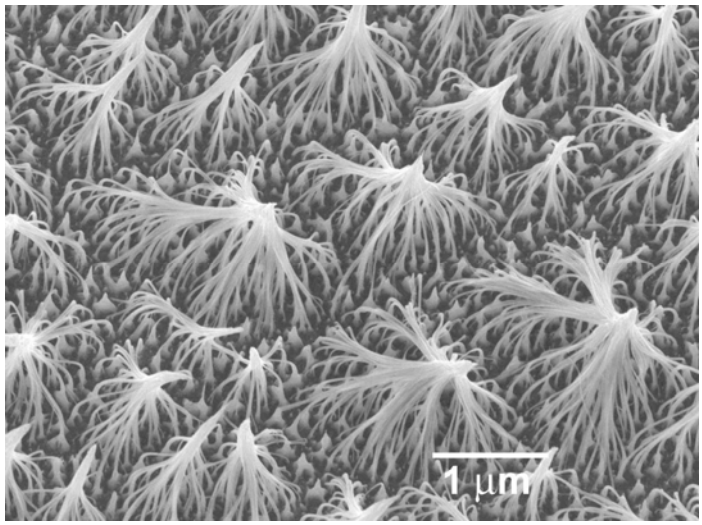

Figure 4-3 SEM image showing the nanotips bundling together grown on the ZnO thin film at 95 ^{o}C aqueous solution for 24 hours.

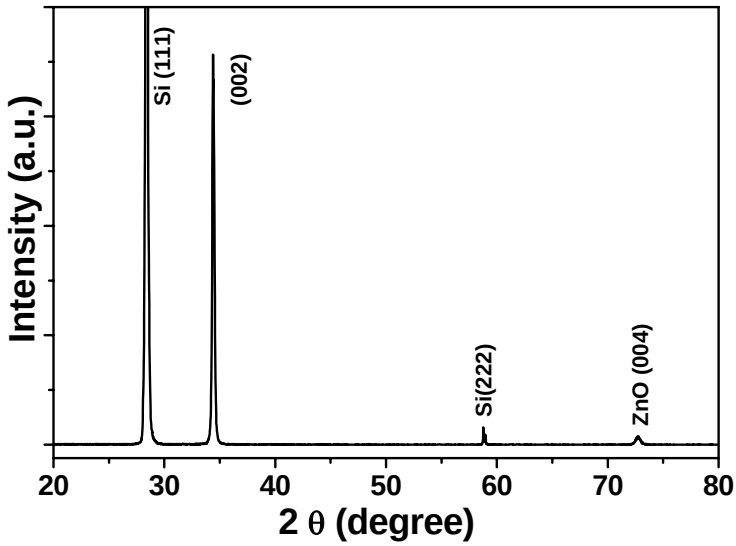

Figure 4-4 X-ray diffraction pattern of ZnO nanotip arrays grown on the ZnO film.

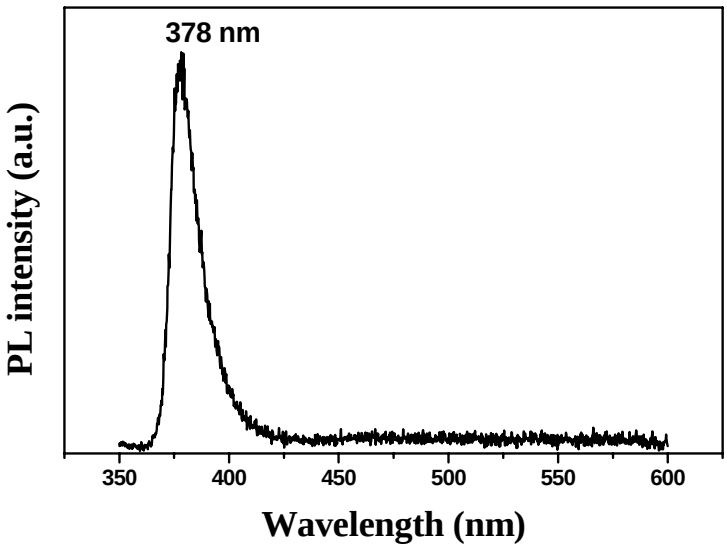

Figure 4-5 PL spectrum of ZnO nanotip arrays measured at room temperature.

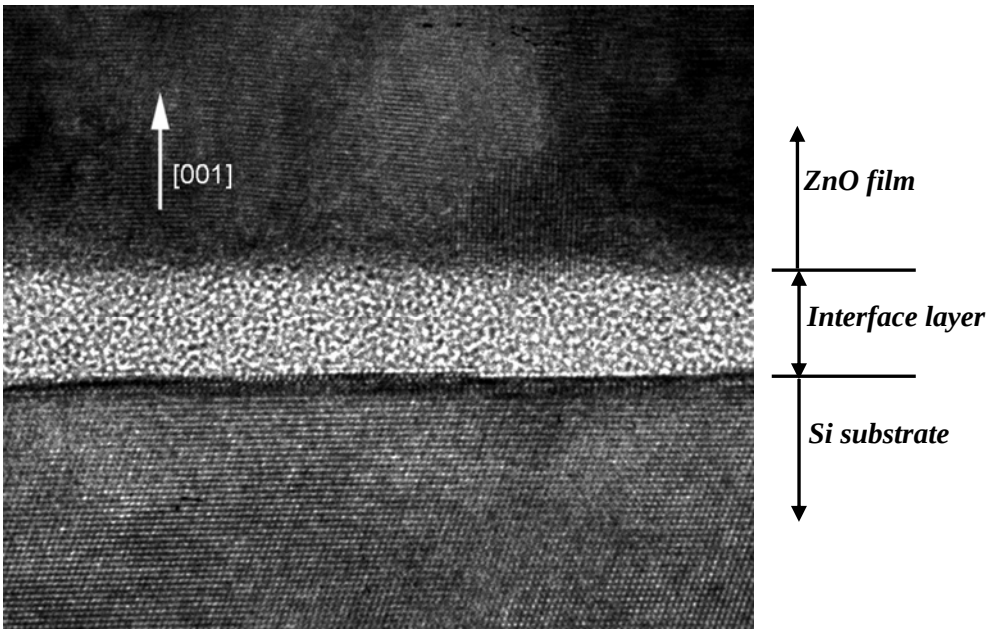

Figure 4-6 High resolution TEM cross-section micrograph of the interface region.

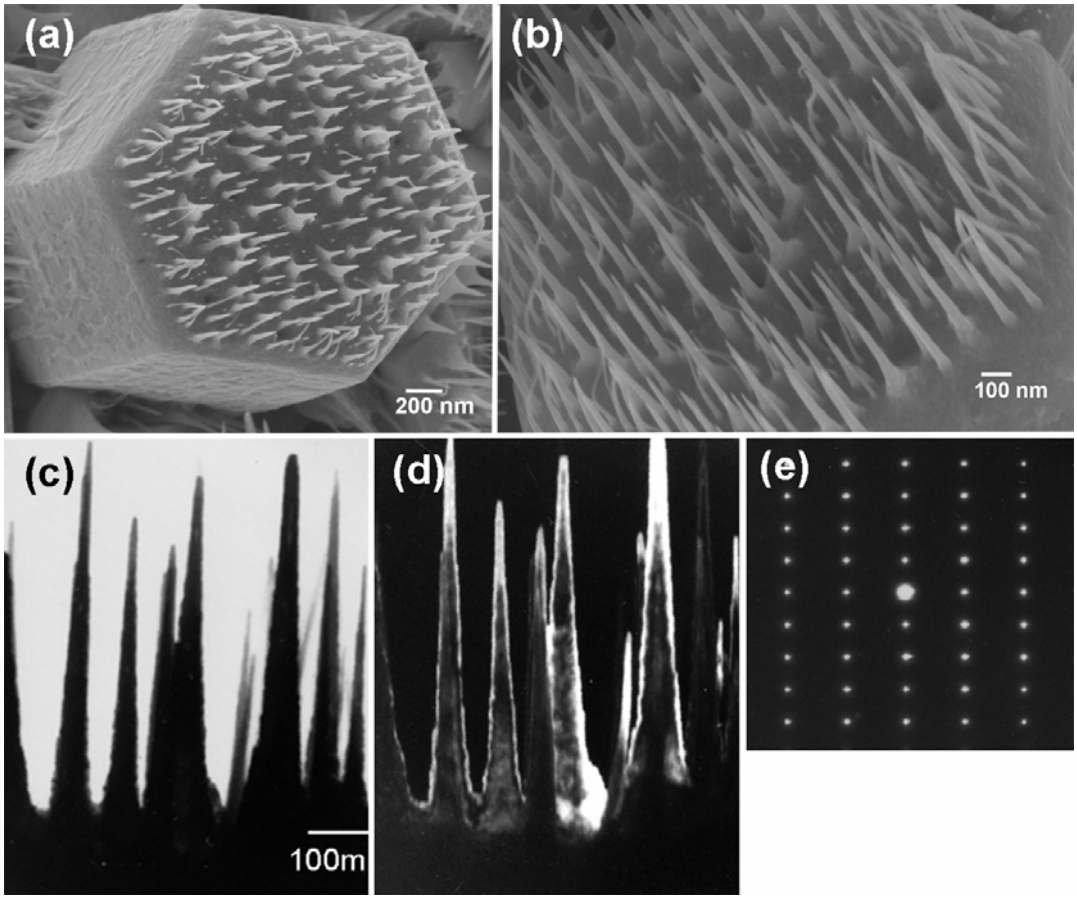

Figure 4-7. (a,b) SEM images show the as-grown ZnO nanotip arrays self-organized on the ZnO microrod. (c) Bright-field and (d) dark-field TEM images from the nanotips-microrod junction region and (e) the corresponding diffraction pattern of microrod.

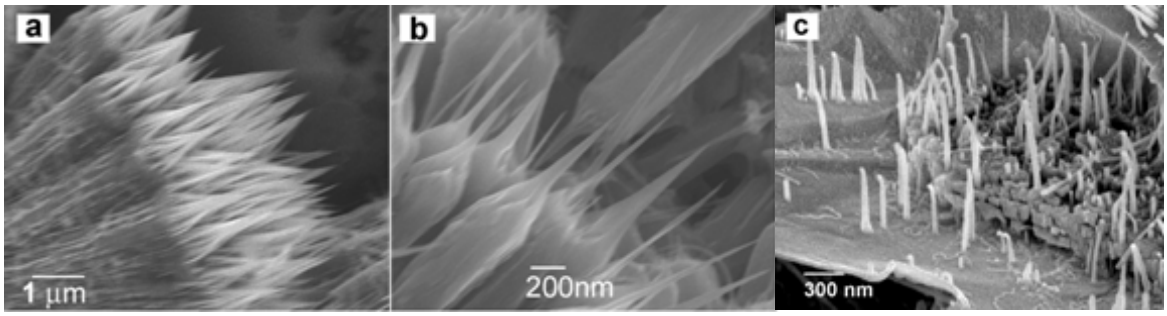

EM images showing novel geometric structures of ZnO (a) nanopaintbrushs

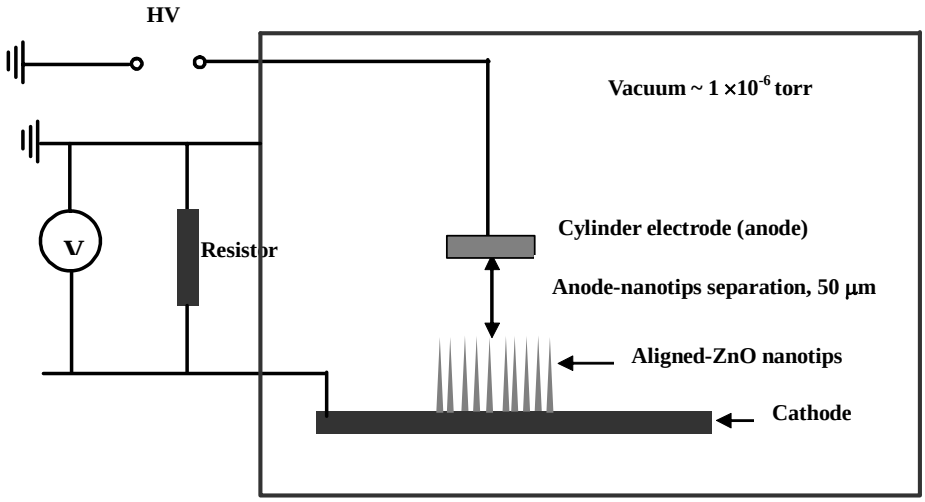

Figure 4-9 Schematic diagram of experiment setup to study field-emission properties of ZnO nanotips arrays.

Chapter 4 ZnO Nanotip Arrays: *Figure section*

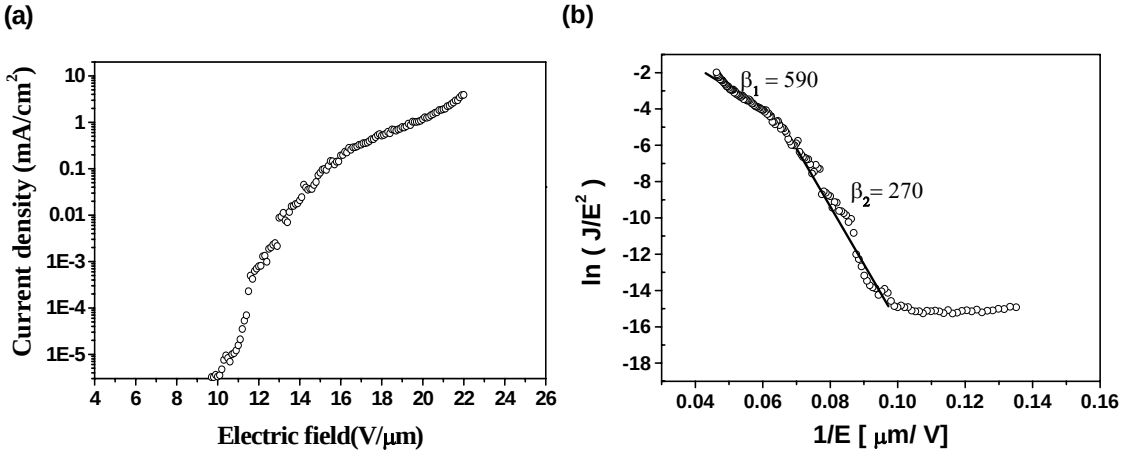

Figure 4-10 (a) Field emission current density vs electric field of ZnO nanotip arrays on Si substrate and (b) the corresponding F-N plot.

4.5 Reference

[1] A. Rothschild, S. R. Cohen, R. Tenne, Appl. Phys. Lett. 75 (1999) 4025.

[2] V. V. Poborchii, T. Tada, T. Kanayama, Appl. Phys. Lett. 75 (1999) 3276.

[3] J. I. Sohn, S. Lee, Y. H. Song, S. Y. Choi, K. I. Cho, K. S. Nam, Appl. Phys. Lett. 78 (2001) 901.

[4] H. C. Lo, D. Das, J. S. Whang, C. H. Hsu, C. F. Chen, L. C. Chen, K. H. Chen, Appl. Phys. Lett. 83 (2003) 1420.

[5] C. J. Lee, T. J. Lee, S. C. Lyu, Y. Zhang, H, Ruh, H. J. Lee, Appl. Phys. Lett. 81 (2002) 3648.

[6] J. Zhou, N. –S. Xu, S. –Z. Deng, J. Chen, J. –C. She, Z. –L. Wang, Adv. Mater. 15 (2003) 1835.

[7] J. Chen, S. Z. Deng, N. S. Xu, S. H. Whang, X. G. Wen, S. H. Yang, C. L. Yang, J. N. Wang, W. K. Ge, Appl. Phys. Lett. 80 (2002) 3620.

[8] M. H. Huang, S. Mao, H. Feick, H. Yan, Y. Wu, H. Kind, E. Weber, R. Russo, P. Yang, Science 292 (2001) 1897.

[9] M. J. Zheng, L. D. Zhang, G. H. Li, W. Z. Shen, Chem. Phys. Lett. 363(2002) 123.

[10] H. T. Ng, J. Li, M. K. Smith, P. Nguyen, A, Cassell, J. Han, M. Meyyanppan, Science 300 (2003) 1249.

[11] J. –J. Wu, S. –C. Liu, Adv. Mater. 14 (2002) 215.

[12] K. Ogata, K. Maejima, Sz. Fujita, Sg. Fujita. J. Cryst. Growth 248 (2003) 25.

[13] Z. R. Dai, Z. W. Pan, Z. L. Wang, Adv. Funct. Mater. 13 (2003) 9.

[14] W. I. Park, G. –C. Yi, M. Kim, S. J. Pennycook, Adv. Mater. 15 (2003) 526.

[15] L. Guo, Y. L. Ji, H. Xu, P. Simon, Z. Wu, J. Am. Chem. Soc. 124 (2002) 14864.

[16] L. Vassieres, K. Keis, S. –E. Lindquist, A. Hagfeldt, J. Phys. Chem. B 105 (2001) 3350.

[17] Z. R. Tian, J. A. Voigt, B. Mckenzie, M. J. Mcdermott, J. Liu, J. Am. Chem. Soc. 124 (2002) 12954.

[18] C. –H. Hung, W. –T. Whang, Materials Chemistry and Physics 82(2003) 705.

[19] W. I. Park, G. Yi, M. Kim, S. L. Pennycook. Adv. Mater. 14 (2002) 1841.

[20] S. Muthukumar, H. Sheng, J. Zhong, Z. Zhang, N. W. Emanaetoglu, Y. Lu, IEEE Trans. Nanotechnol. 2 (2003) 50.

[21] L. Vassieres, Adv. Mater. 15 (2003) 464.

[22] K. Govender, D, S. Bolye, P. O'Brien, D. Binks, D. West, D. Coleman, Adv. Mater. 14 (2002) 1221.

[23] K. Vanhausden, W. L. Warren, C. H. Seager, D. R. Tallant, J. A. Voigt, B. E. Gnade, J. Appl. Phys. 79 (1996) 7983.

[24] C. –T. Hsieh, J. –M. Chen, H. –H. Lin, H. –C. Shih, Appl. Phys. Lett. 83 (2003) 3383.

[25] R. A. Laudise, E. D.Kolb, A. J. Caporaso, J. Am. Ceram. Soc. 47 (1964) 9.

[26] D. M. Bagnall, Y. F. Chen, Z. Zhu, T. Yao, M. Y. Shen, T. Goto, Appl. Phys. Lett. 73 (1998) 1038.

[27] Y. –K. Tseng, C. –J. Huang, H. –M. Cheng, I. –N. Lin, K. S. Liu, I. –C. Chen, Adv. Funct. Mater. 13 (2003) 811.

[28] C. X. Xu, X. W. Sun, Appl. Phys. Lett. 83 (2003) 3806.

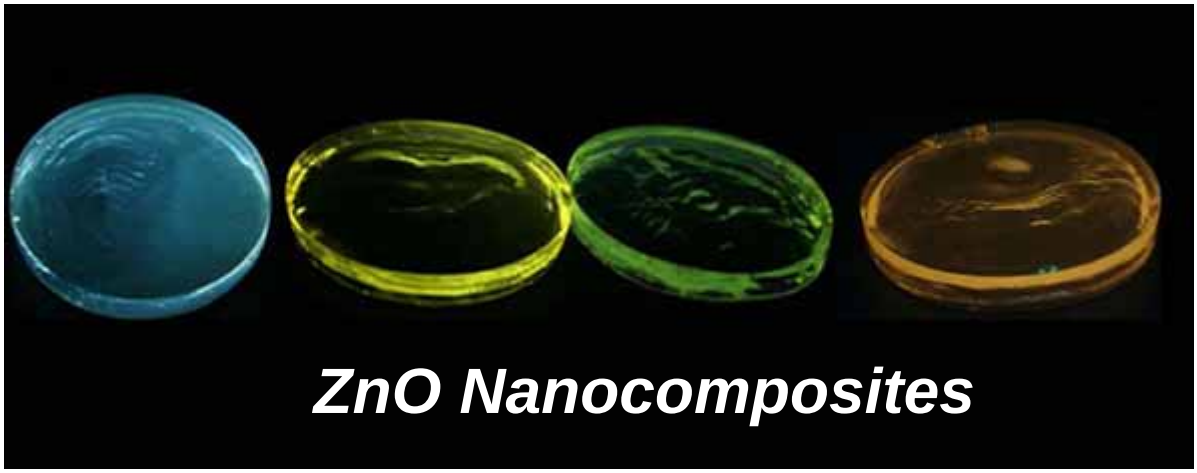

Chapter 5

Effect of Surface Stabilization of Nanoparticles on Luminescent Characteristics in ZnO/Poly(hydroxyethyl methacrylate) Nanohybrid Film

5.1 Introduction

Nanoparticles (NPs) or nanocrystals (NCs) of semiconductor materials have been extensively studied in last decade for use in light emitting diodes, lasers, photovoltaic solar cells and biolabels [1-6]. Many research groups have focused on the superior emitting properties of nanocomposites by dispersing the quantum-sized particles into a polymeric matrix [7-11]. The hybrid nanocomposites not only inherit the high luminescent characteristic of the quantum dots but also possess advantages of polymers such as flexibility, film integrity, and conformity. The control of the particle size, size distribution and dispersion homogeneity over entire matrix is the critical prerequisite to assure the optical and electrical properties of the nanocomposites for nanodevice applications. Up to now, to hybridize the inherently hydrophilic inorganic nanoparticles into a polymer matrix *via* bulk polymerization of an organic monomer is still a technological challenge [12,13]. Generally, passivating nanoparticle surfaces with appropriate capping agents such as long-chain

aliphatic thiols[14,15] or amines [8] is the most efficient method to hinder the innately instable nanoparticles from aggregation and thus enhance the compatibility of the inorganic nanoparticles with the organic matrix.

Among metal oxide materials, zinc oxide (ZnO) with its wide band gap (3.4 eV) and large exciton binding energy (60 meV) has been particularly interesting for catalysts, sensors and optoelectronic devices [16-18]. Since the luminescence characteristics of ZnO quantum dots are size-dependent [19-23], so the size control is quite important. The strategies to control the particle sizes include encapsulating organic capping agent on the nanoparticles surface such as alkylthilos, polymer micelles [24,25] , or using coordinating solvent such as dimethyl sulfoxide, *N*,*N''*-dimethylformamide and tri-n-octylphosphine oxide [26-29]. Although the size of nanoparticles can be manipulated by the capping agents [24,25], the nanoparticles under ambient conditions still will gradually and irreversibly aggregate together, especially when the solvent is evaporated. More importantly, the aggregated nanoparticles cause serious drawbacks in the photoluminescence, in term of wavelength shift and intensity decay [19,20]. Recently, stable-luminescent powder-like ZnO/SiO_2 hybrids prepared by spray drying of SiO_2 and ZnO nanoparticles colloids at 200 ^oC were reported [30]. In addition, Okuyama et [31] al. described the preparation of tunable emission ZnO nanocomposites *via* the incorporating of different size of particles in the presence of poly(ethyl glycol) solutions. However, the long term stability of nanoparticles in both solution and bulk polymers is still an unsolved problem.

In this article, we intend to modify the ZnO nanoparticles surfaces to promote the stability of colloid suspensions and nanocomposites, thus preserving the luminescent properties of nanoparticles in the nanohybrid bulks. We prepared a series of stabilized quantum size ZnO with various particle sizes, and chemically hybridized the nanoparticles into bulk polymers. The surface of the nanoparticles was stabilized by the absorption and hydrolysis of an unsaturated aliphatic silane of 3-(Trimethoxysilyl)propyl methacrylate (TPM), *via* a mild sol-gel reaction. The colloidal ZnO nanoparticles were first dispersed in 2-hydroxyethyl methacrylate (HEMA) monomers and then thermally polymerized to form a stable nanohybrid film. Besides, the unsaturated chain of TPM on the ZnO nanoparticles can be polymerized with 2-hydroxyethyl methacrylate, making the particles uniformly dispersed in the Poly(2-hydroxyethyl methacrylate) (PHEMA) matrix (Scheme 5-1). With this approach, we have prepared a series of high transparent

nanocomposites with uniform and well-defined size of ZnO nanoparticles. The colloidal ZnO nanoparticles and the nanoparticles/polymer composites were also characterized with X-ray diffraction (XRD), Fourier transform infrared (FTIR), transmission electron microscopy (TEM), UV-vis absorbance and photoluminescence spectrum (PL), Fourier transform infrared (FTIR) and ^{1}H NMR spectroscopy.

5.2 Experiment Section

Materials. Zinc acetate dihydrate ($Zn(Ac)_2 \cdot H_2O$) (SHOWA, 99.0%), lithium hydroxide monohydrate (LiOH H_2O) (TEDIA, 99.0%), 3-(Trimethoxysilyl)propyl methacrylate (TPM) (Aldrich, 98.0%) and absolute ethanol (Nasa, 99.5%,) were used as received. 2-hydroxyethyl methacrylate (HEMA, 97.0%) and methyl methacrylate (MMA, 99.0%) from Acros were distilled under vacuum before use. 2,2'-Azobisisobutyronitrile (AIBN, 99.0%) from SHOWA was recrystallized from methanol.

5.2.1 Synthesis of ZnO Nanoparticles

Green-emitting ZnO nanoparticles with an average diameter of 3.2 nm were prepared following the previous reports [18] with minor modification. In a typical run, 3.29 g of $Zn(Ac)_2 \cdot H_2O$ was dissolved in 150 mL boiling ethanol then refluxed at 80 ^oC in a nitrogen atmosphere, and held at this temperature for 3 h under vigorous stirring. To end of this process, 90 mL of ethanol was removed by distillation and the solution was subsequently diluted to original volume by adding same amount fresh ethanol. The reaction mixture was then cooled to 0 ^oC. A 90 mL aliquot of 0.87g $LiOH \cdot H_2O$ in ethanol was dropped into the stock solution under constant stirring within 2h, several hours of stirring with sonication assistance were needed to completely dissolute $LiOH \cdot H_2O$ in the ethanol. The stock solution was then stirred continuously at room temperature for 2h until ZnO nanoparticle colloids became transparent. Finally, the nanoparticles solution was filtered through 0.1 μm glass fiber filter to remove any insoluble precipitants. Blue-emitting nanoparticles with an average diameter of 2.2 nm were synthesized in a similar way, except the molar ratio of $LiOH/Zn(Ac)_2 \cdot H_20$ was raised to about 3.5 [31]. In addition, orange-emitting ZnO nanoparticles (6.1 nm diameter) were synthesized according to the method developed by Hoyer et.al [32].

5.2.2 Synthesis of TPM-modified ZnO Nanoparticles

To stabilize the surface of ZnO nanoparticle colloids, 0.3 g TPM in 10 ml ethanol was injected into 200 ml of as-prepared ZnO nanoparticles colloids over about 1 hour at 0 ^{o}C. The mixture was then further stirring at room temperature for 12 h followed by filtration with a 0.1 μm glass fiber filter to remove any insoluble precipitants.

5.2.3 Preparation of Nanoparticels Powder

To obtain the ZnO nanopowder for characterization, the ZnO nanoparticle colloids (unmodified and TPM-modified samples) were precipitated by adding a excess of anti-solvents as hexane or heptane into ethanol solution (volume ratio: heptane/ethanol >2), [33] as called "washing process". Briefly, 100ml nanoparticles solution was poured into 300 ml heptane to cause nanoparticles precipitation. The resulting products were isolated by centrifugation (3000 rpm, 5 min), decantation and rewashing several times for removing all residue. The resulting product was then collected and dried in vacuum. The amount of TPM stabilizing agent absorbed on ZnO nanoparticles surface can be estimated by the TGA analysis and was found to be about 4.3 wt %.

5.2.4 Preparation of ZnO Nanocomposites

Unmodified and TPM-modified ZnO nanoparticles colloids were first purified through "washing process" and redispersed in 250 ml of fresh ethanol. Then, 5 ml of nanoparticle colloids (ZnO content of ~1 wt %) were mixed with 10 g HEMA monomer under stirring at room temperature for 2h. Ethanol solvent was distilled by using a rotatory evaporation at about 40 ^{o}C. To polymerize ZnO NPs-monomers, 0.2 wt % AIBN radical initiator was added into the precursor solution. The mixture was then gently stirred for several hours until the solution became clear. Finally, the ZnO nanoparticles/polymer hybrid materials were obtained by pouring the solution in a Teflon mold (30 mm diameter × 3mm height) by subsequently bulk polymerization in an oven at 70 ^{o}C for 6 h, and further postheating at 100 ^{o}C for 2 h after being removed from the mold.

5.2.5 Preparation of Polymer Lasing Structure

Preparation of distrbuted feedback resonator

The polymerization belongs to photocatalytic reaction at inorganic

nanoparticle/monomer. By Holography methods, we use two ultra-violet (UV) laser to have an interference and produce a continuous distribution of bright-dark at the surface of samples. According to the different laser intensity distribution, the diffusion of zinc oxide nanoparticle and monomer are relative. That will produce a regular high and low at surface of thin film and it called grating surface.

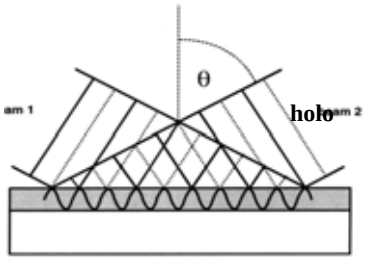

$$\Lambda = \frac{\lambda_{writing}}{2(\sin\theta_{holo})}$$

grating producing diagram

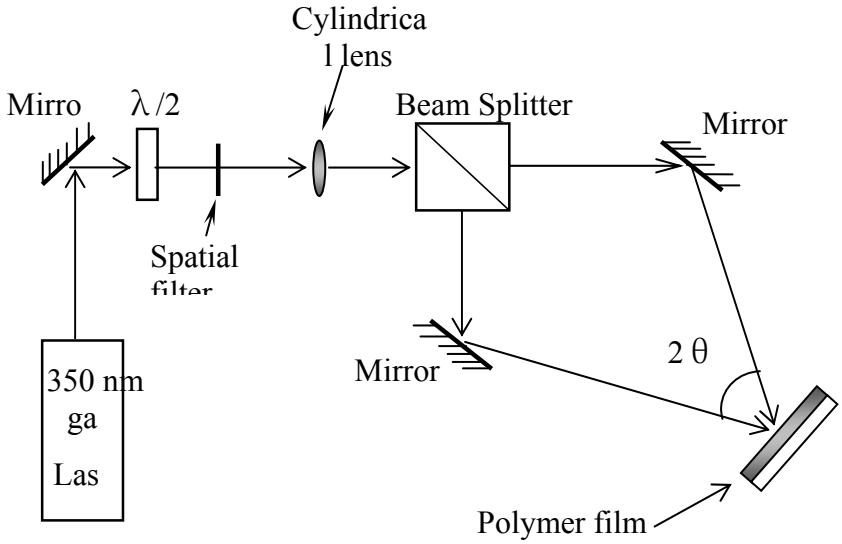

experimental optical path diagram

Analysis of ASE （Amplified Spontaneous Emission）

Limitation of experiment：

（1）pulse laser

（2）The main target is to observe the morphology of surface and the distribution of inorganic/organic phases after production of grating, or analysis of ASE.

Coupled Wave Theory

Germany scientist Kogelnik have reported coupled wave theory and explained the threshold of DFB laser and output wavelength of threshold at1969.

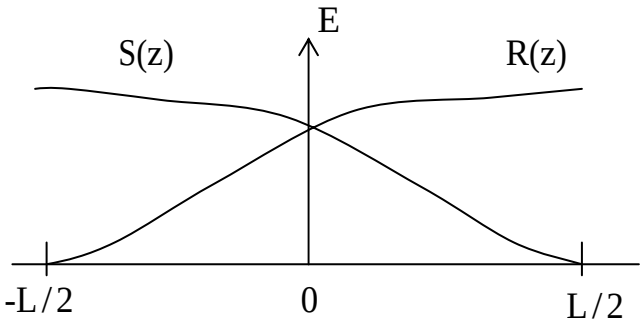

Only at Bragg's condition, we can get the same progressive wave and reflected wave, and have the maximal amplitude. So electric field intensity of DFB laser can be described by equation (1) :

$$E(z)=R(z)\exp(-j\beta_0 z)+S(z)\exp(j\beta_0 z) \qquad (1)$$

z is direction of along resonator, and can be substituted by scalar wave equation ,

$$\frac{\partial^2}{\partial z^2} E + k^2 E = 0$$

And we can get coupled wave equation by comparing to coefficient of an exponential function

$$\begin{aligned} -R' + (\alpha - j\delta)R &= j\kappa S \\ S' + (\alpha - j\delta)S &= j k R \end{aligned} \qquad (2)$$

β_0 : effective wave factor at Bragg' s condition
k : wave vector
L : length of resonator
κ : coupled coefficient,

real components

$$\kappa = \frac{\pi n_1}{\lambda_0} + \frac{1}{2} j\alpha_1$$

imaginary components

n_1 : amplitude of refractive index change; n : average of refractive index in medium
α_1 : amplitude of gain constant changing; α : average of gain constant in medium
λ_0 : Bragg' s wavelength

δ normalized frequent parameter, $j = (-1)^{1/2}$

$$\delta \equiv (\beta^2 - \beta_0^2)/2\beta = \beta - \beta_0 = n(\omega - \omega_0)/c \qquad (3)$$

δ is the difference between vibrate frequency（ω）and Bragg's frequency（ω_0）. δ=0 at Bragg' s frequency. We can assumeβ/β_0=1 because δ is very small.

coupled wave equation is to describe wave propagation of DFB laser in gain and periodic disturbation condition.

At first, we can easy to know the solution of coupled wave equation：

$$R = A_1\exp(\gamma z) + A_2\exp(-\gamma z)$$

$$S = B_1\exp(\gamma z) + B_2\exp(-\gamma z) \qquad (4)$$

Complex propagation constant, γ , is to content dispersion relation：

$$\gamma^2 = \kappa^2 + (\alpha - j\,\delta)^2 \qquad (5)$$

And the solution substitute for boundary condition

$$R(-L/2)=S(L/2)=0 \qquad (6)$$

We can get a complex eigenvalue equation. We can get a resonant gain α and normalized frequency coefficient δ. So coupled wave equation is to solve threshold at each mode of threshold and threshold of each mode. If we know coupled constant (κ)and length of resonator（L）, the character of electric field, threshold, and resonant frequency can be decided at each mode. In other words, the structure of resonator and dispersion of medium affect characters of laser. The importance is to solve eigenvalue equation but the equation is too complex, we just can use numerical analysis by computer. In order to simplify, we just discussion two limit condition at α_1=0 and n_1 = 0.

And we can know each character of resonator from κ.

$$\kappa = \frac{\pi n_1}{\lambda_0} + \frac{1}{2} j\alpha_1$$

1.Index coupling ：α_1=0 , κ is real value.

If we have the stop band be produced, threshold wavelength is at two sides of stop band.

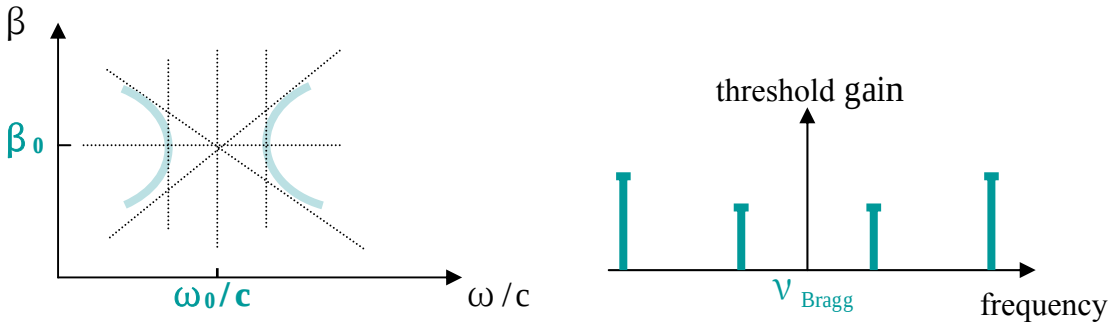

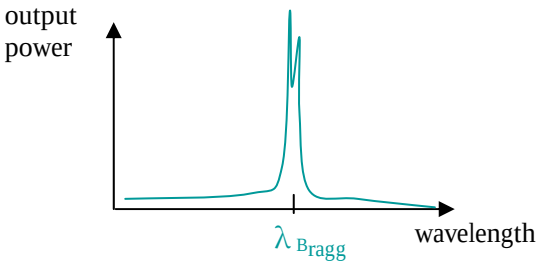

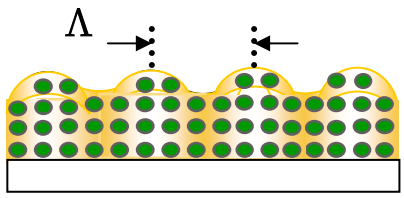

2. Gain coupling： $n_1 = 0$, κ is imaginary value.
No stop band, the threshold is at ν_{bragg} （or λ_{bragg}）

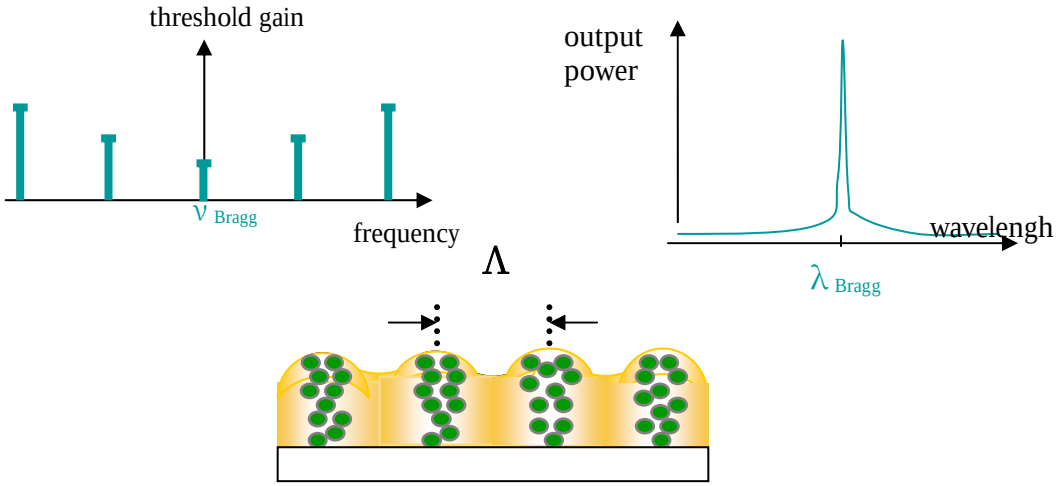

3. Complex coupling：have real components and imaginary components
Complex coupling is combine index and gain coupling. This condition conform to the realistic condition. We can know which mode of coupling is getting advantage from wavelength type of final output.

5.3 Characterization

All measurements for characterization were performed at room temperature. X-ray powder diffraction patterns was carried out with MAC Sience MXP18 X-ray diffractometer （30 kV, 20 mA）with copper targets at a scanning rate of 4^o/min. The Fourier transform infrared (FTIR) spectra of the samples were obtained with a Nicolet PROTÉGÉ-460 by the KBr method. ^{1}H NMR spectra were recorded on a Varian Unity-300 NMR spectrometer. Thermal gravimetric analyses of the ZnO nanoparticles were carried out with a Du Pont TGA 2950 at a heating rate of 10 ^{o}C/min with a nitrogen purge. UV-vis absorbance spectra were performed on an Aligent 8453 spectrometer using a 1cm quartz cuvette. Transmission electron microscopy (TEM) was carried out on a JOEL 2000FX electron microscope operation at 200 kV. The nanoparticles samples were prepared by directly placing a drop of solution on a holey copper grid covered with a continuous carbon film. The specimens of nanocomposites were ultramicrotometed with a diamond knife on a Leica ultracut Uct to obtain about 100 nm thick films. Subsequently, these films were placed on mesh 200 copper net and a layer of carbon about 3 nm thick was deposited for TEM observation. The photoluminescence properties of ZnO nanoparticles solutions and nanocomposites were acquired on a Hitchai F4500 fluorescence spectrometer equipped with an excitation source of 325 nm wavelength. The PL quantum efficiencies of ZnO nanoparticles colloids were measured by using quinine dye in H_2SO_4 aqueous solution as a PL reference [34].

5.4 Result and Discussion

5.4.1 Stability of ZnO Nanoparticle Colloids

TEM

Figure 5-1shows the TEM image of fresh unmodified ZnO nanoparticles dispersed in ethanol. The TEM image reveals spherical particles and the average diameter was estimated to about 3.2 nm. The size distribution histogram in Figure 1 suggests a nearly uniform size distribution.

UV-vis

Figure 5-2 illustrates UV-vis absorption spectra of unmodified ZnO nanoparticles and TPM-modified ZnO nanoparticles in ethanol solution. The UV-vis absorption spectra of the two colloidal solutions which were recorded after 2 h aging reveal a well-defined exciton

band at around 320 nm and a dramatic blue shift compared with the bulk excition absorption (373 nm) [35]. Such features in the exciton band are mainly responsible for the characteristics of quantum size effects (particle size ≤ 7 nm) [36]. Generally, the fresh ZnO nanoparticles prepared from zinc acetate dihydrate in ethanol solution can be electrostatically stabilized by negatively-charged repulsion between carboxylic acid groups on nanoparticles surfaces [21]. However, as the aging times were prolonged, the absorption shoulder of unmodified ZnO nanoparticles obviously undergoes a series of red-shifts (Figure 5-2a), which are mainly results from the development of some degree of aggregation between primary clusters [19]. Moreover, the aggregated clusters accompanied with the formation of turbid suspensions in the solution. As shown in the inset of Figure 5-2a, the ZnO nanoparticle settled to the bottom of the UV cell about two months later at room temperature. In contrast, the profiles in absorption spectra of TPM-modified ZnO nanoparticles recorded at different aging time are almost identical (Fig 5-2b). The solution with TPM-modified ZnO nanoparticles remains optically clear at room temperature during 2 months storage (inset in Figure 5-2b) and remains stable for at least six months without any obvious colloidal aggregation. The stabilities of the TPM-modified ZnO particles are very excellent, implying that the aggregation phenomena of ZnO nanoparticles are strongly quenched by the present of TPM stabilizers on the particle surface.

Monitoring the UV-vis absorption spectra of the ZnO colloidal solution is a useful and available tool to characterize the particle growth because the onset of absorption is associated with particles size [19-21,33]. According to the experimental relationship between average diameter (D) and absorption shoulder ($\lambda_{1/2}$) of the ZnO nanoparticle colloids reported by Meulenkamp [33], the particle sizes based on the following calibrated equation can be calculated.

$$1240/\lambda_{1/2} = 3.301 + 294.0/D^2 + 1.09/D \qquad (1)$$

Thus, the average diameter of ZnO nanopartices can be obtained and the results are shown in Figure 5-3. Clearly, the size of unmodifed ZnO particles increased to about 6.7 nm after 10 days aging. In comparison, the particle sizes of the TPM-modified ZnO remained virtually unaltered from those of the fresh nanoparticle. After a period of 10 days at room temperature, the average diameters of TPM-modified particles estimated to be still about 3.2 nm.

XRD

To further clarify the effect of TPM stabilizers on the aggregation state of nanoparticles, the crystal sizes of ZnO with different aged times were estimated by X-ray diffraction. Figure 5-4 depicts typical powder x-ray diffraction patterns of unmodified and TPM-modified ZnO nanoparticles, taken for samples aged at 30 ^{o}C for 2 h, 3 days and 6 days after nanoparticle preparation. All diffraction peaks of these two profiles are consisted with typical wurtzite structure of bulk ZnO. Additionally, the aging time increase significantly influences the half-width of broadening peaks in the unmodified ZnO samples, as shown in Figure 4a. In principle, the average ZnO crystal sizes (D) can be obtained by using Scherer's equation, $D = 0.89\lambda/(\beta\cos\theta)$, where λ is the x-ray wavelength (1.54 Å), β is the half-width of the diffraction peak, and θ is the Bragg diffraction angle. By calculating the XRD diffraction peak broadening at (110), the average crystallite size of unmodified ZnO were estimated about 3.1 nm for 2 h, 4.3 nm for 3 days and 5.2 nm for 6 days. This result clearly indicates that the crystal growth process of the unmodified ZnO nanoparticles can easily occur even during aging at 30 ^{o}C, which agrees with previous results [19]. In contrast to the unmodified ZnO, the TPM-modified nanoparticle only slightly increased in crystal size from about 3.1 nm to 3.3 nm after aging 6 days (Figure 5-4b). All these results were consisted with our observation in UV-vis spectra.

FTIR To confirm that the trimethoxy silane functionality of the TPM stabilizer capped/absorbed on the surface of ZnO nanoparticles, the purified powders were prepared through the "washing step" four times to ensure the removing all of unreacted TPM stabilizer molecules. Figure 5 shows the IR spectra of (a) unmodified ZnO and (b) TPM-modified ZnO nanoparticles. The absorption band at 1579 cm^{-1} and 1415 cm^{-1} in both samples are assigned to the surface-absorbed carboxylate anions complex with zinc center [20-21], indicating that the acetate group is chemisorbed on the ZnO nanoparticle surface. The addition of stabilizing agent on ZnO nanoparticles surface resulted in the different IR spectrum (Figure 5b). The characteristic absorption peaks of the TPM stabilizer ascribed to –OH stretching vibration at 3450 cm^{-1}, C=O stretching vibration at 1704 cm^{-1}, –SiOH stretching vibration at 880 cm^{-1} [37], and the peak at 1179 cm^{-1} was the characteristic peak of Si–O–Si symmetrical stretching vibration [38].

^{1}H NMR

Purified powders of umodified ZnO and TPM-modified ZnO nanoparticles were

dispersed in DMSO-d_6 for the ^{1}H NMR measurement. Figure 5-6 shows ^{1}H NMR of the pure TPM stabilizer, unmodified ZnO nanoparticles and TPM-modified ZnO nanopaticles. In the ^{1}H NMR spectrum of TPM stabilizer (curve a), the resonance peaks at 6.02 and 5.65 ppm are assigned to the methylene protons (peaks H_1); and the three resonance peaks at 4.03, 1.66 and 0.62 ppm are assigned to the α-CH_2, β-CH_2 and γ-CH_2 protons (peak H_3, H_4 and H_5) to methacrylate, respectively. The resonance peak at 3.47 ppm is caused by methyl protons of trimethoxysilane (peak H_6). In curve 6b of the unmodified ZnO nanoparticles, the peak at 1.72 ppm is attributed to the methyl proton of acetate group, confirming the existence of the acetate group absorbed on the ZnO nanoparticles surface. Comparing ^{1}H NMR spectrums of pure TPM stabilizer and TPM-modified ZnO nanoparticles (curves a and c), clearly the chemical shifts of H_4 and H_5 are not observed and the chemical shifts of H_1, H_2, H_3 become significant broadening in the TPM-modified ZnO nanoparticle sample. The broadening of the proton NMR spectrum is most likely due to inhomogeneities of local chemical environment in the magnetic field. Usually, when the proton are attached or absorbed at the surface of nanoparticles, the proton motion will become more restricted and the proton peak will become broader, or disappear [39].

Base on the above FTIR and ^{1}H NMR observations, it is reasonable to conclude that the trimethoxysilyl group of the TPM stabilizer absorbed on the as-prepared ZnO nanoparticle surface and yield a thin layer of organic silica nanonetwork *via* a hydrolysis-condensation reaction. We believe that the TPM stabilizer probably provided effective steric hindrance of the silica nanonetwork surrounding on the ZnO surfaces preventing colloid aggregation, thus leading to the excellent stability of ZnO nanoparticles in ethanol solution.

5.4.2 Optical Properties and Morphology of ZnO/PHEMA Nanocomposites

Photoluminescence

As shown in Table I, the photoluminescent properties (emission bands and quantum efficiencies) of ZnO nanoparticles in ethanol solution before and after addition of TPM stabilizer are similar, suggesting that the presence of such silica network on the

ZnO nanoparticle surfaces causes no significant fluorescence degradation or particle aggregations. Figure 5-7 shows the PL spectra of the unmodified ZnO nanoparticle solutions and ZnO/PHEMA nanocomposites with an excitation wavelength at 325 nm. The TPM-modified ZnO nanocomposite with average diameter 3.2 nm is found to be remarkably similar to the initial unmodified nanoparticle solution, as shown in Figure 5-7a. In contrast, the emission peak of unmodified ZnO nanocomposite has a red shift. In Figure 7b, the ZnO/PHEMA nanocomposite with average diameter 2.2 nm of TPM-modified ZnO gives a blue emission peak at 466 nm. Although the emission peaks of the 2.2 nm modified and unmodified ZnO nanocomposites all have red shifts, the TPM stabilizer obviously reduces the degree of shift. Since the emission bands of quantum-sized ZnO nanoparticle depend on the particle size [19,21,23], the longer emission wavelength of ZnO/PHEMA nanocomposites without TPM stabilizer may contribute to the larger agglomerates and particle size increases in the course of thermal polymerization.

Due to good miscibility and dispersibility of the ZnO nanoparticle in HEMA monomers solution, stable optical transparent ZnO/PHEMA nanocomposites were readily obtained by common thermal polymerization. Figure 5-8 shows photographs of the ZnO/PHEMA nanocomposites (ca. 1% wt of ZnO nanoparticles) under daylight and under UV light. Both TPM-modified and unmodified ZnO/PHEMA nanocomposites afford excellent optical transparent (Figure 5-8a). Additionally, utilizing the precise size control and surface modification of ZnO nanoparticles into bulk nanocomposites allows adjusting the emission colors from blue to orange Figure 5-8(b–d). Moreover, the luminescent properties of ZnO/PHEMA nanocomposoites display remarkable stability. For example, the emission peaks and intensities of these highly transparent nanocomposites were found to maintain similar values even after being aged over three months (see Table I).

TEM

TEM was employed to examine the stability and dispersibility of the ZnO nanoparticles undergoing thermal polymerization at 70 ^{o}C and postheating procedure at 100 ^{o}C. As a representative example in Figure 5-9a, large aggregate clusters in the unmodified ZnO/PHEMA nanocomposites were easily observed. In contrast, the 3.2 nm TPM-modified ZnO particles are well dispersed in the entire PHEMA matrix and the particles size almost unchanged (Figure 5-9b). These observations are consistent with the results of photoluminescence spectra, clearly supporting the idea that the TPM-surfaced modification really supports superior stability and dispersibility of ZnO nanoparticles into the polymer matrix compared to the unmodified ZnO nanoparicles, probably because of the covalent attachment between nanoparticles and polymers.

5.4.3 Optical Properties of ZnO/PMMA Nanocomposites

To further evaluate influence of TPM on the dispersibility of ZnO nanoparticles in polymeric bulk, poly(methyl methacrylate) (PMMA) were used to replace PHEMA in the preparation of ZnO nanocomposites. Figure 5-10 is the photographs of ZnO/PMMA nanocomposites (a) under daylight and (b) under UV lamp with the samples (I) 3.2 nm unmodified ZnO, (II) 3.2 nm TPM-modified ZnO and (III) 6.1 nm unmodified ZnO. Both unmodified ZnO samples I and III revealed the particle precipitation and aggregation from the PMMA matrix, as the emission regions of samples in Figure 5-10b. In contrast, sample (II) shows a relatively transparent and uniform appearance compared to the unmodified samples, indicating that the TPM stabilizer play an important role on the optical quality of bulk nanocomposites.

5.5 Conclusion

In conclusion, the preparation of surface-modified ZnO nanoparticles with a layer of silica nanonetwork through a mild sol-gel route using TPM stabilizing agent have been demonstrated. The TPM stabilizer was shown to provide the high dispersion stability of ZnO nanoparticles in ethanol solution and preserve the size of nanoparticles near constant over the long periods of time. The TPM-modified ZnO nanoparticles have better spatial separation than the unmodified ZnO nanoparticles in the nanohybrid film. Furthermore, the room temperature PL measurements also show that this surface-modified method can preserve the superior luminescence of ZnO nanoparticles in the nanohybrid films as well as in the initial nanoparticles solution. The surface modification method is believed to be an

efficient approach to finely adjust the luminescent color and uniformity of bulk nanocomposites for developing novel electro-optical application.

Semi-conducting conjugated polymer can be used for gain medium of optical device, such as PPV ,poly(p-phenylene vinylene) and m-LPPP, (methyl added Ladder-type Poly-Para-Phenylene), is one of the news studies. The semi-conducting polymers have a large potential, because they have larger quantum fluorescence efficiency and cross-section probability of exciting emission. Besides, we can change the wavelength by changing chemical structure. Because of the special characterizes, they are always studied in thesis field. The basic theory of the luminous quantum-dot/polymer composites is the same as Semi-conducting conjugated polymer. The difference is,

1. The semi-conducting conjugated polymer:

Uni-system: The most of methods are using chemical synthesizing to get polymer or copolymer. When application for preparing thin film devices, using good solvent to solve polymer become polymer solution. And we dry the solvent after coating at substrates.

2. The luminous quantum-dot/polymer:

Bi-system: luminous quantum-dot and polymer (inorganic/organic) By changing size of quantum-dot we can regulate luminous wavelength. And we can have the more applications by changing surface functionality of quantum dot.

By pulse laser exciting, the quantum dots can be a role of gain medium and scattering center that can extend photon path and induced the more photons.

In thesis field, the ultimate target is to achieve electro-luminescence device of organic solid laser. For the target, we need larger gain medium and higher current density by increasing intrinsic mobility and reducing threshold in materials. Such as organic solid laser can compete with traditions inorganic semiconductor laser, and there are many advantages at low cost, low temperature process, and have mass production in different substrates.

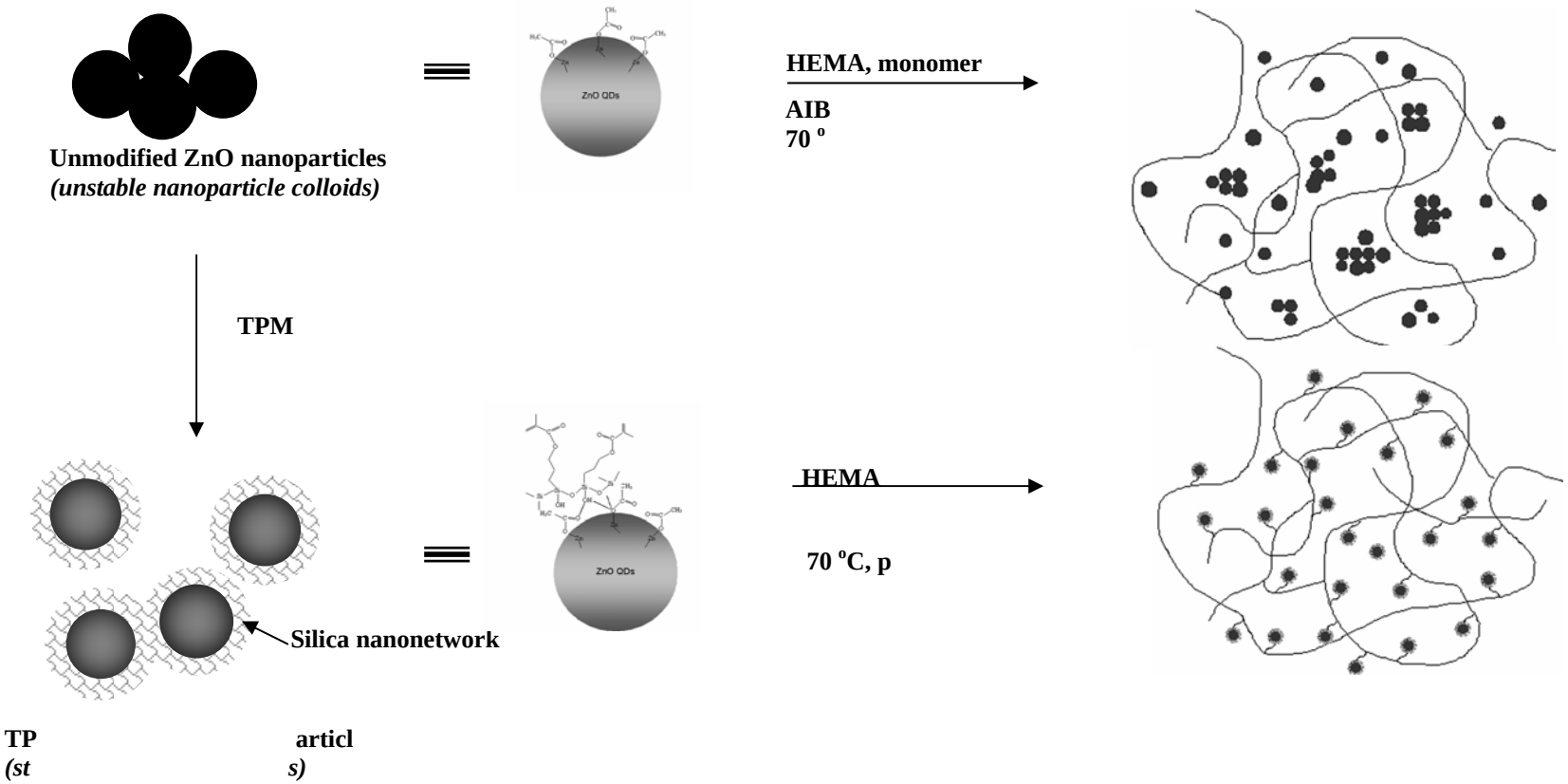

Sheme 1. The synthesis procedure of ZnO/PHEMA nanocomposites.

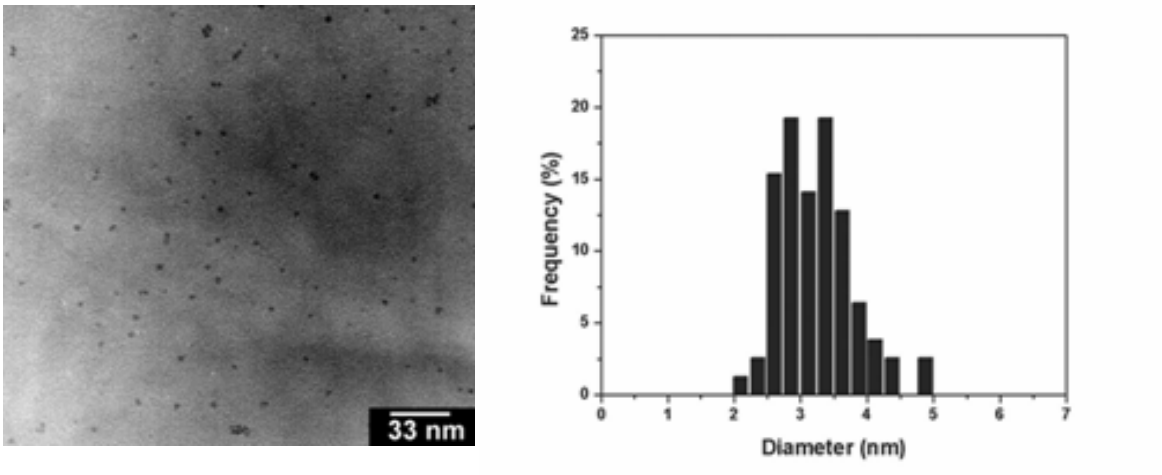

Figure 5-1 TEM image and size distribution histogram of fresh unmodified ZnO particles.

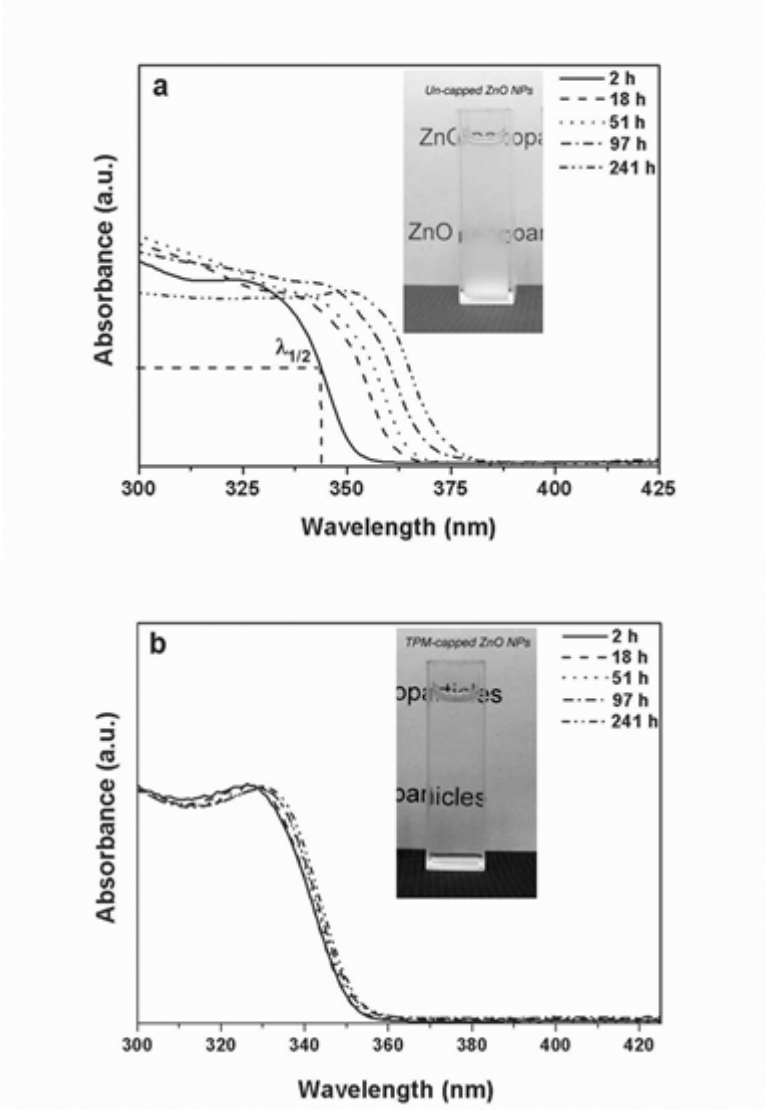

Figure 5-2 Time dependence of UV/vis absorption spectra: (a) umodified ZnO nanoparticles and (b) TPM-modified ZnO nanoparticles in ethanol. Inset are photographs of the ZnO nanoparticle colloids aging at room temperature for 2 months.

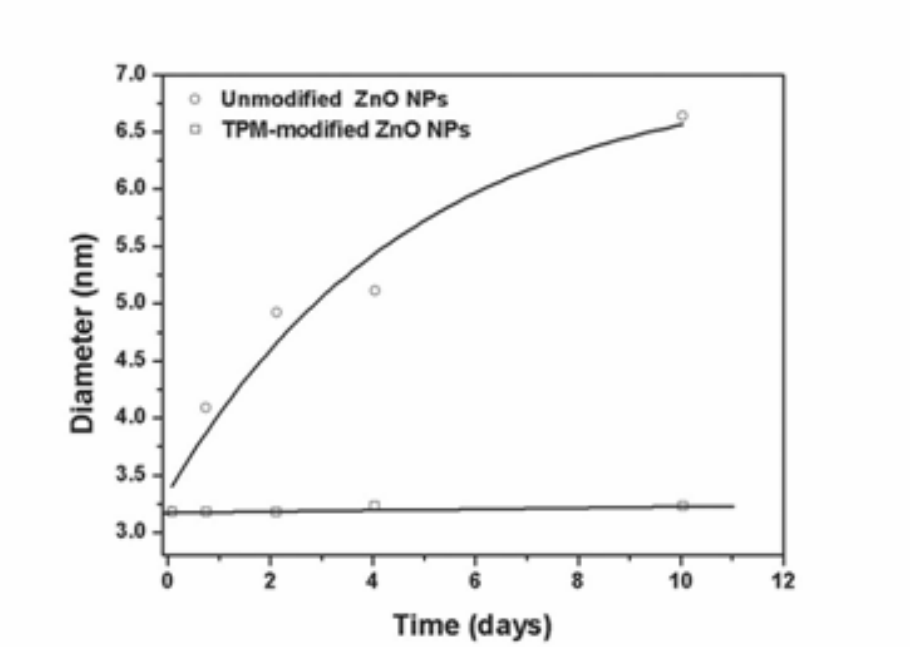

Figure 5-3 Particle diameters versus aging time of the ZnO particles in ethanol.

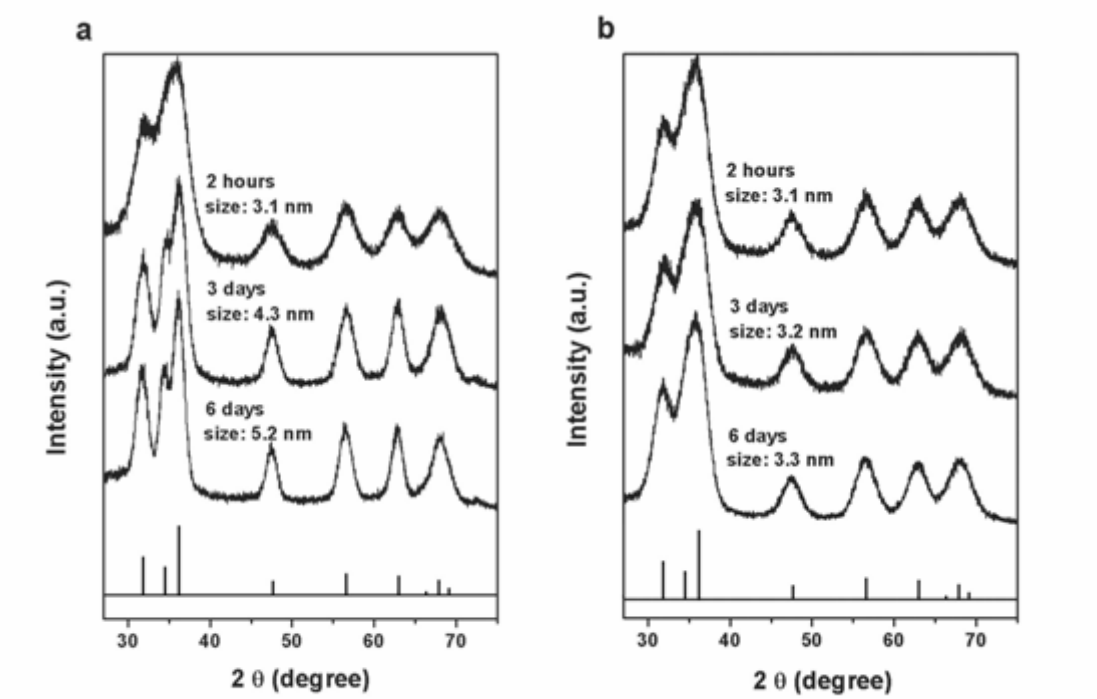

Figure 5-4 Powder x-ray diffraction spectra of (a) umodified ZnO nanoparticles, (b) TPM-modified ZnO nanoparticles prepared with different aging time. The diffraction pattern of wurtzite ZnO crystal from JCPDS database is shown in bottom for comparison.

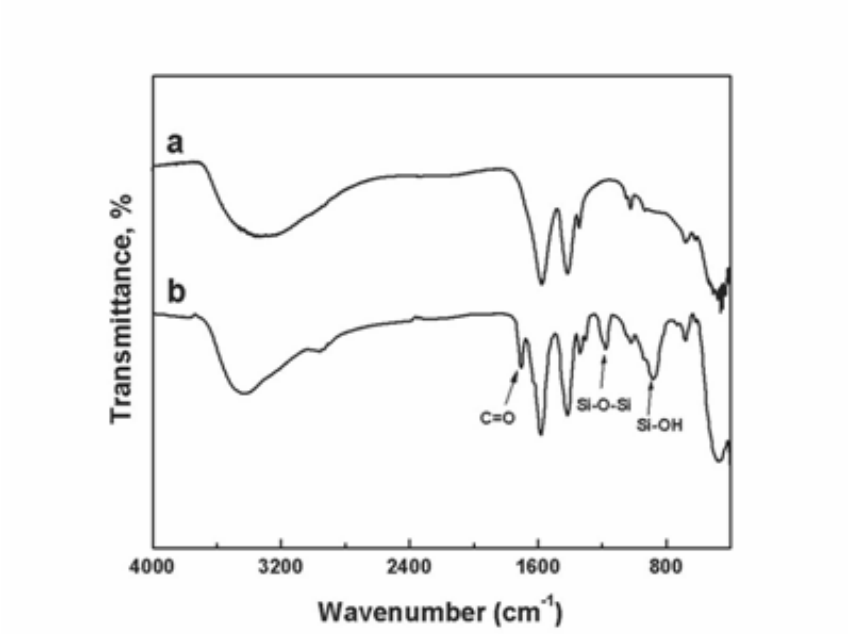

Figure 5-5 FTIR spectra of the (a) unmodified ZnO nanoparticles and (b) TPM-modified ZnO nanoparticles.

Table Ⅰ Luminescence properties of ZnO NPs in solution and ZnO/PHEMA nanocomposites.

ZnO particle size (nm)[a]	PL λ_{max}					
	TPM-modified ZnO			Unmodified ZnO		
	in ethanol solution (nm)	in ZnO/PHEMA nanocomposite (nm)	Φ^c (%)	in ethanol solution (nm)	in ZnO/PHEMA nanocomposites (nm)	Φ^c (%)
3.2	510	508(510)[b]	6.2	506	530(530)[b]	7.8
2.2	453	467(468)[b]	10.5	447	515(520)[b]	10.2

a: NPs diameters calculated from the shoulder of absorption spectra.
b: PL was recorded after three months of storage.
c: Fluorescence quantum yields of ZnO NPs in ethanol solution were obtained with quinine dye as a standard.

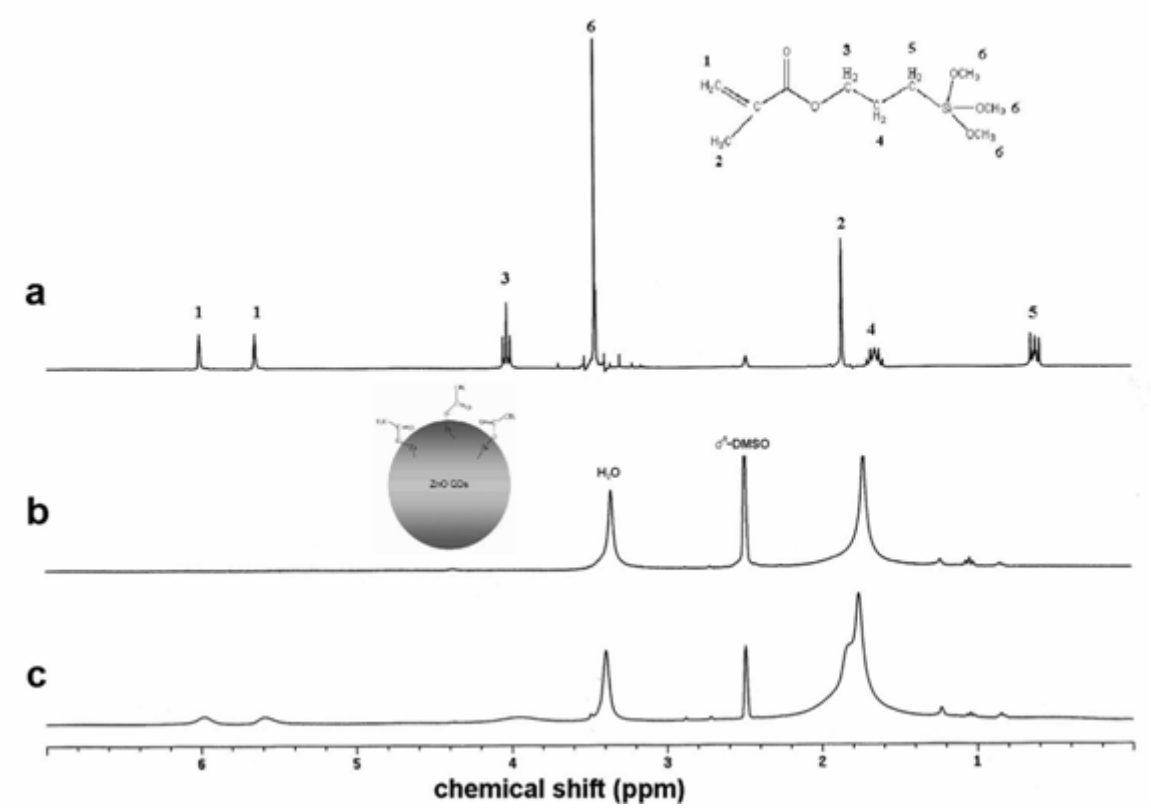

Figure 5-6 ^{1}H NMR spectra of the (a) pure TPM stabilizer, (b) unmodified ZnO nanoparticles and (c) TPM-modified ZnO nanoparticles dispersed in DMSO-d_6.

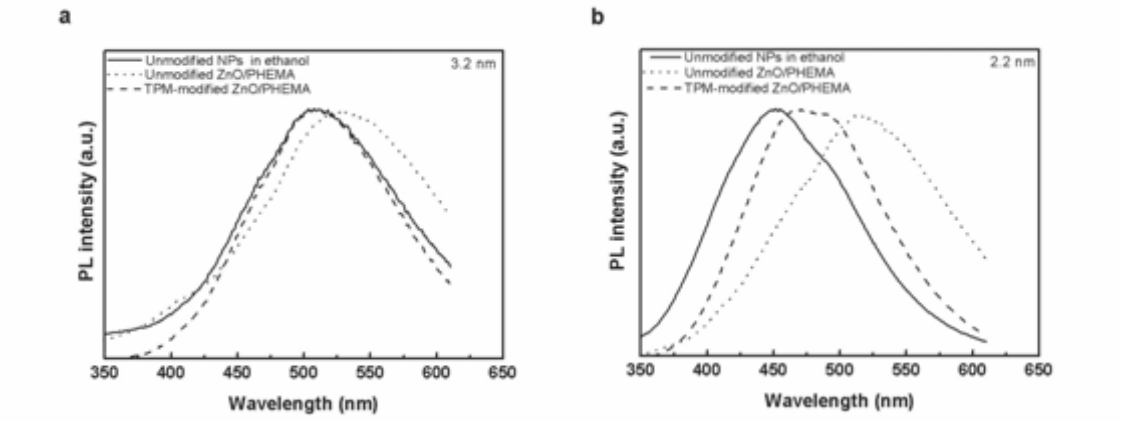

Figure 5-7 Photoluminescence spectra of unmodified ZnO nanoparticles in ethanol solution., and modified and unmodified ZnO/PHEMA nanocomposites

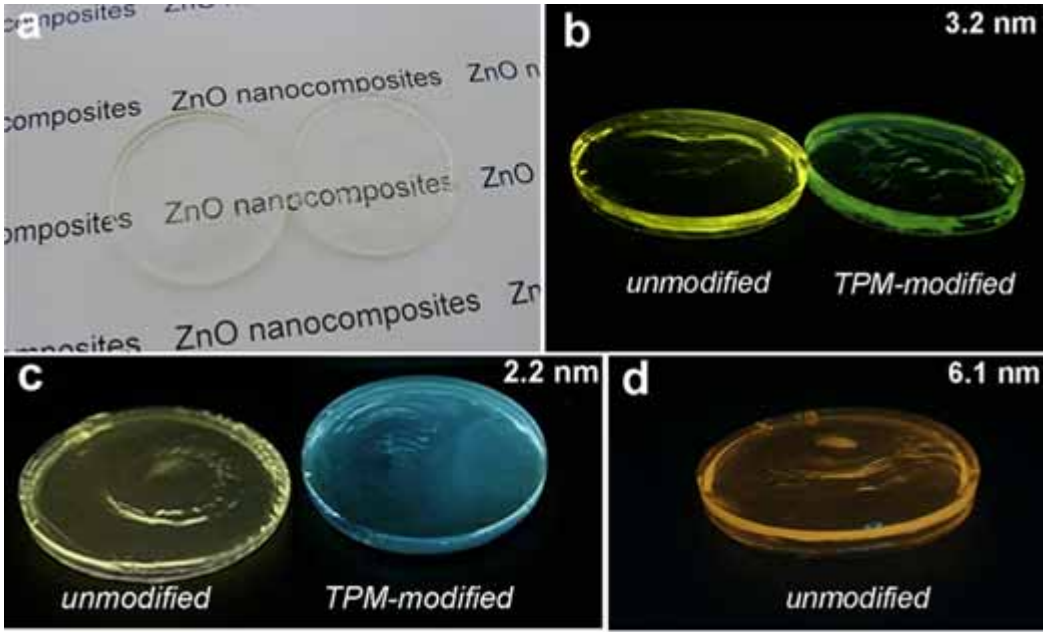

Figure 5-8 Photographs of transparent ZnO/PHEMA nanocomposites with various particles sizes (a) under daylight and (b)–(d) under an UV lamp. The luminescence images of nanocomposites fabricated by ZnO particles with an average diameter of (b)

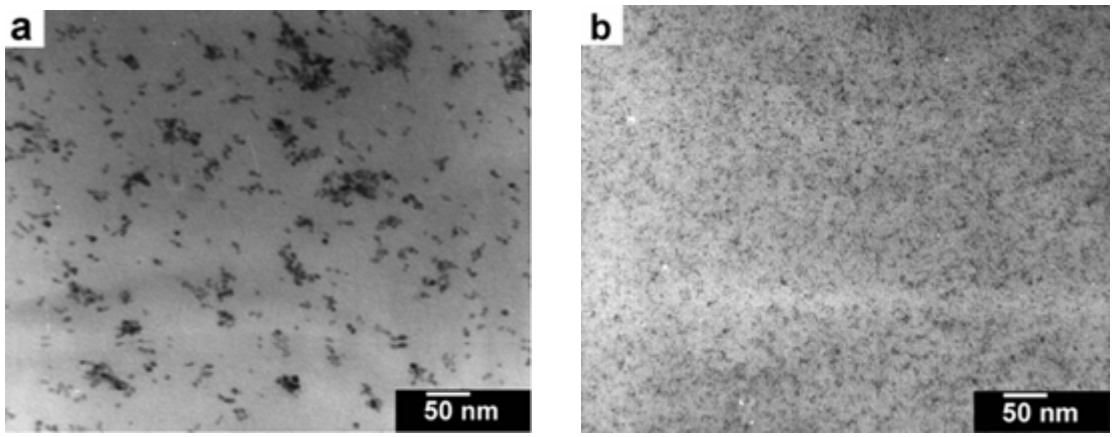

Figure 5-9 Cross-section TEM images: (a) 6.1 nm unmodified ZnO particles in PHEMA matrix and (b) 3.2 nm TPM-modified ZnO particles in PHEMA matrix.

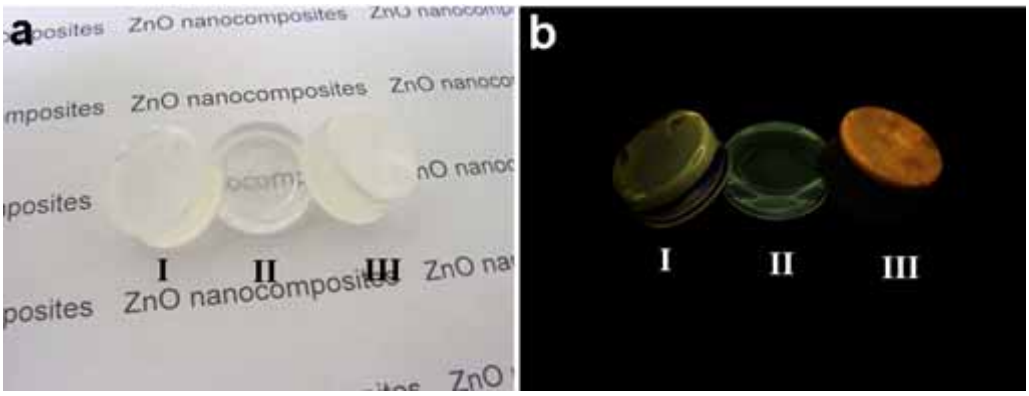

Figure 5-10 Photographs of ZnO/PMMA nanocomposites (a) under daylight and (b) under an UV lamp with the samples of (I) 3.2 nm unmodified ZnO, (II) 3.2 nm

5.6 Reference

[1] V. L. Colvin, M. C. Schlamp and A. P. Alivisatos, *Nature* 370 (1994) 354.

[2] A. P. Alivisatos, *Science* 271 (1996) 933.

[3] M. H. Nayfeh, O. Akcakir, G. Belomonin, N. Barry, J. Therrien and E. Gratton, *Appl*. *Phys*. *Lett*., **77** (2000) 4086.

[4] C. Roland, V. Meunier, B. Larade and H. Guo, *Phys. Rev. B* 66 (2002) 035332.

[5] M. P. Bruchez, M. Moronne, P. Gin, S. Weiss and A. P. Alivisatos, *Science* 281 (1998) 2013.

[6] Y. Yang, J. Huang, S. Liu and J. Shen, *J*. *Mater*. *Chem*., **7** (1997) 131.

[7] J. Lee, V. C. Sundar, J. R. Heine, M. G. Bawendi and K. F. Jensen, *Adv*. *Mater*., 12 (2000) 1102.

[8] H. Zhang, Z. Cui, Y. Wang, K. Zhang, X. Ji, C. Lü, B. Yang and M. Gao, *Adv*. *Mater*., 15 (2003) 777.

[9] S. C. Farmer and T. E. Patten, *Chem*. *Mater*., 13 (2001) 3920.

[10] N. Gaponik, D. V. Talapin, A. L. Rogach, A. Eychmuller and H. Weller, *Nano*. *Lett*., 2 (2002) 803.

[11] M. Moffitt, H. Vali and A. Eisenberg, *Chem*. *Mater*., 10 (1998) 1021.

[12] F. M. Pavel and R. A. Mackay, *Langmuir*, 16 (2000) 8568.

[13] C. H. Chew, T. D. Li, L. H. Gan, C. H. Quek, and L. M. Gan, *Langmuir*, 14 (1998)

6068.

[14] M. Brust, M. Walker, D. Bethell, D. J. Schiffrin and R. Whyman, *J. Chem. Soc., Chem. Commun.*, 1994, 801-802.

[15] C. L. Li and N. Murse, *Langmuir*, 20 (2004) 1.

[16] K. Hara, T. Horiguchi, T. Kinoshita, K. Sayama, H. Sugihara and H. Arakawa, *Sol. Energy Mater. Sol. Cells*, 64 (2000) 115.

[17] S. Bachir, C. Sandouly, J. Kossanyi and J. C. Ronfard–Haret, *J. Phys. Chem. Solids*., 57 (1996) 1869.

[18] D. J. Goyal, C. Agashe, M. G. Takwale, V. G. Bhide, S. Mahamuni, and S. K. Kulkarni, *J. Mater. Res.*, 8 (1993) 1052.

[19] L. Spanhel and M. A. Anderson, *J. Am. Chem. Soc*., 113 (1991) 2826.

[20] S. Monticone, R. Tufeu and A. V. Kanaev, *J. Phys. Chem. B*. 102 (1998) 2854.

[21] S. Sakohara, M. Ishida and M. A. Anderson, *J. Phys. Chem. B*. 102 (1998) 10169.

[22] H. –M, Xiong, X. Zhao, J. –S. Chen, *J. Phys. Chem. B*. 105 (2001) 10169.

[23] E. M. Wang and P. C. Searson, *Appl. Phys. Lett*., 74 (1999) 2939.

[24] N. S. Pesika, Z. Hu, K. J. Stebe and P. C. Searson, *J. Phys. Chem. B*. 106 (2002) 6985.

[25] L. Guo, S. Yang, C. Yang, P. Yu, J. Wang, W. Ge, and G. K. L. Wong, *Appl. Phys. Lett*., 76 (2000) 2901.

[26] G. Rodriguez-Gattorno, P. Santiago-Jacinto, L. Rendon-Vazquez, J. Nemeth, I. Dekany

and D. Diaz, *J. Phys. Chem. B*, 107 (2003) 12597.

[27] M. Shim and P. Guyot-Sionnest, *J. Am. Chem. Soc.,* 123 (2001) 11651.

[28] P. D. Cozzoli, M. L. Curri, A. Agostiano, G. Leo and M. Lomascolo, *J. Phys. Chem. B*. 107 (2003) 4756.

[29] J. Hambrock, S. Rabe, K. Merz, A. Birkner, A. Wohlfart, R. A. Fischer and M. Driess, *J. Mater. Chem*., 13 (2003) 1731.

[30] Mikrajuddin, F. Iskandar, K. Okuyamaa and F. G. Shi, *J. Appl. Phys*., 89 (2001) 6431.

[31] M. Abdullah, I. W. Lenggoro, K. Okuyama and F. G. Shi, *J. Phys. Chem. B*. 107 (2003) 1957.

[32] P. Hoyer, R. Eichberger and H. Weller, *Ber. Bunsen-Ges. Phys. Chem.*, 97 (1993) 630.

[33] E. A. Meulenkamp, *J. Phys. Chem. B*. 102 (1998) 5566.

[34] W. R. Dawson and M. W. Windsor, *J. Phys. Chem.,* 72 (1968) 3251.

[35] M. Haase, H. Weller and A. Henglein, *J. Phys. Chem.*, 92 (1988) 482.

[36] U. Koch, A. Fojtik, H. Weller and A. Henglein, *Chem. Phys. Lett.*, 122 (1985) 507.

[37] M. Nandi, J. A. Coklin, L. Salvati and A. Sen, *Chem. Mater*., 3 (1991) 201.

[38] X. –Y. Shang, Z. –K. Zhu, J. Yin, and X. –D. Ma, *Chem. Mater*., 14 (2002) 71.

[39] O. Kohlmann, W. E. Steinmetz, X. –A. Mao, W. P. Wuelfing, A. C. Templeton, R. W. Murray and C. S. Johnson, Jr, *J. Phys. Chem. B*. 105 (2001) 8801.

Chapter 6

Conclusion

6.1 Conclusions

This project presents the study on the synthesis and characteristic of low-dimensional ZnO nanostructures, the well-controlled diameter of ZnO nanorods, the growth of well-aligned ZnO nanotip arrays on the different ZnO substrates, and the investigation of effect of surface stabilization of nanoparticles on luminescent characteristics in ZnO/poly(hydroxyethyl methacrylate) nanohybrid film.

A novel two-step procedure for preparing large-scale growth of single crystal ZnO nanorods on nanostructured substrates by soft solution method without metal catalyst is proposed. The low-temperature growth can be achieved via the help of ZnO nanostructured substrate which offers a desirable route for large-scale ZnO nanorods growth. XRD, Raman, SEM, TEM and HRTEM analysis indicate that the diameters of single crystal ZnO nanorods with hexagonal wurtzite structure have a finite size distribution. The room

temperature PL spectra of the ZnO nanorods exhibit a strong UV emission of 378 nm and a weak green emission of 580 nm. The low-temperature growth process requires no expensive and precise vacuum equipment, so permitting large-scale fabrication with a relatively low cost. In addition, the high optical transparency and electrical conductivity of the ITO glass substrates also provide a great potential in future optoelectronic nanodevice applications.

As seen in Chapter 4, highly aligned and free-standing ZnO nanotip arrays grown on the ZnO films by soft chemical method are proposed. The soft growing method also has been extended to synthesize well-aligned nanotip arrays on ZnO microrods. X-ray diffraction analysis shows that the ZnO nanotips are hexagonal wurtzite structure, and the *c*-axes of nanotips are perfectly along the substrate surface normal. HRTEM demonstrates the ZnO nanotip to be a single crystal. Room temperature photoluminescence of the ZnO nanotips has a strong UV emission band at 378 nm. The field emission of ZnO nanotip arrays shows a turn-on field of about 10.8 V/μm at a current density of 0.1 $\mu A/cm^{-1}$ and emission current density up to about 1 mA/cm^2 at a bias field of 19.5 V/μm.

Lastly, high transparent and stable luminescent ZnO/Poly(hydroxyethyl methacrylate) nanocomposites have been synthesized via a nanoparticle surface modified method. 3-(Trimethoxysilyl)propyl methacrylate (TPM) was used as the stabilizing agent in the simple, mild sol-gel route to prepare the TPM-modified ZnO nanoparticles. The TPM stabilizer was shown to provide the high dispersion stability of ZnO nanoparticles in ethanol solution and preserve the size of nanoparticles near constant over the long periods of time. The TPM-modified ZnO nanoparticles have better spatial separation than that of unmodified ZnO nanoparticles in the nanohybrid film. Furthermore, the room temperature PL measurements also show that this surface-modified method can preserve the superior

luminescence of ZnO nanoparticles in the nanohybrid films as well as in the initial nanoparticles solution. The surface modification method is believed to be an efficient approach to fine adjust the luminescent color and uniformity of bulk nanocomposites for developing novel electro-optical application.

Publications

1. C.H. Hung and W.T. Whang*, 2003, “A Novel Low-temperature Growth and Characterization of Single Crystal ZnO Nanorods”, Materials Chemistry and Physics. **82**, 705(2003). (*主持人)(SCI) 計畫編號：NSC-91-2216-E-009-013

2. P.J. Chiang and W.T.Whang*, 2003, “The Synthesis and Morphology Characteristics Study of BAO-ODPA Polyimide/TiO_2 Nano Hybrid Films”, Polymer Vol. 44, 2249(2003)(*主持人)(SCI)
計畫編號：NSC-91-2216-E-009-013

3. P.J. Chiang and W.T. Whang, 2004,“Physical and Mechanical Properties of Polyimide/titania Hybrid Films”, Thin Solid Films, Vol 447-48, 359(2004).
計畫編號：NSC-91-2216-E-009-013

4. S.C. Suen and W.T. Whang*, B.W. Wu, and Y.F. Lai, 2004,“Low temperature fabrication of carbon nanofibers by self-assembling of polycyclic aromatic hydrocarbon molecule”, Applied Physics Letters, Vol 84(16), 3157(2004). (*主持人)(SCI)
計畫編號：NSC-92-2216-E-009-003

5. P.J. Chiang and W.T. Whang*, 2004,“Effect of titania content and plasma treatment on the interfacial adhesion mechanism of nano titania-hybridzed polyimide and copper system”, Polymer, Vol 45, 4465(2004).(主持人)
計畫編號：NSC-92-2216-E-009-003

6. C.H. Hung and W.T. Whang*, 2004, “Low Temperature Solution Approach Towards Highly Aligned ZnO Nanotips and Self-Oriented Nanotips-Rod Arrays”, J. Crystal Growth, Vol 268**,** 242(2004). (*主持人)(SCI)
計畫編號：NSC-92-2216-E-009-003

7. C.H. Hung and W.T. Whang*, 2005, “Effect of surface stabilization of nanoparticles on luminescent characteristics in ZnO/poly(hydroxyethyl methacrylate) nanohybrid films”, J. Mater. Chem., Vol 15(2)**,** 267~274(2005). (*主持人)(SCI)
計畫編號：NSC-92-2216-E-009-003

8. Shou-Chian Hsu, Wha-Tzong Whang*, Chin-Hsien Hung, Pei-Chun Chiang, Yi-Nan Hsiao, 2005, “Effect of the Polyimide Structure and ZnO Concentration on the Morphology and Characteristics of Polyimide/ZnO Nanohybrid Films”, Macromolecular Chemistry and Physics, Vol 206(2), 291-298, (2005)(*主持人)(SCI)

計畫編號：NSC-92-2216-E-009-003

9. Y.N. Hsiao, W.T. Whang*, S.H. Lin and K.Y. Hsu, 2005, “Effect of ZnMA on Optical and Holographic Characteristics of Doped PQ/PMMA Photopolymer”, Jpn. J. Appl. Phys., Vol 44(2), 914~919(2005) (*主持人)(SCI)
計畫編號：NSC-92-2216-E-009-003